The SSP greenhouse gas concentrations and their extensions to 2500

Malte Meinshausen[1,2,3], Zebedee Nicholls[1,2], Jared Lewis[1], Matthew J. Gidden[4,5], Elisabeth Vogel[1,2], Mandy Freund[1,6], Urs Beyerle[7], Claudia Gessner[7], Alexander Nauels[1,5], Nico Bauer[3], Josep G. Canadell[8], John S. Daniel[9], Andrew John[1,10], Paul Krummel[11], Gunnar Luderer[3], Nicolai Meinshausen[12], Stephen A. Montzka[13], Peter Rayner[2,1], Stefan Reimann[14], Steven J. Smith[15], Marten van den Berg[16], Guus J.M. Velders[17,18], Martin Vollmer[14], Hsaing Jui (Ray) Wang[19]

[1] Climate & Energy College, The University of Melbourne, Parkville, Victoria, Australia
[2] School of Earth Sciences, The University of Melbourne, Parkville, Victoria, Australia
[3] Potsdam Institute for Climate Impact Research (PIK), Potsdam, Germany
[4] IIASA Institute for Applied Systems Analysis, Laxenburg, Austria
[5] Climate Analytics, Berlin, Germany
[6] Marine and Atmospheric Research, CSIRO, Hobart, Tasmania, Australia
[7] Institute for Atmospheric and Climate Science, Swiss Federal Institute of Technology, Zurich (ETH Zurich), Switzerland
[8] Global Carbon Project, CSIRO Oceans and Atmosphere, Canberra, ACT, Australia
[9] NOAA, Earth System Research Laboratory, Chemical Sciences Division, Boulder, Colorado, USA
[10] Department of Infrastructure Engineering, The University of Melbourne, Parkville, Victoria, Australia
[11] CSIRO Oceans and Atmosphere, Aspendale, Victoria, Australia
[12] Seminar for Statistics, Swiss Federal Institute of Technology (ETH Zurich), Zurich, Switzerland.
[13] NOAA, Earth System Research Laboratory, Global Monitoring Division, Boulder, Colorado, USA
[14] Empa, Laboratory for Air Pollution/Environmental Technology, Swiss Federal Laboratories for Materials Science and Technology, Dübendorf, Switzerland
[15] Joint Global Change Research Institute, Pacific Northwest National Laboratory, College Park, MD, USA
Potsdam, Germany
[16] PBL Netherlands Environmental Assessment Agency, the Netherlands
[17] National Institute for Public Health and the Environment (RIVM), Bilthoven, Netherlands
[18] Institute for Marine and Atmospheric Research Utrecht (IMAU), Utrecht University, Utrecht, The Netherlands
[19] School of Earth and Atmospheric Sciences, Georgia Institute of Technology, Atlanta, GA 30332-0340, USA

Correspondence to: M. Meinshausen (malte.meinshausen@unimelb.edu.au)

Abstract. Anthropogenic increases of atmospheric greenhouse gas concentrations are the main driver of current and future climate change. The Integrated Assessment community has quantified anthropogenic emissions for the Shared Socioeconomic Pathways (SSP) scenarios, each of which represents a different future socio-economic projection and political environment. Here, we provide the greenhouse gas concentrations for these SSP scenarios – using the reduced complexity climate-carbon cycle model MAGICC7.0. We extend historical, observationally-based concentration data with SSP concentration projections from 2015 to 2500 for 43 greenhouse gases with monthly and latitudinal resolution. CO_2 concentrations by 2100 range from 393 to 1135 ppm for the lowest (SSP1-1.9) and highest (SSP5-8.5) emission scenarios respectively. We also provide the concentration extensions beyond 2100 based on assumptions in the trajectories of fossil fuels and land use change emissions, net negative emissions, and the fraction of non-CO_2 emissions. By 2150, CO_2 concentrations in the lowest emission scenario are approximately 350 ppm and approximately plateau at that level until 2500, whereas the highest fossil-fuel driven scenario projects CO_2 concentrations of 1737 ppm and reaches concentrations beyond 2000ppm by 2250. We estimate that the share of CO_2 in the total radiative forcing contribution of all considered 43 long-lived greenhouse gases increases from 66% for present day to roughly 68% to 85% by the time of maximum forcing in the 21st century. For this estimation, we updated simple radiative forcing parameterisations that reflect the Oslo Line by Line model results. In comparison to the RCPs, the five main SSPs (SSP1-1.9, SSP1-2.6, SSP2-4.5, SSP3-7.0 and SSP5-8.5) are more evenly spaced and extend to lower 2100 radiative forcing and temperatures. Performing 2 pairs of 6-member historical ensembles with CESM1.2.2, we estimate the effect on surface air temperatures of applying latitudinally and seasonally resolved GHG concentrations. We find that the ensemble differences in the March-April-May (MAM) season provide a regional warming in higher northern latitudes of up to 0.4K over the historical period, latitudinally averaged of about 0.1K, which we estimate to be comparable to the upper bound (~5% level) of natural variability. In comparison to the comparatively straight line of the last 2000 years, the greenhouse gas concentrations since the onset of the industrial period and this studies' projections over the next 100 to 500 years unequivocally depict a 'hockey-stick' upwards shape. The SSP concentration time series derived in this study provide a harmonized set of input assumptions for long-term climate science analysis; they also provide an indication of the wide set of futures that societal developments and policy implementations can lead to

- ranging from multiple degrees of future warming on the one side or approximately 1.5ºC warming on the other.

1 Introduction

The climate modelling community periodically undertakes large model intercomparison exercises with the latest and most sophisticated set of climate models, to gain a better understanding of the response of the climate system to a range of potential emission or concentration scenarios (Taylor et al., 2012;Meehl et al., 2007). The atmosphere-ocean general circulation models (AOGCMs) are physical climate models that may include biogeochemical model components, such as vegetation or some atmospheric chemistry, but they are not able to project CO_2 concentrations from emissions due to an incomplete, imbalanced or non-existent carbon cycle. The climate models that have this ability to project CO_2 concentrations from emissions, are often referred to as Earth System Models (ESMs) (Lawrence et al., 2016;Jones et al., 2016). These ESMs are also often run in 'CO_2-concentration driven mode' for computational ease and to allow for an easier separation between carbon cycle feedbacks and climate responses. As of today in phase 6 of the Coupled Model Intercomparison Project (CMIP6) (Eyring et al., 2016), both AOGCMs and ESMs use concentrations from all non-CO_2 greenhouse gases to perform multi-gas experiment (such as the future scenario projections) due to either missing non-CO_2 gas cycles or prohibitive computational costs of including such cycles.

This study provides and describes the standardised set of greenhouse gas (GHG) concentration futures for CO_2, CH_4, N_2O and 40 other minor greenhouse gases. For the historical period, this GHG concentration data for CMIP6 was provided by the companion paper Meinshausen et al. (2017). This study provides the GHG concentration data until 2100 on the basis of the emission scenarios derived from socio-economically explicit Integrated Assessment Models' (IAMs) under the SSP framework (Gidden et al., 2019). We also provide an extension of the concentration data until 2500 on the basis of simplified assumptions.

These concentrations datasets are part of the protocols for several CMIP6 experiments, most notably ScenarioMIP (O'Neill et al., 2016) and AerChemMIP (Collins et al., 2017), that require concentration-driven runs (see search.es-doc.org for a full description). While greenhouse gases are arguably the most important influence of humankind on future climate in terms of radiative forcing, there is a wide range of other forcers, including anthropogenic aerosols (Hoesly et al., 2018), land-use patterns, aerosol optical properties (Stevens et al., 2017), as well as natural forcers like solar (Matthes et al., 2017) and volcanic effects (Toohey et al., 2016). These forcers are described in the companion papers and compiled in the input4mip interface to be used for the historical and future ESM experiments (Durack and Taylor, 2019), available on https://esgf-node.llnl.gov/projects/input4mips/.

Our future greenhouse gas concentration datasets from 2015 onwards are provided for a total of nine SSP scenarios. These nine scenarios comprise five high-priority scenarios for the Sixth Assessment report by the IPCC report, which is the group of four "Tier 1" scenarios highlighted in ScenarioMIP (O'Neill et al., 2016) in addition to the SSP1-1.9 scenario that reflects most closely a 1.5°C target under the Paris Agreement. Specifically, these "high priority" scenarios for IPCC AR6 are (1) the SSP1-2.6 "2°C-scenario" of the "sustainability" SSP1 socio-economic family, whose nameplate 2100 radiative forcing level is 2.6 W/m^2. This SSP1-2.6 scenario approximately corresponds to the previous' scenario generation Representative Concentration Pathway (RCP) 2.6. Secondly, the (2) SSP2-4.5 of the "middle of the road" socio-economic family SSP2 with a nominal 4.5W/m^2 radiative forcing level by 2100 - approximately corresponding to the RCP-4.5 scenario. Thirdly, (3), the SSP3-7.0 scenario is a medium-high reference scenario within the "regional rivalry" socio-economic family, while (4), the SSP5-8.5 marks the upper edge of the SSP scenario spectrum with a high reference scenario in a high fossil-fuel development world throughout the 21st century. The additional high priority scenario that IPCC AR6 considers is SSP1-1.9 to better reflect the research regarding the Paris Agreement's 1.5°C target. It should be noted that the radiative forcing labels, such as "2.6" in the SSP1-2.6 scenario, are indicative "nameplates" only, approximating total radiative forcing levels by the end of the 21st century. Those labels are merely indicative, given that actual radiative forcing uncertainties (and differences across ESMs that implement the same concentrations,aerosol abundances, ozone fields and landuse patterns) are substantial.

In addition to these five high-priority scenarios, we provide concentrations for four additional SSP scenarios, namely the three remaining "Tier 2" ScenarioMIP experiments, featuring a low reference

scenario SSP4-6.0 within the socio-economic context of the an "inequality" dominated world, as well as its moderate mitigation scenario SSP4-3.4. Similarly, there is the geophysically interesting emissions "overshoot" scenario, SSP5-3.4-OS, as it initially follows the high emission SSP5-8.5 scenario until 2030 before exhibiting the steepest annual reduction rates of all SSP scenarios and the most net negative emissions by 2100. Lastly, we also consider the SSP3-7.0-LowNTCF variant of the SSP3-7.0 scenario with reduced near-term climate forcer (NTCF) emissions. Given that the SSP3-7.0 scenario is the one with the highest methane and air pollution precursor emissions, the SSP3-7.0-LowNTCF variant investigates an alternative pathway for the AerChemMIP intercomparison project (Collins et al., 2017) that exhibits very low methane, aerosol and tropospheric ozone precursor emissions - approximately in line with the lowest other SSP scenarios for those species like SSP1-1.9 and SSP1-2.6. Note that the NTCF nomenclature is equivalent to the term Short-Lived Climate Forcer, SLCF, which is now more commonly used by the research community and IPCC context.

The presented historical global-mean and hemispheric-mean surface mole fractions in this study transition smoothly from the end of the historical dataset (Meinshausen et al., 2017), 2014, into the start of the projections, 2015. Also, the latitudinal gradient and seasonality, and their temporal evolution, are consistent with the historical dataset - which in all cases are tied directly to past measurements. We used a reduced complexity carbon-cycle model, MAGICC (Meinshausen et al., 2011c;Meinshausen et al., 2011a), to produce global-mean future greenhouse gas concentration time series for each of the considered SSPs. The same model, albeit an earlier version, was also previously used to provide the RCP greenhouse gas concentrations projections (Meinshausen et al., 2011b). The MAGICC version used for this study (version 7.0) is calibrated to closely represent C4MIP carbon cycle responses, includes a permafrost module (Schneider von Deimling et al., 2012) and updated radiative forcing and non-CO_2 gas cycle parameterisations (in particular for CH_4 and N_2O) that represent recent literature findings (Prather et al., 2012; Holmes et al., 2013). The calibrated carbon cycle of MAGICC has previously been shown to reflect well the CMIP5 ESM response range (Friedlingstein et al., 2014). Given the nearly two-year time difference between the completion of historical and future greenhouse gas concentrations, we also updated the historical observational datasets to reflect observations until early 2018 for CO_2, CH_4 and N_2O, as well as most other gases considered here.

This study first describes the methods with separate parts for the updated observational data until 2018 (Section 2.1), the emission input data from the IAM scenarios and the input preparation steps undertaken (2.2), the extensions of the emissions and concentrations beyond 2100 (2.3) the MAGICC model setup (2.4), and the projections of latitudinal gradients (2.5) and seasonality (2.6). We also provide a new simplified formula to reflect the Oslo Line By Line model (OLBL) radiative forcing results (Etminan et al., 2016) in order to provide the radiative forcing aggregation of the output (2.7) and discuss additional methodological steps (2.8). We then show the results and compare these to other recent observational datasets (Section 3 "Results"). A discussion section follows (Section 4 "Discussion"), which includes a closer look at the two most dominant GHG forcers CO_2 and CH_4 and their correlation (4.1), a discussion on the most recent GHG concentration developments (4.2) and the comparison with RCPs concentrations (4.4) as well as temperatures and sea level rise projections (**Error! Reference source not found.**). We describe the limitations of the dataset (5), which includes issues like the integration of observational and modelled future data, missing uncertainty estimates, potential biases in future seasonality and latitudinal gradients, and a lack of reference scenarios for Montreal-controlled substances. Section 6 concludes.

2 Methods

As for the historical concentrations, we provide 43 greenhouse gases future concentration projections, namely CO_2, CH_4, N_2O, 17 ozone depleting substances, namely CFC-11, CFC-12, CFC-113, CFC-114, CFC-115, HCFC-22, HCFC-141b, HCFC-142b, CH_3CCl_3, CCl_4, CH_3Cl, CH_2Cl_2, $CHCl_3$, CH_3Br, Halon-1211, Halon-1301, Halon-2402, and 23 other fluorinated compounds, namely 11 HFCs (HFC-134a, HFC-23, HFC-32, HFC-125, HFC-143a, HFC-152a, HFC-227ea, HFC-236fa, HFC-245fa, HFC-365mfc, HFC-43-10mee), NF_3, SF_6, SO_2F_2, and 9 PFCs (CF_4, C_2F_6, C_3F_8, C_4F_{10}, C_5F_{12}, C_6F_{14}, C_7F_{16}, C_8F_{18}, and c-C_4F_8). Our projections refer to atmospheric dry air mole fractions as does the historical data presented in Meinshausen et al. (2017), even though the projections are sometimes loosely referred to as 'concentrations'. For CO_2, the usual unit is parts per million (ppm), for CH_4 and N_2O, the usual unit is parts per billion (ppb) and other gases are usually denoted in parts per trillion (ppt).

2.1 Updated observational data

The historical concentrations (until the end of 2014) were derived from various observational datasets of greenhouse gas concentrations, or literature studies in the case of some of greenhouse gases with lower concentrations. The observational data was binned by latitudinal and longitudinal boxes, averaged for monthly values and complemented by interpolations. The historical timeseries for every greenhouse gas were separated into three elements as part of the spatio-temporal binning: i) latitudinal gradient, ii) seasonality pattern and iii) global mean. This separation then permitted the use of longer observational timeseries, such as the high latitudinal CH_4 firn data – implicitly correcting for the high latitude differences to the global mean that one would expect. Interpolations, regressed latitudinal gradients and seasonality patterns were employed to derive the historical dataset, but no gas cycle models.

With additional observational data being available for 2015, 2016 and 2017, the previously used observational datasources from the AGAGE and NOAA networks (Dlugokencky, 2015a, b;Prinn et al., 2018), including multiple NOAA/ESRL/GMD flask measurements, were updated and used to determine the initial years of the future concentration timeseries. The result of this is that – depending on the gases - the same concentrations are used across all nine SSPs in the initial years (Table 1). As outlined below, we employed MAGICC7.0 and its calibrated gas cycles to produce concentration time series from SSP emissions beyond the observationally based period.

2.2 Emission data and their harmonisation

For the emission driven MAGICC7 runs that produce the future global-mean greenhouse gas timeseries, we use the SSP emission data for CO_2, CH_4 and N_2O, HFCs, PFCs and SF_6 which is available from the SSP database at IIASA (https://tntcat.iiasa.ac.at/SspDb). This emission data has already been subject to several categorisation and harmonisation steps to obtain regionally consistent (in case of CO_2 and CH_4) and sectorally resolved data (for more details, see Gidden et al., 2019). We complemented those harmonisation steps to consider the following species in the five RCP regions (OECD90, REF (Economies in Transition), LAM (Latin America), MAF (Middle East and Northern Africa) and ASIA): CO_2, CH_4 and N_2O in addition to black carbon (BC), carbon monoxide (CO), ammonium (NH_3), non-CH_4 volatile organic compounds (NMVOC), nitrates (NOx), organic carbon (OC) and sulphate aerosol (SOx). For those 10 species, we also distinguished between fossil & industrial sources and land-use related sources.

Regional landuse CO_2 emissions are not provided in the SSP database (Gidden et al., 2019), so we downscaled to the RCP regions based on historical regional emission shares in the year 2015. Given landuse CO_2 emissions can be negative in some SSP scenarios, a simple scaling approach in the regional harmonisation would yield unrealistic results (i.e. regions with low or negative current net landuse emissions, like the OECD, would end up with positive emissions and the other world regions would be strongly negative in the future. Instead, we applied a normalisation that assumes a negative 1.5 GtC base level against which historical regional emission shares are continued into the future, scaled with global emissions.

Mathematically, the constant regional scaling factor is hence applied to the offset emission level, so that the future regional emissions $E_r(y)$ in year y are:

$$E_r(y) = E_g(2015) \times s_{2015} + \Big(E_g(y) - E_g(2015)\Big) \times r$$

where

$$r = \frac{E_r(2015) + 1.5}{\sum_{r=1}^{n}(E_r(2015) + 1.5)}$$

With r being the regional share of emissions relative to that 1.5GtC offset level, s being the regional share of emissions in 2015 relative to zero, i.e. $s_{2015} = E_r(2015)/E_g(2015)$, $E_r(y)$ being the regional emissions in year y and $E_g(y)$ being the global emissions, i.e. the sum of the n regional emissions. Specifically, the factors s_{2015} and r for were the following for the regions Asia, Latin America, Middle East and Africa, OECD-90 and Economies in Transition: 0.483, 0.282, 0.189, 0.043, 0.003, for s_{2015} and 0.232 0.209, 0.199, 0.182, 0.178 for r, respectively. This choice has little effect because the regional split up of CO_2 emissions only marginally and indirectly affects the latitudinal concentrations in our chosen method. A very small difference arises for different regional landuse CO_2 emission assumptions because MAGICC7 scales albedo effects with landuse CO_2 emissions and these albedo effects impact temperatures and in turn the carbon cycle again.

Landuse related CH_4 and fossil & industrial CO_2 and CH_4 emissions were already harmonised with historical emissions and also regionally available (Gidden et al., 2019;Gidden et al., 2018). N_2O emissions were only available as global total from the SSP database based on PRIMAP (Gütschow et al., 2016),

which is why we assume constant regional and sectoral emission shares. This assumption does not have a bearing on final global concentrations.

For the emissions of fluorinated gases, that are listed in the Kyoto Protocol and considered here (PFCs, HFCs and SF_6), namely C_2F_6, CF_4, HFC-125, HFC-134a, HFC-143a, HFC-227ea, HFC-23, HFC-245fa, HFC-43-10mee, and SF_6, MAGICC7 takes the global and aggregated SSP emissions of the gas baskets as inputs, as provided by the IAM modellers using constant emission shares based on a future gas-specific scenario by Guus Velders (Velders et al., 2015) and described in Gidden et al. (2019). The basket of PFCs, HFCs and SF_6 is reported in the SSP database at IIASA (https://tntcat.iiasa.ac.at/SspDb/). Some few data points were corrected in consultation with the respective IAM modelling teams, namely the SSP1-1.9 emission level in 2100 for CF_4 and C_2F_6, for which we assumed the rate of decline prolonged from the 2080 to 2090 to the 2090 to 2100 period. HFC-32 emissions were complemented from a Kigali-Agreement consistent scenario, which has also been derived from the scenarios by Velders et al. (2015). Those scenarios were published until 2050 and we use in addition an extension up to 2100 by proportional downscaling of the GWP-weighted HFC basket – using SSP GDP and population data with an assumption of constant GDP and population after 2100.

The ozone depleting substances controlled under the Montreal Protocol, namely CFC-11, CFC-12, CFC-113, CFC-114, CFC-115, HCFC-22, HCFC-141b, HCFC-142b, CH_3Br, CH_3Cl, CH_3CCl_3, CCl_4, Halon-1202, Halon-1211, Halon-1301, Halon-2402 are here assumed to follow the WMO 2014 scenario (WMO, 2014) from 1951 to 2099, as presented in detail in Velders and Daniel (2014a). For times before 1951 and after 2099, the previous WMO A1 Baseline emission scenario from year 2006 (WMO, 2006) is assumed which is near-zero and close to the respective WMO 2014 values in 1951 and 2099.

Harmonized emissions of aerosol and ozone precursor species are also available for the SSP scenarios (Hoesly et al., 2018), but not discussed in this paper. These non-GHG emissions are used here as part of the complete scenario specification needed to produce future temperature and GHG concentration pathways.

2.3 Extension of emissions and concentrations beyond 2100

In 2011, the RCPs were extended beyond 2100 to provide the basis for longer-term scenario studies (Meinshausen et al., 2011b), then called 'Extended Concentration Pathways' (ECPs). Studying this longer-term behaviour of the climate system is of interest for quantities that exhibit a strong long-term commitment or non-linear behaviour (e.g. sea-level rise, ice sheet dynamics). The RCP concentration extensions were – for some gases and scenarios – based on pragmatic extensions of emissions, like an RCP8.5 CO_2 emission stabilisation from 2100 to 2150 with a subsequent ramp-down until 2250. For other RCPs, concentrations were held constant and the inverse CO_2 emissions exhibited a near-exponential decline.

Here, we present the extensions beyond 2100 of the ScenarioMIP and AerChemMIP SSPs (although we do not use a new acronym like ECPs at the time of the RCPs). The final choices differ, in some respects, from the initial sketch of these extensions that was offered in the ScenarioMIP overview paper (O'Neill et al., 2016). As described below, the collaborative exercise by the IAM modellers and MAGICC team updated the original SSP extension design. In summary, the extension principles are:

1) From 2100 onwards, net negative fossil CO_2 emissions are brought back to zero during the 22nd century, while positive fossil CO_2 emissions are ramped down to zero by 2250.
2) Land use CO_2 emissions are brought back to zero by 2150.
3) Non-CO_2 fossil greenhouse gas emissions are ramped down to zero by 2250.
4) Land use-related non-CO_2 emissions are held constant at 2100 levels.

In the initial ScenarioMIP design (O'Neill et al., 2016), fossil CO_2 emissions for SSP5-3.4-OS and SSP1-2.6 are negative at 2100 levels until 2140 and gradually increase to zero until 2190 and 2185, respectively (**Figure 2**, panel a). We did not assume permanent net-negative CO_2 emissions to maintain proximity to the original scenario design and in the light of biophysical and economic limits of negative emissions, as well as potential side-effects (Fuss et al., 2018;Smith et al., 2016). For all scenarios with net negative fossil fuel extensions, we implemented extensions assuming constant emissions until 2140 (as suggested), but reaching zero emissions in 2190. The only exception is the SSP5-3.4-OS scenario, which was ramped back to zero by a slightly earlier date (2170) so that fossil and landuse emissions (in combination with

MAGICC7.0's default setting – see section 2.4) met the design criteria of an approximate merge with SSP1-2.6 concentrations in the longer-term, i.e. after 2150.

In the initial ScenarioMIP extension sketch for SSP5-8.5, total CO_2 emissions were envisaged to be "less than 10 GtC/yr" by 2250 **Figure 2**, panel c). Having considered multiple options, we opted for a straight ramp down of fossil CO_2 emissions to zero by 2250 due to its simplicity. Landuse CO_2 emissions for SSP1-2.6 in the initial ScenarioMIP design were held constant at 2100 levels indefinitely. SSP5-3.4-OS levels were designed to reach the same net negative landuse CO_2 levels by 2120 (**Figure 2**, panel b). However, the extensions presented here assume that all landuse CO_2 emissions linearly phase-out between 2100 and 2150, as continuing negative landuse CO_2 emissions are inconsistent with fixed 2100 landuse and land cover patterns. In the original scenario design suggestion by O'Neill et. al, all non-CO_2 greenhouse gas emissions were kept constant at 2100 levels. However, the final extensions presented here assume differentiated extension rules by sector. Specifically, we assumed a linear phase-out of all fossil and industrial non-CO_2 emissions by 2250 (incl. aerosols etc) (see e.g. **Figure 2**, panel c). Similarly, synthetic industrial gases were assumed to be phased out by 2250 instead of assuming constant emissions (panel g, h). For landuse-related non-CO_2 emissions, the assumption has been maintained that 2100 emission levels are held constant. That assumption seemed approximately consistent with constant landuse and land cover patterns as food production activities would continue to produce certain levels of N_2O and CH_4 emissions (panel d). In comparison to a uniform approach of holding all emissions constant at 2100 levels, the chosen differentiation to phase out fossil and industrial related emissions over time while holding land-use related emissions constant seemed more consistent with plausible futures.

2.4 Projecting global-mean concentrations with the MAGICC climate model

For projecting the SSP greenhouse gas concentrations, we updated several gas cycles and also used MAGICC's permafrost module, which was not switched on when projecting the RCP concentrations. The sections below describe these updates.

2.4.1 Methane cycle

The methane (CH_4) cycle in MAGICC projects CH_4 concentrations based on anthropogenic CH_4 emissions as an input. Internally, MAGICC derives natural CH_4 emissions by closing the CH_4 budget over a user-defined historical period (here assumed 1994 to 2004, previously 1966 to 1976). The atmospheric CH_4 lifetime as modelled in MAGICC changes over time both because of projected changes in tropospheric OH concentrations and an increased stratospheric Brewer-Dobson circulation under increased climate change (Meinshausen et al., 2011a). On top of this, increased CH_4 emissions are modelled to affect (alongside several other reactive gas emissions like CO, NMVOC and NOx) tropospheric OH concentrations (as described for our modelling framework in Meinshausen et al., 2011a; based on Ehhalt et al., 2001). Thus, there is a feedback loop where increased CH_4 emissions lead to decreased OH-related CH_4 sinks and in turn longer CH_4 lifetimes and longer lifetimes of other GHGs, such as HCFCs and HFCs. The increased Brewer-Dobson circulation, on the other hand, leads to stronger CH_4 removals, lowering the overall lifetime. As a net effect, CH_4 lifetimes tend to be shorter in the lower emission scenarios and longer in the higher emission scenarios, such as RCP8.5.

In this study, we calibrate nine of MAGICC's CH_4 cycle parameters (see its description and parameter denotations in Appendix A2.1 of Meinshausen et al. (2011c)) to the modelled CH_4 projections by Holmes et al. (2013). They included, like MAGICC, the temperature sensitivity of CH_4's OH-related lifetime, thereby updating results of Prather et al. (2012). These newly calibrated parameters are (a) the initial CH_4 lifetime $\tau'_{CH4,tropos}$ (9.95 yrs, updated from 9.6 yrs), (b) the temperature-sensitivity of CH_4's OH-related lifetime $S_{\tau CH4}$ (0.07 K^{-1}, updated from 0.058 K^{-1}), (c) a scaling factor on the sensitivity of CH_4's lifetime to OH-changes S^{OH}_{scale}(0.725, formerly 1), which is newly introduced and applies to all S^{OH}_{x} factors shown in equation A30 in Meinshausen (2011c), (d) the unscaled sensitivity of OH to CH_4 concentration changes $S^{OH}_{CH_4}$ (-0.5377, updated from the unscaled -0.32), noting that this update largely offsets the effect of the newly introduced scaling factor S^{OH}_{scale}, (e) the other sensitivities of tropospheric OH to changes in NO_x, CO, and VOC, namely $S^{OH}_{NO_x}$, S^{OH}_{CO}, S^{OH}_{VOC} (updated to 9.3376e-3, -1.13e-4, and -3.142e-4 from 4.2e-3, -1.05e-4, and -3.15e-4, respectively). Also, we updated the partial soil related lifetime of CH_4 (150 years rather than 160 years), following Prather et al. (2012).

The net effect of the newly calibrated MAGICC is that Holmes et al. (2013) CH_4 projections are closely matched across the range of RCPs (Supplementary Figure 1, left column). Both OH-related and total CH_4 lifetimes exhibit similar changes over time as in Holmes et al. (Supplementary Figure 1, middle columns), with the slight upward offset explained by our historical budgeting approach deducting somewhat lower natural CH_4 emissions (which MAGICC assumes constant over time) (Supplementary Figure 1, right column).

2.4.2 Nitrous oxide projections

Prather et al. (2012) suggested that the RCP projections for N_2O concentrations performed with MAGICC6 were somewhat too low for the lower RCP2.6 scenario and slightly too high for the higher RCP8.5 scenario (although within their uncertainty ranges). Here, we use their model to back out natural emission assumptions and lifetimes to allow a multi-variable calibration of MAGICC7 to the median of the RCP N_2O concentration range suggested and these other variables by Prather et al. (2012) (Supplementary Figure 2).

To set up this calibration, we complement RCP emission pathways by historical N_2O emissions from PRIMAP-hist (Gütschow et al., 2016). We also used observed N_2O concentrations until 2014 (Meinshausen et al., 2017) to complement the future Prather et al. concentrations. The natural N_2O emission levels are calibrated (as part of the overall calibration that optimised lifetimes, budgeting periods and lifetime sensitivities) with a budgeting approach over the 10 years prior to 1991, resulting in a slightly lower assumed natural N_2O emission level of 8.013 MtN-N_2O compared to Prather et al (9.1 MtN-N_2O) and AR5 (11.0 MtN-N_2O). Nonetheless, the total natural and anthropogenic emissions are similar for present-day conditions, because Prather et al. assumes lower anthropogenic emissions (6.5 MtN-N_2O) compared to the RCP pathways, which assume in average 7.9 MtN-N_2O. Apart from the budgeting period, MAGICC7's N_2O gas cycle has three further N_2O parameters, which we calibrate to the Prather et al. results. Those are (a) the initial N_2O lifetime τ^0_{N2O} (updated from 123 years to 139 years), the sensitivity coefficient $S_{\tau_{N2O}}$ which scales the N_2O lifetime with the factor $\left(\frac{C^t_{N2O}}{C^0_{N2O}}\right)^{S_{\tau_{N2O}}}$, where C^t_{N2O} is the current atmospheric burden at time t, and C^0_{N2O} the pre-industrial burden ($S_{\tau_{N2O}}$ updated from -0.05 to -0.04). Lastly, we calibrated the sensitivity of the stratospheric lifetime, with which N_2O's partial stratospheric

lifetime is adjusted in response to a change in the Brewer-Dobson circulation (0.04 percent change of partial lifetime per percent change of meridional flux).

2.4.3 Additional gas cycles

We extended the number of fluorinated gases to cover the full range of 43 greenhouse gases in MAGICC (i.e. including HFCs) from 12 to 23 and the number of ozone depleting substances from 16 to 18. Specifically, the newly modelled fluorinated species are perfluorocarbons C_3F_8, C_4F_{10}, C_5F_{12}, C_7F_{16}, C_8F_{18}, CC_4F_8, hydrofluorocarbons HFC-152a, HFC-236fa, HFC-365mfc, as well as NF_3, and SO_2F_2. The newly modelled ozone depleting substances are methylene chloride CH_2Cl_2, with a very short lifetime of 0.4 years, and methyl chloride CH_3Cl, with a lifetime of around one year (for lifetimes, see Table 8.A.1 of IPCC AR5 WG1 Chapter 8 (Myhre et al., 2014)). We scale the partial stratospheric lifetime (HFC-152a, 39 years; HFC-236fa, 1800 years; HFC-365mfc, 125 years; NF_3, 740 years; and SO_2F_2 with 630 years – taken from Table 1-3 in WMO (2014)) with a change of the Brewer Dobson circulation strength. The Brewer-Dobson circulation is assumed to increase 15% per degree of warming beyond 1980, derived from Butchart and Scaife's finding of an approximately 3% increase per decade (Butchart and Scaife, 2001) and assuming a 0.2ºC warming per decade (Meinshausen et al., 2011a). Calibrating our gas-cycle models to the results by Holmes et al. (2013), it seemed however that our Brewer-Dobson circulation speed-up shortened the longer-term lifetimes in higher-warming scenarios substantially more than predicted by the results of Holmes et al. (2013). Assuming no change in the height-age distribution of the air parcels that travel through the stratosphere, the speed-up of this meridional circulation could 1:1 lower stratospheric lifetimes. However, assuming shorter residence times could offset some of the effect. We proceeded with a pragmatic approach and calibrated an effectiveness/scaling factor of 0.3 to match methane concentration projections by Holmes et al. (2013). That means that every 1% increase in the Brewer-Dobson circulation, the partial stratospheric lifetimes are reduced by 0.3%. However, we acknowledge that this effectiveness factor possibly summarizes multiple underlying differences between un-scaled MAGICC results and the Holmes et al. (2013) projections that are unrelated to the Brewer-Dobson circulation.

We assume that partial lifetimes related to the (changing) tropospheric OH sink scale with the OH- and temperature-dependent methane lifetime. .

2.4.4 Permafrost feedbacks

Earth system feedbacks from permafrost melting and its associated CO_2 and CH_4 releases were underrepresented in CMIP5 climate models, leading – inter alia – to an ad-hoc adjustment of remaining carbon budgets by 27 GtC (100 $GtCO_2$) in the IPCC Special Report on 1.5°C warming. Also, they were not part of the concentration projections for the RCP scenarios. Here, we include a representation of permafrost feedbacks based on the MAGICC permafrost (Schneider von Deimling et al., 2012), leading to additional cumulative CO_2 emissions of 25 to 88 GtC by 2100, 42 to 378 GtC by 2200 and 51 to 542 GtC by 2300 for the lowest (SSP1-1.9) and highest (SSP5-8.5) scenario, respectively (***Table 2***). Thus, our permafrost module is in line with the IPCC Special Report on 1.5°C warming assumptions for the lowest scenarios (25 GtC versus 27 GtC). While we do not entertain the probabilistic version in this study, our default settings are comparable to the median values reported in Schneider von Deimling (2012). In the highest scenarios (SSP5-8.5), these permafrost related Earth System Feedbacks cause CO_2 concentrations that are up to 200 ppm higher by 2200 (**Figure 3**a). A later study included a more complex offline model with deep carbon deposits, a vertical soil resolution and abrupt thaw processes like thermokarst lake formations. Generally, the results are comparable, although our settings might underestimate 21st century contributions and overestimate long-term cumulative emissions in comparison to Schneider von Deimling (2015).

In addition to elevated CO_2 concentrations, the permafrost module also estimates future CH_4 emissions related to permafrost thawing, i.e. annual emissions of up to 75 $MtCH_4$/yr in the highest SSP5-8.5 scenario by 2200. Cumulatively, 0.34 GtC to 1.07 GtC of carbon are projected to be released as 451 $MtCH_4$ to 1431 $MtCH_4$ over the course of the 21st century across the 9 considered SSP scenarios (Table 2), with even more coming in the 22nd century. The extra emissions lead to 10-240 ppb higher CH_4 concentrations in 2200 (Figure 3b). Most of the carbon decomposition is assumed to happen as aerobic decomposition in the mineral soils, stretching from the more southerly zonal permafrost bands to the higher latitudes from now to 2200 (**Figure 3** e to h).

2.5 Projecting latitudinal gradients

Compared to the previous input datasets for CMIP intercomparisons, which consisted of global-mean values only, latitudinal gradients (and seasonality) are new elements. For the historical period, these latitudinal gradients and seasonally changing surface air concentrations can be estimated from the large set of in situ and flask sampling sites with monthly sampling resolution. Further back in time, when there was insufficient latitudinal coverage, the latitudinal gradient was decomposed into two empirical orthogonal functions (EOFs, the principal components). The multiplier or score (also known as the principal component time series) for the first EOF was regressed against global anthropogenic emissions. Except for CO_2, the score for the second EOF was kept constant. For CO_2, we assumed a simplified approach by both assuming a zero intercept for the regression of global emissions versus the first EOF and a phase-out back in time of the second EOF score. These lead to the simplified and uncertain assumption that the pre-industrial CO_2 gradient was zero (Figure 9b in Meinshausen et al. (2017)). For a more detailed description of the interpolation and assimilation algorithms for the historical data, see Meinshausen et al. (2017).

For the future, there are obviously no observations from which the changes in the latitudinal gradients can be derived. We hence apply the regression procedure from the historical dataset into the future i.e. we project the score of the first EOF of the latitudinal gradient of each greenhouse gas with its global emissions. That makes the simplifying assumption that, in the future, the sources (and sinks) of these gases remain approximately constant in terms of their latitudinal location (not in terms of their magnitude). For CO_2 in the very low emission scenarios, like SSP1-1.9 with net negative CO_2 emissions, that leads to a plausible reversal of the latitudinal gradient if the northern hemisphere is the main location for the natural and anthropogenically induced net CO_2 sink.

There are large natural CH4 emission sources, predominantly in the northern hemisphere. Also, anthropogenic emissions are higher in the northern hemisphere. This largely explains the observed atmospheric concentration gradient: At the end of the historical period (2010 to 2014), CH4 concentrations are 80 ppb above the global average in the Northern mid-latitudes while Southern hemispheric concentrations gently slope towards a minimum of 60 ppb below the global average at the pole (Figure 11b in Meinshausen et al., 2017). As for CO_2, we use anthropogenic CH_4 emissions to

extrapolate the first EOF score into the future. Given that CH_4 emissions do not converge to zero in any scenario, let alone become negative, the strong North-South gradient is maintained in all scenarios.

2.6 Projecting seasonality

Seasonality of concentrations is by far most strongly pronounced for CO_2, given the large seasonal sink (photosynthesis) and source (heterotrophic respiration) pattern of the northern hemispheric terrestrial biomass. Projecting future seasonality changes depends on a correct understanding of the past seasonality changes and how those seasonality changes are related to changes in ecosystem productivity (Forkel et al., 2016;Graven et al., 2013;Welp et al., 2016), increased cropland productivity (Gray et al., 2014) and other factors. Here, we use the net ecosystem productivity (NPP) as a proxy for future seasonality changes and regress the historically derived seasonality change EOF score with modelled future net ecosystem exchange by MAGICC7. NPP in MAGICC7 is projected to increase strongly in the highest SSP5-8.5 scenario, while following a maximum-then-decline pattern in the lower SSP1-1.9 scenario. At the end of the historical period, the total seasonality is derived to have a minimum concentration deviation of -10.1 ppm in Northern mid-latitude August. Given these projected NPP changes in the high SSP5-8.5 scenario, the projected total seasonality increases to approximately twice that by 2100, a projection that comes with a high degree of uncertainty.

For all other gases for which we identified a significant seasonal cycle in the historical observational data, we assume that the relative seasonality (i.e. the magnitude of monthly anomalies relative to the annual mean) stays constant, i.e. that the absolute seasonality concentration changes scale with global-mean concentrations.

2.7 Simplified formula to reflect radiative forcing from CO_2, CH_4 and N_2O

In order to present CO_2, CH_4 and N_2O in our compilation of 43 greenhouse gases and their relative importance for future effective radiative forcings (ERFs), we use simplified radiative forcing formula (for radiative forcing after stratospheric temperature adjustments) that represent the Oslo line-by-line model results – which now takes into account the short-wave absorption of CH_4, among other aspects (Etminan et al., 2016). While Etminan et al. provided simplified formulas for their Oslo line-by-line model results, we here adjust those simplified formulas, resulting in a virtual elimination of the model fit errors by

Etminan of up to 3.6% for CO_2 (see Table 1 in Etminan et al. (2016) and our **Figure 4**d and **Table 3** below). Aside from slight model mis-fits, the original Etminan simplified formula for CO_2 has a validity range of only up to 2000 ppm CO_2 concentrations. Their simplified formula is an adaptation of the classical approach to approximate radiative forcing by $\alpha * ln\left(\frac{C}{C_0}\right)$, where α is a scaling coefficient, C the CO_2 concentration at time t and C_0 the concentration at the reference state, normally the pre-industrial reference value. Etminan et al. introduce the overlap of the absorption spectra between CO_2 and N_2O and also modulate the logarithmic approximation by quadratic and linear terms. When using their suggested coefficients (a_1, b_1 and c_1 in their Table 1), the factor α in front of the $ln\left(\frac{C}{C_0}\right)$ part reaches a maximum at $C_0 - \frac{b_1}{2a_1}$, i.e. at around 1777 ppm, when assuming C_0 as the pre-industrial concentration(277.15 ppm). For CO_2 concentrations beyond 1777 ppm, the alpha value decreases, leading to an unrealistic flattening off above 2000 ppm (and eventual decline well above 3000 ppm). The highest projected SSP concentration (SSP5-8.5) reaches beyond the nominated validity range of 2000 ppm. Hence, we adapt the CO_2 radiative forcing formula to assume a constant α, once α reaches its maximal value (which is around 1808 ppm with our optimised parameter settings – see **Table 3**).

In summary, building on the work of Etminan, our optimised modifications of the simplified radiative forcing expressions for CO_2, CH_4 and N_2O as presented in **Table 3** have the two advantages of (a) representing the 48 Oslo line-by-line model results within rounding errors and also (b) extending its likely validity range in line with previous forcing approximations (and pending examinations by line-by-line models) to higher CO_2 concentrations. However, there is one disadvantage of our simplified formula. While our formula starts from fixed C_0, N_0, and M_0 values at pre-industrial levels, the formulas presented in Etminan cater for the option to set C_0, N_0 and M_0 at any value within the validity range. Hence, our formula would have to be applied twice to calculate the difference in terms of radiative forcing between a C_1, N_1, M_1 and a C_2, N_2, M_2 concentration state, if both are different from pre-industrial levels C_0, N_0 and M_0.

We also take into account new findings regarding rapid adjustments (Smith et al., 2018). In the multi-model analysis by Smith et al. (2018), CO_2 is suggested to have a slightly (~5%) higher effective radiative forcing than its instantaneous radiative forcing after stratospheric temperature adjustments alone, an

adjustment also used here. While the tropospheric rapid adjustments in the case of CO_2 is substantial, it is largely offset by the corresponding water vapour adjustment and the cloud-related rapid adjustments (Figure 3 in Smith et al., 2018). Following Smith et al. (2018), we assume that rapid adjustments largely cancel out for CH_4.

2.8 Data-flow, mean-preserving higher resolutions, and merging with historical files.

In this study's projections, the data is provided in 15° latitudinal bands with monthly resolution. These are constructed from the global-mean time series generated by MAGICC7, with the modulation towards latitudinal annual means by the time-changing latitudinal gradients (section 2.5). These latitudinal annual means are then turned into monthly data values using the latitudinally and monthly resolved seasonality fields.

There are two additional post-processing steps involved. For one, the mean-preserving interpolation routines from Section 2.1.9 of Meinshausen et al. (2017) are used to generate a monthly surface air mole fraction field at a finer 0.5° latitudinal resolution. The other step is merging the projections with the historical concentrations. To ensure a smooth transition from the previously derived historical concentration fields to the ones derived in this study, we use the latitudinally resolved differences in the month of December 2014 between the historical fields derived in Meinshausen et al. (2017) and the raw data produced here. We then add those December 2014 differences to the 2015 future datasets, phasing them out linearly over 12 months.

3 Results

This study's projected greenhouse gas concentrations provide the 'official' greenhouse gas concentrations for the SSP scenarios. They help enable the CMIP6 exercises and span a wide range of possible futures. Below, the results are presented for the various gases. The complete data repository of all projected mole fractions in various data formats, with interactive plots and factsheets is available at http://greenhousegases.science.unimelb.edu.au. The subset of the data recommended for the nine SSPs that are part of the ScenarioMIP and AerChemMIP experiments in netcdf format is also available on https://esgf-node.llnl.gov/search/input4mips/.

3.1 Carbon Dioxide

The projected CO_2 concentrations range from 393 to 1135 ppm in 2100, with the low scenario SSP1-1.9 decreasing to 350 ppm by 2150 (**Figure 5**g). Given the assumption of zero CO_2 emissions in the lower scenarios beyond that, the lower end of the projected CO_2 concentrations is not projected to decrease much further. On the upper end, under the SSP5-8.5 scenario global-average concentrations are projected to increase up to 2200 ppm by 2250 (**Table 4** and **Table 5**, and see also online "GHG factsheets" at greenhousegases.science.unimelb.edu.au). The latitudinal gradient implies a difference of annual-average northern midlatitudes to South pole concentrations of about 6 ppm in current times (**Figure 5**b). As future seasonality is correlated with projected NPP, the CO2 seasonality change pattern (**Figure 5**a.1) is scaled with the a normalized projected NPP (**Figure 5**a.2). Future latitudinal gradients are derived by projecting the first two principal components or EOFs, where the first (dark blue line in **Figure 5**c) is regressed against global emissions – with the implied future scaling factor show in **Figure 5**d (dark blue line). The second EOF (turquoise line in **Figure 5**c) is assumed constant in the future (turquoise line in **Figure 5**d). The applied projection methods result in a continuous projection of CO_2 concentration from the observationally derived historical values, including their latitudinal gradients and seasonality (**Figure 5**h). By approximately 2060, a zero latitudinal gradient is projected in the lowest SSP1-1.9 scenario (**Figure 5**b) because CO_2 emissions revert from positive to net negative. Under the highest SSP5-8.5 scenario, the northern midlatitude to South Pole difference expands to more than 23 ppm by 2100 (not shown in plot, but viewable in online data repository at greenhousegases.science.unimelb.edu.au).

3.2 Methane

Global-mean CH_4 surface air mole fractions across the SSP scenarios are projected to range from 999.7 ppb to 3372 ppb by 2100, with maximal northern hemispheric averages being ~60 ppb higher than the global average (**Table 4**). The largest difference between average Northern and Southern hemispheric concentrations (up to 120 ppb by 2100, **Table 5**) is in the highest CH_4 emissions scenario (SSP3-7.0) and whilst the smallest difference (~70 ppb) is seen in the scenarios with the lowest global CH_4 emissions (SSP1-1.9, SSP1-2.6 and SSP5-3.4OS). While SSP5-8.5 is projected to be the scenario with the highest radiative forcing, because of high CO_2 emissions, SSP5-8.5 is not the highest CH_4 emissions scenario,

with both SSP3-7.0 and SSP4-6.0 suggesting higher total CH_4 emission by 2100 (and in our extensions beyond 2100) (**Figure 2**f).

3.3 Nitrous Oxide

N_2O concentrations are not projected to decrease at any point before 2200, regardless of the SSP scenario we consider. Even under the lowest emissions scenarios, SSP1-1.9 and SSP1-2.6, current global-average concentrations are projected to increase from 328.5 ppb in 2015 to 361 ppb by 2100 (**Table 5**). Under the highest N_2O scenarios (SSP3-7.0 and SSP3-7.0-lowNTCF), concentrations are projected to increase to 422 ppb by 2100 and over 500 ppb by 2500. Both seasonality and the latitudinal gradient is rather subdued for N_2O, as it is both a long-lived greenhouse gas and does not exhibit strong seasonal variability in either sources or sinks.

3.4 Ozone Depleting Substances and other chlorinated substances

As all ozone depleting substances' emissions are assumed to follow a single emission scenario as a result of the Montreal Protocol (Velders and Daniel, 2014b), the SSP concentration scenarios exhibit no substantial variation across their projected concentrations. For example, by 2100, CFC-11 and CFC-12 concentrations are assumed to vary from 51.4 to 56.2 ppt, and from 114.3 ppt to 133.5 ppt, respectively (**Table 4**). These differences across the concentration scenarios are hence not a result of different emission assumptions but solely due to factors that influence the substances' lifetimes. The stratospheric partial lifetime of these substances is affected by a change in the meridional Brewer-Dobson circulation, assumed to strengthen with increasing climate forcing. The tropospheric OH-related partial lifetime is scaled by changing OH concentrations. Those OH concentrations are in turn mainly affected by CH_4 abundances and emissions of other reactive gases (CO, NMVOC, NOx). Overall, the concentrations and radiative forcing contributions of all ozone depleting substances are assumed to strongly reduce until 2100 and beyond, following the phase-out schedules under the Montreal Protocol (**Figure 10**). See section 4.2 for a discussion of the unexpectedly slow declines of CFC-11 (Montzka et al., 2018) and other species, though.

3.5 Other fluorinated greenhouse gases

The fluorinated gas' emissions with a virtually zero ozone depleting potential - HFCs, PFCs, SF_6 and NF_3 - vary across the SSP scenarios. Most SSP scenarios assume strong decreases for several of these substances (e.g. NF_3 and SF_6,), while SSP5-8.5 assumes strong increases for most of the 21st century (**Figure 2**h,i). Until recently, these fluorinated gases were not controlled under the Montreal Protocol. With the 2016 Kigali Amendment, however, a select number of HFCs have been included in the Montreal Protocol and GWP-weighted emissions of these particular HFCs will have to be phased-down globally in coming decades. When aggregating all these non-ozone depleting fluorinated gases into HFC-134a equivalent concentrations, the SSP scenarios project a wide range of 2100 values, ranging from 278 ppt to more than ten-fold that value, i.e. 2985 ppt (last row in **Table 4**). While the HFC projections are derived from the IAM modelling team assumptions regarding the SSPs, several of the resulting HFC projections would exceed the phase-out emission levels agreed to in the Kigali Agreement.

3.6 Radiative forcing since 1750

In this section, we aggregate all 43 greenhouse gases' radiative forcing effect using the updated radiative forcing formula for CO_2, CH_4, and N_2O and standard radiative efficiencies from IPCC AR5 (section 2.7). Across the nine SSP scenarios, it is apparent that CO_2 makes the largest contribution to future warming (blue parts in **Figure 7**), constituting between 68% and 85% of GHG radiative forcing by 2100, and 68% to 92% of radiative forcing by the time of maximum GHG-induced radiative forcing (***Table 6***). In the scenario with the greatest radiative forcing, SSP5-8.5, radiative forcing in 2100 is projected to be approximately 8 W/m^2 and 9.7 W/m^2 for CO_2 or all GHGs, respectively (right-axis bars in **Figure 7**i). This greenhouse gas induced radiative forcing is projected to increase to nearly 13 W/m^2 by 2250 under SSP5-8.5. On the lower side, the SSP1-1.9 scenario exhibits a CO_2 radiative forcing of around 1 W/m^2 in 2150 and beyond, with total greenhouse gas induced forcing stabilising around 1.5 W/m^2 – equivalent to CO_2 concentrations of approximately 370 ppm (right axis in panel a of **Figure 7**).

4 Discussion

In this section, we discuss the SSP greenhouse gas concentration projections in relation to the last 2000 years of observations and cumulative carbon emissions, which are an important metric for mitigation efforts. We also provide a comparison to previous RCP pathways.

4.1 CO_2 and CH_4 concentrations

After CO_2, the greenhouse gas with the second largest radiative forcing contribution in the 21st century is CH_4 (**Figure 7**). To a large extent, greenhouse gas induced future warming is hence influenced by the concentrations of CO_2 and CH_4. Two examples in which methane and CO_2 forcings and their relative strength are important. i: Firstly, discussions about the benefit of the mitigation of short-lived forcers often accounts for CH_4 as a short-lived forcer, which usually contributes most of the climate benefits of any short-lived forcer mitigation strategy (Rogelj et al., 2015;Rogelj et al., 2014). Hence, when the climate benefits of reducing short-lived forcers are compared to those of reducing CO_2 emissions, the actual comparison is mostly between CH_4 and CO_2. Secondly, deriving the remaining carbon budget from Earth System Model runs from single or a few scenario runs is contingent on those scenarios showing a representative level of CH_4 versus CO_2 concentrations. Here, we consider mid-21st century CH_4 and CO_2 concentrations across the range of SSP scenarios. We place them in the context of the RCP scenarios as well as 475 scenarios of the IPCC Special Report on 1.5°C emissions database (https://data.ene.iiasa.ac.at/iamc-1.5c-explorer/) (**Figure 9**). We focus on mid-century concentrations as they are close to the expected point of peak warming in the scenarios that are in line with the Paris Agreement temperature targets of 1.5°C and well below 2.0°C. The comparison shows that SSP1-1.9 and SSP1-2.6 result in relatively similar CH_4 concentrations by 2050, albeit their CO_2 concentrations differ by approximately 7% (437 ppm versus 469 ppm, respectively, **Table 5**). The other scenario with low CH_4 concentrations in 2050, i.e. SSP3-7.0-lowNTCF, falls outside the scenario space considered here, namely the SR.15 database (https://data.ene.iiasa.ac.at/iamc-1.5c-explorer/, see **Figure 9** below). This is by design, as this scenario is the result of adapting a high emission scenario (SSP3-7.0) so that it features very low short-lived climate forcer emissions (Collins et al., 2017). See also Appendix C in Gidden et al. (2019) for a detailed comparison of SSP3-7.0 and SSP3-7.0-lowNTCF emissions. The comparison of mid-century CO_2 and CH_4 concentrations also reveals that the main reason for higher implied warming

of SSP4-3.4 in comparison to SSP1-2.6 are elevated CH_4 concentrations. Thus, to a limited extent, the SSP4-3.4 and SSP1.2.6 scenarios represent a similar pair of scenarios to the SSP3-7.0 and SSP3-7.0-lowNTCF scenarios, but for a lower level of cumulative CO_2 emissions.

4.2 Most recent concentration observations

While updating the historical observations for our future concentrations, several recent trends are noteworthy. We discuss these in this section, covering CH_4, ozone depleting substances CFC-11, CFC-12, CFC-113 as well as HFC-23 and SF_6.

Regarding CH_4, atmospheric observations show a plateauing of CH_4 concentrations from 1999 to 2005 followed by an increased growth rate from 2007 (Nisbet et al., 2016). Available literature suggests that changes in natural and anthropogenic sources and OH-related sinks are involved (Rigby et al., 2017), for example reduced biomass burning emissions (Worden et al., 2017) or reduced thermogenic fossil-fuel related emissions (Schaefer et al., 2016) to explain the plateau of concentrations until 2006, but large uncertainties remain, particularly related to natural wetland and inland water sources (Saunois et al., 2016). Schaefer et al. (2016) suggest that the renewed onset of increasing CH_4 concentrations could be related to increased emissions from the agricultural sector.

Our CH_4 concentration time series, both the historical ones and the future projections from 2015 onwards, capture this observed increase in the trend **Figure 6**b) – although there is uncertainty as to whether the underlying processes and emission sources are correct. Nevertheless, our employed simple model MAGICC7 also captures this temporary plateau of CH_4 concentrations when run in an emission-driven model, possibly not the earlier parts though (left column in Supplementary Figure 1). Note that the transition in 2017 from observationally-driven concentrations to our model-driven concentration timeseries exhibits a slight offset in concentrations (section 5.3), as MAGICC7 inferred a slightly stronger increase in CH_4 concentrations over 2016 based on the IAM's emissions, than observed (**Figure 6**).

For nitrous oxide, there appears to be a small downward adjustment in the growth rate around 2014, with atmospheric growth in years 2016 and 2017 being slightly lower than in 2014 (**Figure 6**c), although observed 2018 growth rates picked up again and the slight offset seems to be well within the noise of recent growth rate variations. For a close comparison of recent observations and our concentration

timeseries, see the CH_4- and nitrous oxide-related factsheets at http://greenhousegases.science.unimelb.edu.au.

Recent observations regarding substances whose production is largely phased out under the Montreal Protocol are also notable (Montzka et al., 2018;Rigby et al., 2019). CFC-11 measurements show some elevated northern hemisphere values from 2013 onward and the global average concentrations are 5-10 ppt above published projections from 2012 to 2017, which consider compliance with projected Montreal Protocol controls, even though the global concentration continues to decline (Velders and Daniel, 2014b) (see panel h in online CFC-11 factsheets at http://greenhousegases.unimelb.edu.au). Our projections reflect the elevated atmospheric concentrations until 2016, but then continue on the assumption of compliance with the Protocol and those additional emission sources to be halted. By analyzing measurement data from sites around the world, it was also concluded that the additional CFC-11 emissions – roughly a 25% increase since 2012– originate in part from the eastern Asian region (Rigby et al., 2019;Montzka et al., 2018), and an updated study has identified that about half of the global increase can be attributed to 2 provinces in eastern China (Rigby et al., 2019). Although less pronounced, CFC-12 and CFC-113 concentrations have also not declined as expected since 2013, although for neither of these gases emissions are thought to have actually increased in recent years, as is the case for CFC-11 (**Figure 10**b). More notable is the diversion of projected and recently observed concentrations for CFC-114, when comparing against the recent Velders and Daniel projections (2014b). For a discussion of recent concentrations of CFC-13, and inferred emissions of CFC-13 (which also seem to increase due to Asian sources) and the two isomers of CFC-114 as well as CFC-115, see Vollmer et al. (2018).

Chloroform ($CHCl_3$) exhibited a concentration decline since 2000 but is increasing again in the global atmosphere (see Chloroform Factsheet available in the online data repository at http://greenhousegases.science.unimelb.edu.au). Fang et al. (2019) point to a recent strong growth of chloroform emissions in China. The similarly short-lived methylene chloride (CH_2Cl_2) also had almost stagnant atmospheric concentrations around the year 2000, but high growth has been observed in subsequent years, almost doubling atmospheric global-average concentrations from around 20 ppt to 40 ppt by 2017 (Hossaini et al., 2015). See also Chapter 1 of the 2018 Ozone Assessment Report (Engel et al., 2018).

Emissions of HFC-23 originate almost completely as a by-product of the production of HCFC-22. Under the Kyoto Protocol, abated emissions of HFC-23 are eligible to be credited in project based offset mechanisms – leading to a bulk of offset credits under the Clean Development Mechanism and also two former Joint Implementation projects in Russia (Schneider, 2011). It has been shown that so-called 'perverse incentives' likely resulted in additional production – in order to broaden the magnitude of claimable abatement credits (Schneider and Kollmuss, 2015). Given that the monetary value of those offsets credits far exceeded the abatement costs, the Kigali Amendment to the Montreal Protocol in October 2016 lead to a new regulatory approach for HFC emissions (Velders et al., 2015). Nevertheless, rather high individual station measurements (classified as "pollution" events) lead to high monthly average concentrations at the Gosan South Korean station. Together with accelerating growth trends for HFC-23 since 2015, this could point to a continued large increase of emissions (see panel h in HFC-23 related factsheets on http://greenhousegases.science.unimelb.edu.au). Similarly, SF_6 concentrations continue to increase at unprecedented rates. They will remain high for a long time (without other anthropogenic interventions) due to SF_6's very long lifetime. The commonly assumed lifetime so far (also assumed in this study) has been 3200 years (Myhre et al., 2013), although recent findings about a loss mechanism in the polar vortex suggest a lower new best estimate of 850 years (Ray et al., 2017).

4.3 The long-term projections in the context of last 2000 years

As the historical compilation of greenhouse gas concentrations based on firn and ice core records indicated, multiple literature studies indicate relatively flat concentration of CO_2, CH_4 and N_2O over the past 2000 years. Historical fluctuations over the last 2000 years of a few ppm or ppb, e.g. around 1650 for CO_2, are miniscule in comparison to recently observed concentration changes since the onset of industrialisation and projected future changes (**Figure 8**). For example, CO_2 concentrations could reach levels beyond 1500 ppm in the SSP3-7.0 and SSP5-8.5 scenarios and even reach beyond 2000pm by 2200 under SSP5-8.5. CO_2 concentrations in excess of 1500ppm have likely not been present on Earth for more than 40 million years ((Fig. 4 in Royer, 2006) – i.e. before the current Antarctic and Northern hemisphere ice sheets formed. Reflecting the shorter lifetime, concentrations of methane decrease noticeably over the 21st century. The stronger mitigation scenarios include net negative emissions for CO_2, so that CO_2 concentrations recede over the long term to around 350ppm in case of the SSP1-1.9 scenario. Reflecting

the longer lifetime and base level of agricultural emissions, N_2O concentrations are not foreseen to drop below current levels in any of the investigated SSP scenarios over the coming 500 years (**Figure 8**).

4.4 Comparing SSP and RCP concentrations

For every generation of climate scenarios, whether these are the IS92, SRES, RCP or now the SSP scenarios, it is pertinent to clarify the differences and similarities of the new scenario set to the previous one(s). In particular due to the unavoidable delay in the analysis and use of the climate projections in the impact communities, clarifying the comparability to previous scenarios is paramount. Here, we compare both the greenhouse gas concentrations and an indication of global climate effects (section **Error! Reference source not found.**).

Four RCP scenarios are now replaced in the SSP generation of scenarios with five "high priority' scenarios (4 ScenarioMIP "Tier1" cases plus SSP1-1.9) in addition to 4 additional scenarios that investigate additional forcing levels (see panels a,c in **Figure 11**). Aside from this difference in the sheer number of scenarios, compared to the RCPs, the actual concentration levels differ substantially for most corresponding SSP scenarios. For example, the SSP5-8.5 scenario features substantially higher CO_2 concentrations by 2100 and beyond than the RCP8.5 scenario (panels a,b in **Figure 11**). Somewhat compensating though, the CH_4 concentrations by 2100 are substantially lower under the SSP5-8.5 scenario compared to the RCP8.5 scenarios (**Figure 11**c), and that difference is even more pronounced by 2300 due to the different extension principles followed for RCP extensions (Meinshausen et al., 2011b) and those for SSPs (section 2.3). Specifically, the SSP5-8.5 fossil and industrial CH_4 emissions are assumed to be phased out by 2250 with land use-related CH_4 emissions kept constant at 2100 under the SSP5-8.5 extension. That contrasts with the RCP8.5 extension, in which a long term CH_4 concentration stabilisation at very high levels of 3500 ppb was implemented. Similarly, for N_2O, the new SSP5-8.5 scenario implies lower concentrations by 2100 and beyond compared to the RCP8.5 (**Figure 11**e,f). Under the SSP family, the SSP3-7.0 becomes the scenario with the highest emissions and concentrations for both CH_4 and N_2O.

On the lower side of the scenarios, the most marked differences are that the new SSP1-2.6 has higher CO_2 concentrations, compared to the previous RCP2.6 and SSP1-1.9 has the lowest CO_2 concentrations

(**Figure 9** and **Figure 11**a). CH_4 concentrations are very similar across these three scenarios by the middle of the century, whereas by the end of the 21st century, the new SSP1-1.9 and SSP1-2.6 scenarios show reduced levels of only 1000 ppb, substantially below today's CH_4 concentration levels. For N_2O, the story is the other way around: SSP1-1.9 and SSP1-2.6 follow almost identical concentration trajectories while the previous RCP2.6 scenario is lower.

When projecting future concentrations under the old RCP emission scenarios, the new calibration choice for the gas cycles of MAGICC (section 2.4) produce increased CO_2, CH_4 and N_2O concentrations compared to the original RCP concentration timeseries, at least for the upper scenarios (**Figure 11**).

4.5 Estimating the effect of latitudinally and seasonally resolved GHG concentrations on surface air temperatures in ESMs

A much-improved assimilation process results from considering seasonally and latitudinally resolved GHG concentration – as individual station monthly mean measurements can easily be "bias" corrected to account for their latitudinal and seasonal variations to inform the global mean. In addition, however, the latitudinally and seasonally resolved GHG concentration data we provide also offers an opportunity to drive Earth System models with more accurate forcings, so that a comparison of the ESM historical runs with observational data can be performed – excluding ESM biases that might result from GHG concentrations that are applied with a globally uniform GHG concentration levels or spatial fields that are sometimes rather dissimilar from observations (Figures S46 and S47 in Supplementary of Meinshausen et al., 2017). In order to test the approximate magnitude of applying either globally uniform ("yearmean-global") or latitudinally and seasonally resolved GHG concentrations ("lat-mon"), we performed 6 historical ensemble members of the CESM1.2.2 model (Hurrell et al., 2013) under each setup. To increase the signal to noise ratio, we then took the averages over the 155 years of model simulations from 1850 to 2005 across the 6 ensembles, resulting in 930 years of model data under each experiment. Given the seasonality of the data, we average the DJF and MAM monthly means in the "lat-mon" experiment and subtract the the reference scenario's "yearmean-global" respective average. In the DJF and MAM northern hemispheric winter and spring season, one would expect a slight positive warming signal in the higher northern latitudes – given the latitudinal gradient of methane concentrations and the seasonally higher CO_2 concentrations. Indeed, we observe a regional warming signal of up to 0.4K over Northern

American and Eurasian land masses, which is – in the DJF season – however latitudinally overcompensated by a strong cooling signal in the North Atlantic (**Figure 12** a). In the MAM season, the slight cooling signal in the North Atlantic does not fully offset the warming over the land-masses (**Figure 12**b), resulting in a latitudinally averaged warming signal of approximately 0.1K poleward of 65 degrees North (**Figure 12**d). Given the high natural variability in the higher latitudes, we consider the significance of this warming signal by comparing our warming signal to corresponding differences of arbitrarily chosen control run segments. From an approximately 4500-yearlong control run for CESM1.2.2 at pre-industrial conditions, we randomly chose hundred pairs of 930-year long segments to compute the variability of the differences. It turns out that our warming signals are within the min-max range of those 100 sample pairs regarding the latitudinally averaged warming differences, indicating that the expected warming signal due to applying latitudinally and seasonally resolved GHG concentration data is not beyond the min-max variability range. However, for the MAM period, there are only a few (approximately 3-5) of the paired control run differences that result in a higher warming signal compared to the "lat-mon" versus "yearmean-global" differences, suggesting that the GHG warming signal is comparable in magnitude to the variability a the 5% confidence level. This is noteworthy, as many detailed processes are included theses days in ESMs at increasing computational costs that would not create a temperature signal of comparably magnitude. In the DJF period, a strong North Atlantic cooling is reducing the latitudinally aggregated warming signal. Whether that North Atlantic cooling is a result of natural variability in our modestly sized 6-member ensembles or whether it is a dynamical response to generally higher latitude forcing (and possible reduced overturning in the North Atlantic thermohaline circulation branch) cannot be detected from our initial ESM runs. As one would expect, our analysis does not suggest significant latitudinal temperature perturbations at the 5% level for the JJA and SON periods (not shown), when seasonally lower CO_2 concentrations are partially offset by the latitudinal gradient of concentrations in the Northern hemisphere.

5 Limitations

In this section, we provide a number of key limitations that come with the SSP concentration datasets. Some of these limitations arise from the underlying emission scenario data (section 5.1 and 5.2), some due to imperfect matches between recent observational and model results (section 5.3), some are intrinsic

model limitations (section 5.4 and 5.5). Likely the largest limitation is that - by design - this study provides default concentration timeseries for the future but does not represent the uncertainty range of future greenhouse gas concentrations for each scenario (section 5.6).

5.1 Limited emission variations across scenarios for gases other than CO_2, CH_4 and N_2O.

The main focus of Integrated Assessment Models rests on projecting sectorally resolved energy, transport, industry, waste, agricultural and landuse emissions for CO_2, CH_4 and N_2O as well as air pollutant emissions. The other industrial greenhouse gases in the basket of gases of the Kyoto Protocol, namely hydrofluorocarbons (HFCs), perfluorocarbons (PFCs), SF_6 and NF_3 are often modelled as a group or in subgroups. Subsequent downscaling mechanisms can then yield individual gas timeseries, although they often lack specific process dynamics, i.e. follow the same growth and decline trajectory independent of their actual end-use applications. This is certainly a limitation of many of the forward-looking PFC projections.

In terms of the ozone-depleting substances (ODS), a feature, or limitation, is that the presented SSP scenarios do not capture baseline or reference scenarios or in fact any emission-driven scenario variation at all. This is because the future ODS emissions are strongly constrained by the Montreal Protocol phase-out schedules. The real-world uncertainty in ODS emissions comes from non-compliance to the Protocol and from uncertainties in emission factors from banks and bank magnitudes. In our study, in which we assume identical emissions in all of our different scenarios, future variations in concentrations are hence purely climate-driven, i.e. illustrate the effect that circulation or atmospheric chemistry changes across the scenarios can have on the ODS lifetimes. It might be worth considering whether, for future assessments, the climate community's scenarios and the ozone community's scenarios could not be commonly designed. For example, some of the scenarios could include ODS emission futures that reflect lower or even non-compliance with the Montreal Protocol to allow studies on the "world avoided" (Morgenstern et al., 2008;Velders et al., 2007). An integration of scenarios used for the Ozone Assessments and the climate assessments may be desirable.

Finally, another limitations is that a few minor long-lived greenhouse gases are not included in this compilation of 43 gases, such as CFC-13 or the isomer CFC-114a (Vollmer et al., 2018).

5.2 Individual scenario features and overall scenario spectrum

Despite all the multi-year design efforts by large research international communities, there are some inevitable limitations of the overall group of scenarios. In particular, the final set of scenarios might be more appropriate for the earth system research community than for those interested in exploring policy relevant outcomes. For example, one of the scenarios that features new characteristic is the SSP5-3.4-OS scenario. That scenario assumes the greatest net negative emissions after an initial high emissions growth rate. Its high-peak-then-strong-decline feature tests the biophysical models and will be pivotal to examine the asymmetry of the ramp-up and ramp-down characteristics of the carbon cycle, ocean heat uptake and multiple other Earth System properties. Yet, for policy purposes, that is substantially outside the target space of the Paris Agreement, aiming to keep temperatures to below 2°C warming.

A possible shortcoming for the climate science and impact community is that the new SSP generation of scenarios does not provide a very closely matching overlap with the RCP scenarios, as multiple scenario features are substantially different (see e.g. CO_2 and CH_4 concentrations in **Figure 9**). Thus, from a climate science perspective, maintaining a single multi-gas scenario unaltered from the previous generation of scenarios could have provided a useful reference point with which to quantify the change in our climate system knowledge for future projections. Given the amount of human and material resources used for the CMIP6 runs, it is however a question of balance between historical comparability and the capability to link to earlier studies and putting resources into the most relevant, up-to-date, scenarios. However, there is also a desire to use the best available forcing data to simulate the historical period. Because the actual historical evolution of concentrations and SLCF emissions has been different in detail from previous scenarios, and historical emission and concentration estimates are updated over time (e.g. Hoesly et al., 2018), the community has thus far decided to use the most up to date data for each subsequent CMIP exercise.

5.3 Transition issues from observational to modelled concentrations.

MAGICC has been calibrated to allow a smooth continuation from historical time series to future projections. For some gases, this transition is possibly suboptimal. For example, atmospheric measurements since 2013 produced some rather high chloroform ($CHCl_3$) concentrations in the northern

hemisphere, which lead to a stronger latitudinal gradient assumption in the assimilation framework for those recent years. The future projections are not reflecting a continuation of this high implied emission spike and hence revert to a lower latitudinal gradient and slightly smaller global-mean chloroform concentrations (see panel f in the Chloroform factsheet available on http://greenhousegases.science.unimelb.edu.au). A similar transition issue is also present for HFC-23, HFC-245fa, HFC-43-10mee, CH_2Cl_2, Halon-1301 and even more pronounced for HFC-32, whose actual global emissions seem to increase much stronger than assumed in the 2020s in our Kigali-aligned emission scenario by Velders et al. (2015).

5.4 Main limitations due to sequential scenario generation process

The sequential and concentration-driven nature of the main ESM CMIP6 experiments poses the challenge that future projections of greenhouse gas concentrations are required before the ESM results can be evaluated. In other words, the best estimate of future CO_2 concentrations, given a certain emission pathway, will certainly differ at the end of the CMIP6 analysis cycle from the setting with which the MAGICC7 climate model was driven with for this study. This sequential problem could only be avoided with an altered experimental design, performing most future ESM experiments in an emission-driven, but computationally more demanding, design. An advantage of the concentration driven runs is that climate feedbacks and carbon cycle feedbacks can more easily be separated.

In addition to the inconsistencies introduced by the sequential and concentration-driven nature of future climate scenario experiments, there are clearly limitations of MAGICC and its chosen default parameter settings for this study. A full evaluation of the extent to which the chosen parameters yield a concentration response that is representative of the higher complexity atmospheric chemistry model projections that are part of CMIP6 will be of key interest for future studies.

5.5 Variable natural emissions.

Except for the interactive carbon cycle, this study assumes constant natural emissions levels for substances like CH_4, N_2O, CH_3Br, CH_3Cl and others. This is clearly a limitation, as under climate change and human management of the land and ocean, the magnitude of these natural emissions (indirectly

influenced by human activities) will change over time. Future research could build knowledge of the time-varying natural emission sources into the projection model used.

5.6 No uncertainty estimates

A major limitation of our study is the lack of uncertainty estimates. Given the primary purpose of this study of providing a single reference concentration projection as input dataset for the CMIP6 experiments, uncertainty ranges around the projections are not necessary. However, in multiple other potential applications of this dataset, properly derived uncertainty information could have opened up new use cases. For example, simple inversion studies could attempt to derive seasonally varying sink and source patterns from our observationally based historical monthly and latitudinally resolved concentration patterns. Without the appropriate uncertainty information, any inversion approach will have to make ad-hoc assumptions.

6 Conclusion

The projected human-induced increase of atmospheric greenhouse gas abundances over the 21st century swamps all observed variations for the last 2000 years (**Figure 8**). The new SSP scenarios span an even broader range of CO_2 concentration futures, with the higher end (SSP5-8.5) yielding higher concentrations than the previous RCP8.5 scenario and the lower end SSP1-1.9 scenario resulting in CO_2 emissions down to 350 ppm in the longer term (2150). Also, in a more technical aspect, the SSP concentrations are breaking new ground. For the first time, the greenhouse gas projections are available for 43 greenhouse gases, with latitudinal and seasonal variations captured. For example, by 2050, Northern hemispheric concentrations in the SSP3-7.0 scenario are 1.2% and 4.3% higher than Southern hemispheric averages for CO_2 and CH_4, respectively - with corresponding non-negligible implications for radiative forcing (**Table 5**).

Given the substantial efforts that go into the data collection by observational network communities, a worthwhile effort in continuation from the present study would be to build a real-time framework to provide a system that updates GHG historical and future projections, including uncertainties, for a wide range of - perhaps also updated - scenarios from the integrated assessment community. While updates of

observations, gas cycle models or emission scenarios in between the major IPCC or WMO Assessments are useful for a range of scientific studies, the new GHG projections data could be frozen every several years to provide a new range of benchmark scenarios for Earth System Models. Efforts to provide more frequent updates for emissions data are also underway (e.g.Hoesly et al., 2018).

More than 20 years ago, the IPCC started to put forward future concentration scenarios, the so-called IS-92 scenarios. Back then in 1992, CO_2 concentrations were at 356 ppm (Keeling et al., 1976;Keeling and Whorf, 2004). In 2019, atmospheric CO_2 concentrations are 411ppm. In equilibrium and assuming a central climate sensitivity of 3°C, these CO_2 concentrations of 411ppm alone would imply a temperature change of 1.7°C above pre-industrial levels (using the simple and standard CO_2 forcing formula of $RF = 5.35 * \ln(C/C_0)$ with C being the current and C_0 being the pre-industrial concentrations). While zero CO_2 emissions would yield decreasing concentrations, it becomes clear that only a future emission trajectory that effectively reduces atmospheric CO_2 concentration levels below today's levels would provide a reasonable chance to keep warming at or below 1.5°C in the longer term. And even such 1.5°C of warming could come with multi-meter sea level rise by 2300 (Mengel et al., 2018) and the likely demise of coral reefs (Frieler et al., 2013). Thus, while the shown scenarios span a scientifically valid wide range of plausible futures, from a climate impact point of view - and trying to achieve the Paris Agreement targets - all except for the lowest scenarios investigated in this study will hopefully remain hypothetical futures.

7 Data Availability

A supplementary data table is available with global and annual mean mole fractions. The complete dataset with latitudinally and monthly resolved data in netcdf format is available via the Earth System Grid Federation (ESGF) servers at https://esgf-node.llnl.gov/search/input4mips/ with a total of 1656 files for source version 1.2.1. The license for all data is Creative Commons Attribution-ShareAlike 4.0 International License (CC BY-SA 4.0). The digital identifiers of the produced datasets, as provided by the ESGF servers are specific to the 9 SSP scenarios: (SSP5-3.4-over: 10.22033/ESGF/input4MIPs.9867; SSP5-8.5: 10.22033/ESGF/input4MIPs.9868; SSP2-4.5: 10.22033/ESGF/input4MIPs.9866; SSP4-3.4: 10.22033/ESGF/input4MIPs.9862; SSP3-7.0: 10.22033/ESGF/input4MIPs.9861; SSP3-7.0-lowNTCF: 10.22033/ESGF/input4MIPs.9824; SSP1-1.9: doi.org/10.22033/ESGF/input4MIPs.9864; SSP1-2.6:

10.22033/ESGF/input4MIPs.9865; SSP4-6.0: 10.22033/ESGF/input4MIPs.9863) Additional data formats, i.e. CSV, XLS, MATLAB .mat files of the same data are also available via http://greenhousegases.science.unimelb.edu.au.

8 Author contributions.

Together with EV, MM designed the study. ZN and MG performed the emission data collation, downscaling and harmonisation steps. MM, EV, and MF build the MATLAB libraries for this project. MF, ZN and MM did the verification of the final data product in comparison to the historical datasets. The new MAGICC parameterisations were developed by MM, ZN, and AJ. MAGICC runs for the concentration projections and postprocessing of the data was performed by MM, ZN, EV, and MF. ZN coordinated the transfer of data to the Input4MIP project. JL, ZN and AN performed the MAGICC temperature and SLR projections. UB setup and performed the CESM1.2.2 runs with CG leading the analysis. GV contributed the future ODS and halogenated emission projections. MM produced the figures with Figure 8 being produced by JL and MM. All authors contributed to writing and commenting on the manuscript.

9 Acknowledgements

We would like to thank the broad community of scientists, lab technicians, research assistants and respective funding agencies that make the observational records of greenhouse gas concentrations possibly, specifically those of the AGAGE and NOAA networks. See Meinshausen et al., 2017 for a detailed acknowledgement. Without those observational records, our ability to project greenhouse gas into the future would not be possible. We also would like to thank the IAM modelling teams, especially the IMAGE, MESSAGE-Globiom, AIM, REMIND-MagPie and GCAM4 teams, who created chosen SSP benchmark emission scenarios underlying this study. The author team thanks for the discussions with the IAM modellers on the design of the SSP extensions, especially Keywan Riahi, Detlef van Vuuren, David Klein and Shinichiro Fujimori. Lastly, the authors acknowledge the web-teams that make the use of the datasets possible. Specifically, we would like to thank Paul Durack for handling the data integration for the ESGF server. Also, we would warmly like to thank Melissa Makin and Usha Nattala and Uli Felzmann

from the Faculty of Science IT team at the University of Melbourne, who made it possible that the full datasets, factsheets and interactive plots of this study are available in a user-accessible fashion on greenhousegases.unimelb.edu.au. A deep thank goes to Christopher Holmes, who helped tremendously in providing data and code to calibrate MAGICC to abundance projections presented in Prather et al. (2012) and Holmes et al. (2013). We thank Keith Shine for very helpful discussions on section 2.7. MM thankfully acknowledges the support by the Australian Research Council Future Fellowship grant FT130100809. This work was undertaken in collaboration with partners in the European Union's Horizon 2020 research and innovation programme CRESCENDO (grant no. 641816), of which the University of Melbourne is an unfunded partner.

10 Tables

Table 1 - Derivation and construction of future CMIP6 mixing ratio fields for the greenhouse gas concentration series from 2015 onwards. Note that in addition to the steps shown below, a post-processing step was implemented to scale any differences in the December 2014 values between the raw future data and the previously submitted historical greenhouse gas concentration data. Those data differences in monthly latitudinal values for Dec 2014 were linearly scaled to zero until Dec 2015 in order to provide for a smooth transition between historical and future datasets (section 2.8). See section 2.1 for a description of how the observational data was updated.

Gas	Time period	Observational data source	Global and annual-mean C_{global}	Seasonality $\hat{S}_{l,m}$	Seasonality Change $\Delta S_{l,m}$	Latitudinal gradient $\hat{L}$
CO_2	2015 - 2016	NOAA ESRL Carbon Cycle Cooperative Global Air Sampling Network, 1968-2016. Version: 2017-07-28 (updated from historical run version: 2015-08-03), monthly station averages (Dlugokencky, 2015b;NOAA ESRL GMD, 2014c, a, b, d)	Calculated based on observational data source as described in Meinshausen et al. (2017)	Mean over 1984-2013 period.	Leading EOF of residuals from observation – extended into future with projected GPP from MAGICC7.0 calibrated carbon cycle to the UVIC C4MIP model (Friedlingstein et al., 2006). (This is a change from the historical GHG methodology, when we used only observational temperature and CO_2 concentrations) .	Two leading EOFs and their scores derived from latitudinal residuals from annual mean values.
	2016 to 2500	n/a	MAGICC7.0 CO_2 global-mean projections driven by harmonized SSP GHG emissions (Gidden et al., 2019) or extended emissions beyond 2100 (section 2.3).			The score for the first EOF is regressed against global annual fossil fuel & industry emissions from SSP scenarios. Score for the second EOF assumed constant in future.
CH_4	2015-2016	AGAGE monthly station means, incl. pollution events ('.mop') (Cunnold et al., 2002) & NOAA	Calculated based on observational data source as described	Mean over 1985-2013 period. Applied as relative	Absolut seasonality changing given that it is applied	Two leading EOFs and their scores derived from latitudinal residuals from annual mean values. The score for the first EOF is regressed against

		ESRL monthly station data (Dlugokencky, 2015a); Version 2017-07-28;	in Meinshausen et al. (2017).	seasonality, i.e. percent deviation from global-mean.	relative to global-mean.	global annual fossil fuel & industry emissions from SSP scenarios. Score for the second EOF assumed constant in future.
	2016-2500	n/a	MAGICC7.0 CH_4 global-mean projections driven by harmonized SSP emissions extended emissions beyond 2100 (section 2.3).			
N_2O	2015 to 2016	AGAGE monthly station means, incl. pollution events (Prinn et al., 1990) (Version Dec 2017) & Combined Nitrous Oxide data (monthly station averages) from the NOAA/ESRL Global Monitoring Division; Version Thu, Jan 25, 2018 1:50:47 PM	Calculated based on observational data source as described in Meinshausen et al. (2017).	Mean over 1985-2013 period. Applied as relative seasonality, i.e. percent deviation from global-mean.	Absolut seasonality changing given that it is applied relative to global-mean.	Two leadings EOFs and their scores derived from latitudinal residuals from annual mean values; The score for the first EOF is regressed against global total N_2O emissions to extrapolate into the future. Score for the second EOF assumed constant in future.
	2016 to 2500	n/a	MAGICC7.0 N_2O global-mean projections driven by harmonized SSP emissions (Gidden et al., 2019) extended emissions beyond 2100 (section 2.3).			
Other greenhouse gases	2015 to 2017	Data input sources as described in Meinshausen (2017) with several data inputs updated to newer versions of the	Calculated based on observational data source as described in Meinshausen et al. (2017).	Depending on the gas, either assumed zero or mean over recent	Either zero or absolute seasonality changing given that it is applied relative to	The leading EOF and its score derived from residuals from observations; with the score for the leading EOF regressed against global total CH_4

		data, namely: AGAGE monthly station means, incl. pollution events (Prinn et al., 2018) (Version Dec 2017); 04-Feb-18 update of NOAA/ESRL/GMD data (Montzka et al., 2015), were appropriate.		historical period, normally 1990-2013, period. See online factsheets at greenhousegases.science.unimelb.edu.au for a gas-to-gas depiction of the seasonality.	global-mean – depending on the gas.	emissions to extrapolate into the future.
	2016/2017 to 2500	n/a	MAGICC7.0 driven by harmonized SSP emissions or WMO (2014) scenario A1 emission projections (with extensions beyond 2100).			

Table 2 - *Cumulative CO_2 and CH_4 emissions from MAGICC's permafrost module under the considered SSPs. The permafrost module has 50 zonal bands, a mineral and peatland soil module and 50 latitudinal zonal bands. See Schneider von Deimling et al. (Schneider von Deimling et al., 2012) for a detailed description. See* **Figure 3** *for timeseries of induced CO_2 and CH_4 atmospheric concentration changes.*

	Time horizon	SSP1-1.9	SSP1-2.6	SSP2-4.5	SSP3-7.0-LowNTCF	SSP3-7.0	SSP4-3.4	SSP4-6.0	SSP5-3.4-OS	SSP5-8.5
Cumulative CO_2 emissions (GtC)	2100	25	31	46	54	65	38	56	48	88
	2200	42	58	121	252	288	78	167	83	378
	2300	51	74	173	410	444	99	248	101	542
Cumulative CH_4 emissions ($MtCH_4$)	2100	451	549	789	919	1,089	670	953	835	1,431
	2200	884	1,231	2,527	5,083	5,911	1,639	3,467	1,744	7,999
	2300	1,177	1,774	4,246	10,505	11,673	2,404	6,170	2,389	15,096

Table 3 - Simplified expressions for radiative forcing relative to pre-industrial (1750) levels by changes of surface air mole fractions of CO_2, CH_4, N_2O – reflecting the Oslo Line-by-line model results. This table can be compared to Table 1 in Etminan et al. (2016), but note that their formulae can be directly applied to any sets of (C, Co), (M, Mo) and (N, No) within the range of fitting, unlike the case here where Co, Mo and No are pre-specified at pre-industrial levels.

Gas	Simplified Expression	Coefficients	Maximal absolute fit error % (Wm^{-2})
CO_2	$C_{\alpha_{max}} = C_0 - \frac{b_1}{2a_1} \approx 1808\, ppm$ $\alpha' = d_1 - \frac{{b_1}^2}{4a_1}, \quad for\ C > C_{\alpha_{max}}$ $\alpha' = d_1 + a_1(C - C_0)^2 + b_1(C - C_0), for\ C_0 < C < C_{\alpha_{max}}$ $\alpha' = d_1, \quad for\ C < C_0$ $\alpha_{N2O} = c_1 * \sqrt{N}$ $RF_{CO_2} = (\alpha' + \alpha_{N2O}) * ln\left(\frac{C}{C_0}\right)$	a_1 = -2.4785e-07 $Wm^{-2}ppm^{-2}$ b_1 =0.00075906 $Wm^{-2}ppm^{-1}$ c_1 = -0.0021492 $Wm^{-2}ppb^{-0.5}$ d_1 = 5.2488 Wm^{-2} C_0 = 277.15 ppm	0.11% (0.0037 Wm^{-2})
N_2O	$RF_{N2O} = \left(a_2\sqrt{C} + b_2\sqrt{N} + c_2\sqrt{M} + d_2\right) * \left(\sqrt{N} - \sqrt{N_0}\right)$	a_2 =-0.00034197 $Wm^{-2}ppm^{-1}$ b_2 = 0.00025455 $Wm^{-2}ppb^{-1}$ c_2 =-0.00024357 $Wm^{-2}ppb^{-1}$ d_2 = 0.12173 $Wm^{-2}ppb^{-0.5}$ N_0 = 273.87 ppb	1.5% (0.0059 Wm^{-2})
CH_4	$RF_{CH_4} = \left(a_3\sqrt{M} + b_3\sqrt{N} + d_3\right) * \left(\sqrt{M} - \sqrt{M_0}\right)$	a_3 =-8.9603e-05 $Wm^{-2}ppb^{-1}$ b_3 = -0.00012462 $Wm^{-2}ppb^{-1}$ d_3 = 0.045194 $Wm^{-2}ppb^{-0.5}$ M_0 = 731.41 ppb	0.55% (0.0032 Wm^{-2})

Table 4 - Overview of future scenario range of individual GHG concentrations. The table indicates the minimum and maximum surface air mole fra
across the 9 SSP scenarios considered in this study. For spreadsheets with annual data tables per scenario, see greenhousegases.science.unimelb.e
The third column indicates the region, with global ('GL'), Northern hemispheric ('NL') and Southern hemispheric ('SH') data shown for CO_2, CH
N_2O. The last three rows provide the equivalence concentrations. The CFC-11-eq concentrations summarize – in terms of radiative forcing equiva
all greenhouse gases aside from CO_2, CH_4, N_2O and CFC-12. The CFC-12-eq concentrations summarize all the ozone depleting substances (
controlled under the Montreal Protocol, while HFC-134a-eq summarizes the remaining fluorinated gases. Altogether CO_2, CH_4, N_2O, CFC-12-e
HFC-134a-eq together represent the radiative forcing of the entirety of the 43 greenhouse gases considered here (cf. Table 5 in Meinshausen et al., 2

GAS	UNIT	REG	2015	2025	2050	2075	2100	2150	2200	2250	2300
CO_2	ppm	GL	399.9	426.5 - 432.4	437.6 - 562.8	419.7 - 801.7	393.5 - 1135.2	349 - 1737.3	343.4 - 2108.3	343.3 - 2206.4	342 - 2161.7
		NH	401.7	428.2 - 434.9	437.8 - 567.2	419.5 - 808.5	392.9 - 1142.3	348.5 - 1742	343.4 - 2110.7	343.3 - 2206.4	342 - 2161.7
		SH	398.2	424.9 - 429.9	437.5 - 558.3	419.9 - 794.9	394.1 - 1128.2	349.5 - 1732.6	343.4 - 2106	343.3 - 2206.3	342 - 2161.7
CH_4	ppb	GL	1841.9	1865.1 - 2049.1	1358.8 - 2503.7	1184.3 - 2934.1	999.7 - 3372.2	961.8 - 3096.2	927.6 - 2571.6	875.2 - 2107.1	864.4 - 1988.1
		NH	1889.7	1910.3 - 2098.2	1400 - 2554.8	1224.3 - 2989.5	1038.8 - 3430.7	1000.6 - 3151.1	966.1 - 2622.8	913.1 - 2154.7	902.4 - 2035.7
		SH	1794.1	1820 - 1999.9	1317.5 - 2452.5	1144.3 - 2878.7	960.6 - 3313.7	922.9 - 3041.3	889.1 - 2520.3	837.2 - 2059.5	826.4 - 1940.5
N_2O	ppb	GL	328.2	334.9 - 336.4	343.5 - 361.9	348.5 - 391	353.9 - 422.4	361.2 - 472.5	363.4 - 498.5	362.2 - 508.7	360 - 512
		NH	328.5	335.1 - 336.7	343.8 - 362.2	348.8 - 391.3	354.2 - 422.7	361.5 - 472.8	363.7 - 498.8	362.5 - 509	360.3 - 512.3
		SH	327.9	334.6 - 336.1	343.2 - 361.6	348.2 - 390.7	353.6 - 422.1	360.9 - 472.2	363.2 - 498.3	361.9 - 508.4	359.7 - 511.8
SF_6	ppt	GL	8.6	11.3 - 11.9	14.3 - 21.7	16.1 - 32.7	17.2 - 43.5	18.5 - 60.7	19.1 - 70.5	19.1 - 73.1	18.8 - 72
NF_3	ppt	GL	1.4	2.3 - 2.5	3.3 - 5.8	3.8 - 9.3	4 - 12.7	4.2 - 17.4	4.1 - 19.2	3.9 - 18.5	3.6 - 16.6
SO_2F_2	ppt	GL	2.1	2.8 - 3	2.4 - 4	1.6 - 4.4	1.1 - 4.1	0.5 - 2.9	0.2 - 1.8	0.1 - 0.8	0 - 0.2
CF_4	ppt	GL	81.8	88.3 - 89.7	96.1 - 106.3	99.2 - 123.2	101.3 - 136	103.8 - 154.6	105.3 - 165.7	105.7 - 169.4	105.6 - 169.2
C_2F_6	ppt	GL	4.5	5.1 - 5.2	5.7 - 6.9	5.8 - 8.6	5.8 - 10	5.8 - 12.2	5.8 - 13.4	5.7 - 13.8	5.7 - 13.7
C_3F_8	ppt	GL	0.6	0.7 - 0.8	0.9 - 1.1	0.9 - 1.5	0.9 - 1.8	0.9 - 2.2	0.9 - 2.5	0.9 - 2.6	0.9 - 2.5
c-C_4F_8	ppt	GL	1.4	1.7 - 1.8	2.1 - 2.6	2.2 - 3.5	2.3 - 4.1	2.4 - 5	2.5 - 5.5	2.5 - 5.6	2.4 - 5.5
C_4F_{10}	ppt	GL	0.2	0.2 - 0.2	0.2 - 0.3	0.2 - 0.3	0.2 - 0.4	0.2 - 0.5	0.2 - 0.5	0.2 - 0.5	0.2 - 0.5
C_5F_{12}	ppt	GL	0.1	0.1 - 0.1	0.1 - 0.2	0.1 - 0.2	0.1 - 0.2	0.1 - 0.2	0.1 - 0.2	0.1 - 0.2	0.1 - 0.2
C_6F_{14}	ppt	GL	0.3	0.3 - 0.4	0.4 - 0.5	0.4 - 0.7	0.4 - 0.8	0.4 - 1	0.4 - 1.1	0.4 - 1.1	0.4 - 1.1
C_7F_{16}	ppt	GL	0.1	0.2 - 0.2	0.2 - 0.3	0.2 - 0.3	0.2 - 0.4	0.2 - 0.5	0.2 - 0.6	0.2 - 0.6	0.2 - 0.6
C_8F_{18}	ppt	GL	0.1	0.1 - 0.1	0.1 - 0.1	0.1 - 0.2	0.1 - 0.2	0.1 - 0.2	0.1 - 0.3	0.1 - 0.3	0.1 - 0.3
HFC-23	ppt	GL	27.9	31.5 - 32	28.7 - 29.9	25.8 - 27	22.8 - 24.1	17.2 - 19.4	12.8 - 16	9.5 - 13.1	7.1 - 10.7

HFC-32	ppt	GL	9.8	6.5 - 7.5	0.1 - 0.7	0 - 0.2	0 - 0	0 - 0	0 - 0	0 - 0	0 - 0
HFC-43-10MEE	ppt	GL	0.3	0.3 - 0.3	0.1 - 0.4	0 - 0.4	0 - 0.4	0 - 0.2	0 - 0.1	0 - 0	0 - 0
HFC-125	ppt	GL	17.8	52.1 - 78.6	49.8 - 371.6	31.5 - 744.8	22.7 - 988.8	14.2 - 809.2	8.5 - 458.2	3.4 - 137	0.8 - 13.7
HFC-134A	ppt	GL	84.8	109.6 - 143.7	36.1 - 239.4	11.4 - 358	6.6 - 423.3	4.4 - 286.9	2.5 - 145.5	0.6 - 24.6	0 - 0.2
HFC-143A	ppt	GL	16.7	36.7 - 50.9	39 - 234.3	29.6 - 509.6	23.7 - 745.9	16.1 - 748.4	10.4 - 500.9	5.4 - 213.3	2.2 - 53.1
HFC-152A	ppt	GL	7.5	4.6 - 8.2	0.2 - 6.5	0.1 - 7.6	0.1 - 6.5	0.1 - 3.8	0 - 1.8	0 - 0.1	0 - 0
HFC-236FA	ppt	GL	0.1	0.2 - 0.3	0.3 - 1.3	0.3 - 3.1	0.3 - 5.3	0.3 - 7.9	0.3 - 8.2	0.2 - 6.7	0.2 - 4.9
HFC-227EA	ppt	GL	1.1	1.8 - 2.4	1.4 - 6.4	0.8 - 9.8	0.5 - 10.9	0.2 - 8.2	0.1 - 4.7	0 - 1.5	0 - 0.2
HFC-245FA	ppt	GL	2.2	3.6 - 5.8	1.1 - 18.4	0.5 - 34.5	0.5 - 39.1	0.4 - 24.5	0.2 - 12.1	0 - 1.3	0 - 0
HFC-365MFC	ppt	GL	0.9	1.2 - 1.6	0.2 - 2.5	0.1 - 3.8	0.1 - 4.3	0 - 2.7	0 - 1.3	0 - 0.2	0 - 0
CCL_4	ppt	GL	82.1	67.4 - 67.4	32.4 - 32.7	13.3 - 13.8	5 - 5.5	0.6 - 0.8	0.1 - 0.1	0 - 0	0 - 0
$CHCL_3$	ppt	GL	10.4	8.8 - 9.7	5.8 - 9.5	5.5 - 9	5.5 - 8.3	5.4 - 7.4	5.4 - 6.4	5.4 - 5.5	5.4 - 5.4
CH_2CL_2	ppt	GL	37.8	24.7 - 46.7	8 - 59.2	7.7 - 86.2	7.8 - 90	7.6 - 63	7.3 - 35.5	7.1 - 8	7.1 - 7.1
CH_3CCL_3	ppt	GL	3.2	0.4 - 0.4	0 - 0	0 - 0	0 - 0	0 - 0	0 - 0	0 - 0	0 - 0
CH_3CL	ppt	GL	549.8	546.5 - 577.6	466.1 - 582.4	425.6 - 566	421.6 - 556.5	418.5 - 536.2	394 - 509.7	363.7 - 479.1	358.2 - 475.9
CH_3BR	ppt	GL	6.7	6.5 - 6.9	5.3 - 6.9	5 - 6.8	4.9 - 6.6	4.7 - 6.3	4.6 - 5.9	4.4 - 5.5	4.4 - 5.5
CFC-11	ppt	GL	231.5	204.4 - 204.4	137.8 - 138.9	86.3 - 89.4	51.4 - 56.2	17.3 - 22.4	5.5 - 8.7	1.7 - 3.4	0.5 - 1.3
CFC-12	ppt	GL	518	471.6 - 471.7	364.3 - 366	277.6 - 283.6	208.7 - 220.2	114.3 - 133.5	61.2 - 81.4	32.5 - 49.6	17.3 - 30.3
CFC-113	ppt	GL	72.1 - 72.1	64.7 - 64.7	48.7 - 48.9	36.1 - 37	26.4 - 28	13.7 - 16.2	6.9 - 9.4	3.5 - 5.5	1.7 - 3.2
CFC-114	ppt	GL	16.3 - 16.3	15.8 - 15.8	13.9 - 13.9	12 - 12.1	10.3 - 10.6	7.5 - 8.1	5.4 - 6.2	3.8 - 4.7	2.7 - 3.6
CFC-115	ppt	GL	8.5 - 8.5	8.8 - 8.8	9.1 - 9.1	9 - 9	8.6 - 8.7	7.7 - 7.9	6.9 - 7.2	6.2 - 6.6	5.5 - 6
HCFC-22	ppt	GL	233.7 - 233.7	237.2 - 241.1	49.9 - 59.5	4.5 - 8.8	0.3 - 1.4	0 - 0	0 - 0	0 - 0	0 - 0
HCFC-141B	ppt	GL	24.2 - 24.2	27.2 - 27.7	14.1 - 16.2	3.5 - 5.2	0.8 - 1.4	0.3 - 0.5	0.2 - 0.3	0 - 0	0 - 0

HCFC-142B	ppt	GL	22.1 - 22.1	21.2 - 21.5	8.7 - 9.8	1.9 - 3	0.4 - 0.9	0 - 0.1	0 - 0	0 - 0	0 - 0
HALON-1211	ppt	GL	3.7 - 3.7	2.6 - 2.6	0.7 - 0.8	0.2 - 0.2	0 - 0	0 - 0	0 - 0	0 - 0	0 - 0
HALON-1301	ppt	GL	3.3 - 3.3	3.3 - 3.3	2.8 - 2.8	2.1 - 2.1	1.5 - 1.6	0.6 - 0.8	0.3 - 0.4	0.1 - 0.2	0 - 0.1
HALON-2402	ppt	GL	0.4 - 0.4	0.4 - 0.4	0.2 - 0.2	0.1 - 0.1	0 - 0	0 - 0	0 - 0	0 - 0	0 - 0
CFC-11-EQ	ppt	GL	818.9 - 818.9	848.9 - 908.6	528.3 - 1102.9	371 - 1599.7	305.6 - 1975	235 - 1698.5	189.8 - 1126.9	155 - 563.5	135.3 - 323.9
CFC-12-EQ	ppt	GL	1047.8 - 1047.9	967.1 - 969	627.8 - 637.9	433 - 444.4	320.6 - 329.5	175.3 - 197.1	99.2 - 124.3	58.4 - 82.2	38.7 - 57.5
HFC-134A-EQ	ppt	GL	271.1 - 271.1	388.3 - 485.4	327.5 - 1259.5	286.2 - 2274	277.9 - 2984.9	254.7 - 2638	223.2 - 1755.3	186.7 - 864	165.4 - 483.5

Table 5 - Overview of CO_2, CH_4 and N_2O concentrations in the eight SSP scenarios considered in this study with global-average ('GL'), No hemispheric ('NH') and Southern hemispheric ('SH') surface air mole fractions. For annual and latitudinally resolved mole fractions and other green gases, see supplementary material or greenhousegases.science.unimelb.edu.au.

SSP1-1.9			2015	2025	2050	2075	2100	2150	2200	2250	2300	2400	2500
CO_2	ppm	GL	399.9	426.5	437.6	419.7	393.5	349.0	343.4	343.3	342.0	339.2	336.9
		NH	401.7	428.2	437.8	419.5	392.9	348.5	343.4	343.3	342.0	339.2	336.9
		SH	398.2	424.9	437.5	419.9	394.1	349.5	343.4	343.3	342.0	339.2	336.9
CH_4	ppb	GL	1,842.0	1,875.2	1,427.9	1,184.3	1,036.4	969.8	928.9	881.3	1,112.0	870.9	871.4
		NH	1,889.7	1,919.9	1,468.8	1,224.3	1,075.6	1,008.6	967.2	919.2	909.6	908.8	909.3
		SH	1,794.2	1,830.6	1,387.0	1,144.3	997.2	931.1	890.5	843.4	833.8	833.0	833.5
N_2O	ppb	GL	328.2	335.1	343.6	349.0	354.0	361.4	363.9	362.7	360.6	358.2	357.1
		NH	328.5	335.4	343.8	349.3	354.3	361.7	364.2	363.0	360.9	358.5	357.4
		SH	327.9	334.8	343.3	348.7	353.7	361.2	363.6	362.4	360.3	357.9	356.8
SSP1-2.6			**2015**	**2025**	**2050**	**2075**	**2100**	**2150**	**2200**	**2250**	**2300**	**2400**	**2500**
CO_2	ppm	GL	399.9	427.7	469.3	471.0	445.6	411.1	403.2	399.7	396.0	389.5	384.3
		NH	401.7	429.6	470.4	471.2	445.3	410.9	403.2	399.7	396.0	389.5	384.3
		SH	398.2	425.7	468.2	470.8	445.9	411.4	403.2	399.7	396.0	389.4	384.3
CH_4	ppb	GL	1,842.0	1,865.1	1,519.4	1,248.4	1,056.4	977.4	927.6	875.2	1,112.0	863.5	864.0
		NH	1,889.7	1,910.3	1,561.5	1,288.8	1,095.9	1,016.4	966.1	913.1	902.4	901.5	901.9
		SH	1,794.2	1,820.0	1,477.3	1,208.0	1,016.9	938.4	889.1	837.2	826.4	825.6	826.0
N_2O	ppb	GL	328.2	334.9	343.5	348.5	353.9	361.2	363.4	362.2	360.0	357.5	356.4
		NH	328.5	335.1	343.8	348.8	354.2	361.5	363.7	362.5	360.3	357.8	356.7
		SH	327.9	334.6	343.2	348.2	353.6	360.9	363.2	361.9	359.7	357.2	356.1
SSP2-4.5			**2015**	**2025**	**2050**	**2075**	**2100**	**2150**	**2200**	**2250**	**2300**	**2400**	**2500**
CO_2	ppm	GL	399.9	429.0	506.9	575.5	602.8	626.3	643.1	637.0	621.3	597.8	579.2
		NH	401.7	431.2	509.2	577.3	603.6	626.8	643.4	637.0	621.3	597.8	579.2
		SH	398.2	426.9	504.5	573.6	602.0	625.7	642.8	637.0	621.3	597.8	579.2
CH_4	ppb	GL	1,841.9	1,960.7	2,020.2	1,815.7	1,683.2	1,479.6	1,255.4	1,038.1	1,112.0	999.2	997.3
		NH	1,889.7	2,008.0	2,066.6	1,860.7	1,727.7	1,522.4	1,296.6	1,077.6	1,040.9	1,038.7	1,036.8

		SH	1,794.2	1,913.3	1,973.9	1,770.8	1,638.6	1,436.7	1,214.2	998.6	961.8	959.7	957.8
N_2O	ppb	GL	328.2	336.0	356.2	371.5	377.3	378.3	375.9	371.4	367.0	362.0	359.8
		NH	328.5	336.3	356.5	371.8	377.6	378.6	376.2	371.7	367.2	362.3	360.1
		SH	327.9	335.7	355.9	371.2	377.0	378.0	375.6	371.1	366.7	361.7	359.5
SSP3-7.0			**2015**	**2025**	**2050**	**2075**	**2100**	**2150**	**2200**	**2250**	**2300**	**2400**	**2500**
CO_2	ppm	GL	399.9	432.3	540.6	683.0	867.2	1,235.3	1,456.8	1,513.7	1,482.8	1,423.6	1,371.1
		NH	401.7	434.8	543.9	686.8	871.6	1,238.3	1,458.3	1,513.7	1,482.8	1,423.6	1,371.1
		SH	398.2	429.9	537.3	679.2	862.8	1,232.4	1,455.3	1,513.6	1,482.7	1,423.6	1,371.1
CH_4	ppb	GL	1,841.9	2,006.5	2,472.0	2,934.1	3,372.2	3,096.2	2,571.6	2,107.1	1,112.0	1,959.1	1,938.4
		NH	1,889.7	2,055.4	2,524.2	2,989.5	3,430.7	3,151.1	2,622.8	2,154.7	2,035.7	2,006.7	1,986.0
		SH	1,794.2	1,957.7	2,419.8	2,878.7	3,313.7	3,041.3	2,520.3	2,059.5	1,940.5	1,911.5	1,890.8
N_2O	ppb	GL	328.2	336.4	361.8	390.7	421.8	471.4	497.2	507.2	510.5	514.3	516.0
		NH	328.5	336.7	362.1	391.0	422.1	471.7	497.4	507.5	510.8	514.6	516.3
		SH	327.9	336.1	361.5	390.4	421.5	471.1	496.9	506.9	510.2	514.0	515.7
SSP3-7.0-lowNTCF			**2015**	**2025**	**2050**	**2075**	**2100**	**2150**	**2200**	**2250**	**2300**	**2400**	**2500**
CO_2	ppm	GL	399.9	432.4	538.8	677.5	858.7	1,221.5	1,447.2	1,509.7	1,482.8	1,426.1	1,374.1
		NH	401.7	434.9	542.2	681.4	863.2	1,224.6	1,448.7	1,509.7	1,482.8	1,426.1	1,374.1
		SH	398.2	429.9	535.5	673.5	854.1	1,218.5	1,445.7	1,509.7	1,482.7	1,426.1	1,374.1
CH_4	ppb	GL	1,841.9	1,940.3	1,358.8	1,202.5	1,219.9	1,203.5	1,164.6	1,129.1	1,112.0	1,088.0	1,068.8
		NH	1,889.7	1,985.6	1,400.0	1,244.0	1,262.1	1,245.3	1,205.9	1,170.1	1,152.9	1,129.0	1,109.8
		SH	1,794.2	1,895.0	1,317.5	1,161.0	1,177.8	1,161.8	1,123.2	1,088.2	1,071.0	1,047.1	1,027.9
N_2O	ppb	GL	328.2	336.4	361.9	391.0	422.4	472.5	498.5	508.7	512.0	515.8	517.5
		NH	328.5	336.7	362.2	391.3	422.7	472.8	498.8	509.0	512.3	516.1	517.8
		SH	327.9	336.1	361.6	390.7	422.1	472.2	498.3	508.4	511.8	515.5	517.2
SSP4-3.4			**2015**	**2025**	**2050**	**2075**	**2100**	**2150**	**2200**	**2250**	**2300**	**2400**	**2500**

CO_2	ppm	GL	399.9	427.3	472.9	490.2	473.4	408.8	396.2	395.2	392.4	387.5	383.4
		NH	401.7	429.3	474.0	490.3	472.5	408.0	396.2	395.2	392.4	387.5	383.4
		SH	398.2	425.3	471.8	490.1	474.3	409.5	396.2	395.2	392.4	387.5	383.4
CH_4	ppb	GL	1,841.9	2,030.9	2,223.4	2,370.0	2,336.3	2,177.6	2,023.8	1,842.7	1,112.0	1,786.8	1,786.2
		NH	1,889.7	2,078.9	2,271.3	2,417.9	2,383.2	2,223.4	2,068.6	1,886.6	1,832.2	1,830.7	1,830.1
		SH	1,794.1	1,983.0	2,175.4	2,322.2	2,289.5	2,131.7	1,978.9	1,798.8	1,744.5	1,743.0	1,742.3
N_2O	ppb	GL	328.2	335.7	353.9	373.7	394.7	425.2	441.1	446.8	448.2	449.9	450.7
		NH	328.5	336.0	354.2	374.0	395.0	425.5	441.3	447.1	448.5	450.2	451.0
		SH	327.9	335.4	353.6	373.4	394.4	424.9	440.8	446.5	447.9	449.6	450.4
SSP4-6.0			**2015**	**2025**	**2050**	**2075**	**2100**	**2150**	**2200**	**2250**	**2300**	**2400**	**2500**
CO_2	ppm	GL	399.9	428.3	515.6	606.9	668.4	741.0	783.9	786.2	768.7	739.1	714.0
		NH	401.7	430.5	518.2	609.2	669.7	741.8	784.3	786.2	768.7	739.1	714.0
		SH	398.2	426.0	513.0	604.7	667.1	740.1	783.4	786.2	768.7	739.1	714.0
CH_4	ppb	GL	1,841.9	2,049.1	2,503.7	2,688.5	2,645.5	2,382.6	2,111.4	1,864.6	1,112.0	1,791.0	1,785.6
		NH	1,889.7	2,098.2	2,554.8	2,739.6	2,695.8	2,431.2	2,158.3	1,909.8	1,844.7	1,836.3	1,830.9
		SH	1,794.1	1,999.9	2,452.5	2,637.3	2,595.3	2,334.1	2,064.4	1,819.3	1,754.1	1,745.7	1,740.4
N_2O	ppb	GL	328.2	335.9	359.7	383.4	404.7	435.8	451.2	456.1	456.8	457.7	458.1
		NH	328.5	336.2	360.0	383.7	405.0	436.1	451.4	456.4	457.1	457.9	458.4
		SH	327.9	335.6	359.4	383.2	404.4	435.5	450.9	455.8	456.5	457.4	457.8
SSP5-3.4-OS			**2015**	**2025**	**2050**	**2075**	**2100**	**2150**	**2200**	**2250**	**2300**	**2400**	**2500**
CO_2	ppm	GL	399.9	432.2	549.3	554.5	496.6	409.4	404.7	401.8	398.5	392.4	387.5
		NH	401.7	434.7	551.9	553.8	495.6	408.7	404.7	401.8	398.5	392.4	387.5
		SH	398.2	429.7	546.7	555.1	497.7	410.1	404.7	401.8	398.5	392.4	387.5
CH_4	ppb	GL	1,841.9	1,964.3	2,125.1	1,205.4	999.7	961.8	941.9	916.8	1,112.0	910.5	910.6
		NH	1,889.7	2,012.6	2,168.8	1,245.2	1,038.8	1,000.6	980.5	955.2	950.1	948.9	948.9
		SH	1,794.2	1,916.0	2,081.4	1,165.5	960.6	922.9	903.3	878.5	873.4	872.2	872.2
N_2O	ppb	GL	328.2	336.3	356.3	371.1	383.8	398.4	404.7	405.1	403.6	401.9	401.1
		NH	328.5	336.6	356.6	371.4	384.1	398.7	405.0	405.4	403.9	402.1	401.4
		SH	327.9	336.0	356.1	370.8	383.6	398.1	404.4	404.8	403.3	401.6	400.8

SSP5-8.5			2015	2025	2050	2075	2100	2150	2200	2250	2300	2400	2500
CO_2	ppm	GL	399.9	431.8	562.8	801.7	1,135.2	1,737.3	2,108.3	2,206.4	2,161.7	2,080.5	2,010.0
		NH	401.7	434.3	567.2	808.5	1,142.3	1,742.0	2,110.7	2,206.4	2,161.7	2,080.5	2,010.0
		SH	398.2	429.4	558.3	794.9	1,128.2	1,732.6	2,106.0	2,206.3	2,161.7	2,080.5	2,010.0
CH_4	ppb	GL	1,841.9	1,954.5	2,446.5	2,672.3	2,415.3	1,906.9	1,515.6	1,157.3	1,112.0	1,038.5	1,019.0
		NH	1,889.7	2,002.6	2,499.2	2,724.9	2,465.2	1,953.8	1,559.4	1,198.1	1,109.0	1,079.3	1,059.8
		SH	1,794.2	1,906.4	2,393.7	2,619.6	2,365.5	1,860.1	1,471.8	1,116.5	1,027.4	997.7	978.2
N_2O	ppb	GL	328.2	336.3	358.2	377.1	391.8	407.8	413.6	413.0	410.5	407.8	406.6
		NH	328.5	336.6	358.5	377.4	392.1	408.1	413.9	413.3	410.8	408.1	406.9
		SH	327.9	336.0	357.9	376.8	391.5	407.5	413.3	412.7	410.2	407.5	406.3

)4

995
996

997 ***Table 6 -*** Fraction of greenhouse gas induced forcing due to CO_2 concentrations in SSP scenarios at the point of maximal greenhouse gas
998 induced forcing until 2300 (upper row) or in year 2100 (lower row)

	SSP1-1.9	SSP1-2.6	SSP4-3.4	SSP2-4.5	SSP4-6.0	SSP3-7.0	SSP5-8.5	SSP3-7.0-lowntcf	SSP5-3.4-OS
Point of maximal GHG forcing over 2000 to 2300	68%	74%	70%	83%	81%	86%	92%	90%	75%
2100	76%	80%	68%	79%	76%	77%	82%	85%	82%

999

000

Table 7 - SSP Global Mean Surface Air Temperature (GMSAT) and Global Mean Sea Level Rise (GMSLR) projections for the end of the 21st century (2081-2100 average and 2100 estimate) and 2300. GMSAT is shown in Kelvin relative to 1750, GMSLR is shown in metres relative to the 1986-2005 average. Mean and 5th to 95th percentiles are provided for both variables.

	GMT in K			GMSLR in m		
	2081-2100	2100	2300	2081-2100	2100	2300
SSP1-1.9	1.2 (0.6 to 1.8)	1.1 (0.6 to 1.8)	0.6 (0.1 to 1.3)	0.44 (0.30 to 0.62)	0.47 (0.32 to 0.65)	0.80 (0.54 to 1.19)
SSP1-2.6	1.6 (1.0 to 2.4)	1.6 (0.9 to 2.4)	1.3 (0.6 to 2.4)	0.49 (0.35 to 0.69)	0.53 (0.37 to 0.73)	1.07 (0.69 to 1.60)
SSP2-4.5	2.6 (1.7 to 3.8)	2.8 (1.8 to 4.1)	3.8 (1.7 to 6.7)	0.59 (0.41 to 0.82)	0.66 (0.46 to 0.89)	2.02 (1.13 to 3.12)
SSP4-3.4	2.0 (1.3 to 3.1)	2.1 (1.3 to 3.2)	1.8 (0.9 to 3.3)	0.53 (0.36 to 0.75)	0.58 (0.40 to 0.81)	1.30 (0.82 to 1.98)
SSP3-7.0	3.8 (2.6 to 5.7)	4.4 (3.0 to 6.5)	9.8 (5.5 to >15**)	0.68 (0.47 to 0.95)	0.79 (0.56 to 1.07)	4.51 (2.36 to 8.51)
SSP3-LowNTCF	3.4 (2.3 to 5.1)	3.9 (2.6 to 5.8)	9.5 (5.3 to >15**)	0.64 (0.45 to 0.89)	0.74 (0.53 to 1.00)	4.22 (2.22 to 7.63)
SSP4-6.0	3.3 (2.2 to 4.9)	3.6 (2.4 to 5.3)	6.0 (2.9 to 10.8)	0.65 (0.45 to 0.90)	0.74 (0.53 to 1.00)	2.87 (1.53 to 4.72)
SSP5-3.4-OS	2.1 (1.2 to 3.1)	1.9 (1.1 to 3.0)	1.1 (0.3 to 2.3)	0.58 (0.40 to 0.81)	0.62 (0.42 to 0.87)	1.08 (0.66 to 1.68)
SSP5-8.5	5.0 (3.3 to 7.6)	5.8 (3.8 to 8.6)	10.8 (6.4 to >15**)	0.79 (0.54 to 1.13)	0.94 (0.66 to 1.29)	5.31 (2.86 to 10.31)

** MAGICC has an internal cutoff temperature in each land-ocean and hemispheric box at 25K. Any temperatures indications beyond 10K should be considered illustrative only given that the calibrated range of MAGICC covers only lower temperature levels.

11 Figures Captions

Figure 1 - The SSP scenarios and their five socio-economic SSP families. Shown are illustrative temperature levels relative to pre-industrial levels with historical temperatures (front band), current (2020) temperatures (small block in middle) and the branching of the respective scenarios over the 21st century along the five different socio-economic families. The small black horizontal bars on the 2100 pillars for each SSP indicate illustrative temperature levels (obtained by the MAGICC7.0 default setting used to produce the GHG concentrations) for the range of SSP scenarios that were available from the IAM community at the time of creating the benchmark SSP scenarios. The more opaque bands over the 21st century indicate the five SSP scenarios SSP1-1.9, SSP1-2.6, SSP2-4.5, SSP3-7.0 and SSP5-8.5 that are used as priority scenarios in IPCC. The more transparent bands indicate the remaining "Tier 2" SSP scenarios, namely SSP3-7.0-LowNTCF (used in AerChemMIP), SSP4-3.4, SSP4-6.0, and SSP5-3.4-OS. Also shown is a blue indicative bar on the right side, indicating the effect of mitigation action, which reduces temperature levels in 2100 and throughout the 21st century - depending on the respective reference scenario and level of mitigation.

Figure 2 - The anthropogenic emission scenarios to derive SSP concentration scenarios for CO_2 (panels a-c), CH_4 (d to e), nitrous oxide (f), NF_3 (g) and SF_6 (panel i). Shown are the four SSP scenarios for which long-term CMIP6 model experiments are planned (bold lines with color-box labels), namely for SSP5-8.5 (red), SSP5-34-OS (orange), SSP1-2.6 (blue) and SSP1-1.9 (turquoise). Also shown are RCP extensions (Meinshausen et al., 2011b), and those of other SSP scenarios following the same design principles (see text). While the design principles for CO_2 emissions are specific, other gases from fossil and industrial sources are assumed to be phased out by 2225, and landuse-related emissions are assumed to stay constant at their 2100 values. The pre-2100 emission scenarios are derived from harmonised Integrated assessment scenarios, while the post-2100 extensions follow simple extension assumptions.

Figure 3 - The assumed permafrost related emissions by using MAGICC's permafrost module in its default settings for the SSP GHG concentration projections, close to the median of the probabilistic MAGICC permafrost version (Schneider von Deimling et al., 2012). In

the highest scenario, SSP5-8.5, CO_2 and CH_4 concentrations by 2300 would have been about 250 ppm and 150 ppb, respectively, lower without including the permafrost module (panel a and b). The additional CO_2 from mineral soil and peatland carbon decomposition reach a maximum in the highest scenario SSP5-8.5 around 2140 of about 3 GtC emissions per year (panel c), mainly due to the aerobic mineral soil decomposition (panel e). The mineral and peatland soil decomposition under aerobic conditions (panels e and g, respectively), and also the oxidised part of the methane that originates from the anaerobic decomposition (panels f and h) contribute to the net CO_2 emissions from permafrost thawing. The permafrost zonal bands are a simplified approach to represent the range of thawing thresholds and permafrost carbon contents and are described in Schneider von Deimling et al. (2012). See ***Table 2*** for cumulative emissions.

Figure 4 - Simplified parameterisation to emulate 48 Oslo Line by line model results (bright blue open numbered circles). Shown are the IPCC TAR simplified formula for CO_2 (three options), CH_4 and N_2O forcing with their default parameter settings (grey-blue lines) in the background. The simplified formula results by Etminan (2016) are shown as orange lines. Adjusting pre-industrial concentration values to default 1750 values improves the fit of the Etminan simplified formula (red lines in panels a to c and red error terms in panel d). This study's simplified formula results are shown in green, matching the Oslo-line-by-line model results within rounding – and continuing a forcing approximation beyond 2000 ppm CO_2 in line with previously derived formulas (red dashed circle in panel a). See text.

Figure 5 - CO_2 concentrations under the SSP1-1.9 scenario. The base seasonality pattern derived from historical observations with monthly and 15° latitudinal resolution (panel a) is modulated over time using the first EOF of the residuals (panel a.1), scaled with projected NPP into the future (panel a.2). The latitudinal gradient is assumed flat in pre-industrial times, with latitudinal gradients over the observational record being derived from historical observations – and here compared with CMIP5 ESM models – see Meinshausen et al. (2017) (panel b). The projection of the latitudinal gradient uses global total CO_2 emissions regressed against the score (dark blue line in panel d) of the first latitudinal EOF (dark blue line in panel c). The principal component's score of the second EOF's is assumed zero in the future (turquoise line in panel c,d). Resulting surface air mole fractions fields show a return to current CO_2 (~2019) concentrations by the end of the 21st century (panel e and f). Historical NOAA surface flask station datasets (grey dots in panels f, g, h with station indicators provided in legend of panel f) are used for these future projections beyond the end of 2014 reach of the historical dataset (grey shaded background

in panels f, g, h). Various comparison datasets shown, namely the WDCGG timeseries (Tsutsumi et al., 2009), the NOAA Marine Boundary Layer (MBL) product (https://www.esrl.noaa.gov/gmd/ccgg/mbl/) and the NASA AQUA satellite data (ftp://acdisc.gsfc.nasa.gov/ftp/data/s4pa/Aqua_AIRS_Level3/AIRX3C2M.005/), the Petrenko timeseries (made available in the supplement to Buizert et al. (2012). Also shown are the MAGICC global-mean projections (bright blue line "MAGICCconc"). These overview figures are available for all 43 gases and all 9 scenarios on greenhousegases.science.unimelb.edu.au as a total of 387 so-called factsheets. See also Table 12 in Meinshausen (2017) for a description of all data labels.

Figure 6 - Transition between historical runs and future SSP concentrations for CO_2 (panel a), CH_4 (panel b) and N_2O (panel c) surface mole fractions. The observational in situ and flask station datapoints reach into the first years of the future SSP datasets (grey dots). Derived northern-hemispheric (orange), global (black) and Southern hemispheric averages (blue) are shown with annual averages (thick lines) and monthly averages (thin lines with seasonality variability). On the right axis side, the illustrative arrows indicate the min-max range across the scenarios for Northern hemispheric, global and Southern hemispheric annual-average concentrations by 2030 across all 9 SSP scenarios. The NOAA/AGAGE global mean dataseries are shown in green. For description of labels of other comparison data, see Table 12 in Meinshausen (2017).

Figure 7 - Overview of all greenhouse gases within SSP scenarios and their relative importance in terms of radiative forcing. The radiative forcing contributions are stacked, starting with CO_2 (blue shaded area) at the bottom, followed by methane (CH_4), nitrous oxide (N_2O) and the other 40 greenhouse gases. Default radiative forcing efficiencies or parameterisations are used, with CO_2, CH_4 and N_2O being based on a parameterisation of the Oslo-line-by-line model (section 2.7). Seasonal and latitudinal variation is indicated by the three bars on the right of each panel for the global average, northern hemispheric and southern hemispheric monthly mean concentrations for the year 2100. The light-blue shaded areas on the left side of each panel from 1750 to 2014 are based on historical greenhouse gas observations, the 21st century span from 2015 to 2100 (white area) and the extension until 2300 and beyond is based on the MAGICC7.0 model. For the IPCC

AR6, the five scenarios SSP1-1.9 (panel a), SSP1-2.6 (b), SSP2-4.5 (d), SSP3-7.0 (g) and SSP5-8.5 (i) are chosen as key scenarios for knowledge integration across chapters and Working Groups.

Figure 8 - Overview of SSP concentrations of CO_2, CH_4 and N_2O in the context of the historical observational dataset. For the respective main ice core and firn datasets (WAIS, Law Dome, EPICA DML etc.), please see Figure 6b in Meinshausen et al. (2017). The 21st century is shown as grey vertical band.

Figure 9 – The 2050 CO_2 and CH_4 concentrations of SSPs (dark blue circles), RCP (orange circles) and scenarios of the IPCC Special Report on 1.5C warming database (grey dots). All scenarios' concentrations were derived by using the SSP or RCP or SR1.5 harmonised emission scenarios together with the same MAGICC7.0 default settings as used for the CMIP6 SSP concentration projections.

Figure 10 - Atmospheric surface air mole fractions of four CFCs, namely CFC-12 (panel a), CFC-11 (panel b), CFC-113 (panel c) and CFC-114 (panel c). This study's Northern hemispheric averages (orange lines), Southern hemispheric averages (blue lines) and global averages (black lines) are shown in comparison with recent measurements of the NOAA and/or AGAGE networks (grey dots), the global averages derived by Montzka et al. (2018) and the projections by Velders and Daniel (2014b) (dashed lines with diamond markers). The latter can be seen as near-lifetime limited projections whereas observations hint to recent (since 2012) emissions increases , leading to a slower-than-projected fall in global atmospheric concentrations. For an exploration of CFC-11's decline rates, see the recent studies by Montzka et al. (2018) and Rigby et al. (2019). Note that the high "outlier" monthly mean values for CFC-11 and CFC-114 are primarily from the AGAGE Gosan station and include all data, i.e., so-called "pollution" events in which case temporary high concentration air masses pass the measurement station. The apparent disappearance of those high pollution events at the end of 2015 is due to that particular AGAGE data timeseries only having been available until then at the point of this analysis, although a recent publication (Rigby et al., 2019) shows that these enhancements continued at least through 2017.

Figure 11 - Overview of SSP concentrations in comparison with RCP concentrations for CO_2, CH_4 and N_2O. The original RCP scenarios are shown in thicker black lines and various linestyles. Applying the new MAGICC7 default setting used for the SSP scenarios to the RCP emissions results in generally higher concentrations (grey lines).

Figure 12 - Warming signal induced by latitudinally and seasonally resolved GHG concentrations ("lat_mon") compared to an annually and global-mean uniform GHG concentrations ("yearmean_global") in an Earth System Model, namely CESM1.2.2 (Hurrell et al., 2013). We averaged the full historical scenario from 1850 to 2005 across all 6 ensemble members in each setup ("lat_mon" and "yearmean_global") and produced the averages for the December-January-February DJF average (panel a) and the March-April-May averages (b). The latitudinally averaged warming signals that result from using spatially and temporarily resolved GHG concentrations are shown in the lower panels (thick blue lines), here compared against comparable one hundred differenced pairs of 930-year long control run segments (thin grey lines). In the high upper North during the MAM season, the comparison with control run segment differences suggest that these ESM model results show a significant warming at the 5% level, given that only 3 to 5 of the 100 control run differences are higher.

12 References

Buizert, C., Martinerie, P., Petrenko, V. V., Severinghaus, J. P., Trudinger, C. M., Witrant, E., Rosen, J. L., Orsi, A. J., Rubino, M., Etheridge, D. M., Steele, L. P., Hogan, C., Laube, J. C., Sturges, W. T., Levchenko, V. A., Smith, A. M., Levin, I., Conway, T. J., Dlugokencky, E. J., Lang, P. M., Kawamura, K., Jenk, T. M., White, J. W. C., Sowers, T., Schwander, J., and Blunier, T.: Gas transport in firn: multiple-tracer characterisation and model intercomparison for NEEM, Northern Greenland, Atmos. Chem. Phys., 12, 4259-4277, 10.5194/acp-12-4259-2012, 2012.

Butchart, N., and Scaife, A. A.: Removal of chlorofluorocarbons by increased mass exchange between the stratosphere and troposphere in a changing climate, Nature, 410, 799-802, 2001.

Collins, W. J., Lamarque, J. F., Schulz, M., Boucher, O., Eyring, V., Hegglin, M. I., Maycock, A., Myhre, G., Prather, M., Shindell, D., and Smith, S. J.: AerChemMIP: quantifying the effects of chemistry and aerosols in CMIP6, Geosci. Model Dev., 10, 585-607, 10.5194/gmd-10-585-2017, 2017.

Cunnold, D., Steele, L., Fraser, P., Simmonds, P., Prinn, R., Weiss, R., Porter, L., O'Doherty, S., Langenfelds, R., and Krummel, P.: In situ measurements of atmospheric methane at GAGE/AGAGE sites during 1985–2000 and resulting source inferences, Journal of Geophysical Research: Atmospheres, 107, 2002.

Dlugokencky, E. J., P.M. Lang, A.M. Crotwell, K.A. Masarie, and M.J. Crotwell: Atmospheric Methane Dry Air Mole Fractions from the NOAA ESRL Carbon Cycle Cooperative Global Air Sampling Network, 1983-2014. NOAA (Ed.), 2015a.

Dlugokencky, E. J., P.M. Lang, K.A. Masarie, A.M. Crotwell, M.J. Crotwell: Atmospheric Carbon Dioxide Dry Air Mole Fractions from the NOAA ESRL Carbon Cycle Cooperative Global Air Sampling Network, 1968-2014. NOAA (Ed.), 2015b.

Durack, P. J., and Taylor, K.: CMIP6 Forcing datasets summary, http://goo.gl/r8up31, 46, 2019.

Ehhalt, D., Prather, M. J., Dentener, F., Derwent, R. G., Dlugokencky, E., Holland, E., Isaksen, I. S. A., Katima, J., Kirchhoff, V., Matson, P., Midgley, P., and Wang, M.: Atmospheric Chemistry and Greenhouse Gases, in: Climate Change 2001: The Scientific Basis, edited by: Houghton, J. T., Ding, Y., Griggs, D. J., Noguer, M., van der Linden, P. J., Dai, X., Maskell, K., and Johnson, C. A., Cambridge University Press, Cambridge, UK, 892, 2001.

Engel, A., Rigby, M., Burkholder, J. B., Fernandez, R. P., Froidevaux, L., Hall, B. D., Hossaini, R., Saito, T., Vollmer, M. K., and Yao, B.: Update on Ozone-Depleting Substances (ODCss) and Other Gases of Interest to the Montreal Protocol, Chapter 1, in: Scientific Assessment of Ozone Depletion: 2018, World Meterological Organization, Geneva, Switzerland, 2018.

Etminan, M., Myhre, G., Highwood, E., and Shine, K.: Radiative forcing of carbon dioxide, methane, and nitrous oxide: A significant revision of the methane radiative forcing, Geophysical Research Letters, 43, 2016.

Eyring, V., Bony, S., Meehl, G. A., Senior, C. A., Stevens, B., Stouffer, R. J., and Taylor, K. E.: Overview of the Coupled Model Intercomparison Project Phase 6 (CMIP6) experimental design and organization, Geosci. Model Dev., 9, 1937-1958, 10.5194/gmd-9-1937-2016, 2016.

Fang, X., Park, S., Saito, T., Tunnicliffe, R., Ganesan, A. L., Rigby, M., Li, S., Yokouchi, Y., Fraser, P. J., Harth, C. M., Krummel, P. B., Mühle, J., O'Doherty, S., Salameh, P. K., Simmonds, P. G., Weiss, R. F., Young, D., Lunt, M. F., Manning, A. J., Gressent, A., and Prinn, R. G.: Rapid increase in ozone-depleting chloroform emissions from China, Nature Geoscience, 12, 89-93, 10.1038/s41561-018-0278-2, 2019.

Forkel, M., Carvalhais, N., Rödenbeck, C., Keeling, R., Heimann, M., Thonicke, K., Zaehle, S., and Reichstein, M.: Enhanced seasonal CO2 exchange caused by amplified plant productivity in northern ecosystems, Science, aac4971, 2016.

Friedlingstein, P., Cox, P., Betts, R., Bopp, L., von Bloh, W., Brovkin, V., Cadule, P., Doney, S., Eby, M., Fung, I., Bala, G., John, J., Jones, C., Joos, F., Kato, T., Kawamiya, M., Knorr, W., Lindsay, K., Matthews, H. D., Raddatz, T., Rayner, P., Reick, C., Roeckner, E., Schnitzler, K.-G., Schnur, R., Strassmann, K., Weaver, K., Yoshikawa, C., and Zeng, N.: Climate–

Carbon Cycle Feedback Analysis: Results from the C4MIP Model Intercomparison, Journal of Climate, 19, 3337-3353, 10.1175/JCLI3800.1, 2006.

Friedlingstein, P., Meinshausen, M., Arora, V. K., Jones, C. D., Anav, A., Liddicoat, S. K., and Knutti, R.: Uncertainties in CMIP5 Climate Projections due to Carbon Cycle Feedbacks, Journal of Climate, 27, 511-526, 10.1175/jcli-d-12-00579.1, 2014.

Frieler, K., Meinshausen, M., Golly, A., Mengel, M., Lebek, K., Donner, S. D., and Hoegh-Guldberg, O.: Limiting global warming to 2 degrees C is unlikely to save most coral reefs, Nature Climate Change, 3, 165-170, 10.1038/nclimate1674, 2013.

Fuss, S., Lamb, W. F., Callaghan, M. W., Hilaire, J., Creutzig, F., Amann, T., Beringer, T., de Oliveira Garcia, W., Hartmann, J., and Khanna, T.: Negative emissions—Part 2: Costs, potentials and side effects, Environmental Research Letters, 13, 063002, 2018.

Gidden, M. J., Fujimori, S., van den Berg, M., Klein, D., Smith, S. J., van Vuuren, D. P., and Riahi, K.: A methodology and implementation of automated emissions harmonization for use in Integrated Assessment Models, Environmental Modelling & Software, 105, 187-200, https://doi.org/10.1016/j.envsoft.2018.04.002, 2018.

Gidden, M. J., Riahi, K., Smith, S. J., Fujimori, S., Luderer, G., Kriegler, E., van Vuuren, D. P., van den Berg, M., Feng, L., Klein, D., Calvin, K., Doelman, J. C., Frank, S., Fricko, O., Harmsen, M., Hasegawa, T., Havlik, P., Hilaire, J., Hoesly, R., Horing, J., Popp, A., Stehfest, E., and Takahashi, K.: Global emissions pathways under different socioeconomic scenarios for use in CMIP6: a dataset of harmonized emissions trajectories through the end of the century, Geosci. Model Dev., 12, 1443-1475, 10.5194/gmd-12-1443-2019, 2019.

Graven, H. D., Keeling, R. F., Piper, S. C., Patra, P. K., Stephens, B. B., Wofsy, S. C., Welp, L. R., Sweeney, C., Tans, P. P., Kelley, J. J., Daube, B. C., Kort, E. A., Santoni, G. W., and Bent, J. D.: Enhanced Seasonal Exchange of CO2 by Northern Ecosystems Since 1960, Science, 341, 1085-1089, 10.1126/science.1239207, 2013.

Gray, J. M., Frolking, S., Kort, E. A., Ray, D. K., Kucharik, C. J., Ramankutty, N., and Friedl, M. A.: Direct human influence on atmospheric CO2 seasonality from increased cropland productivity, Nature, 515, 398-401, 10.1038/nature13957, 2014.

Gütschow, J., Jeffery, M. L., Gieseke, R., Gebel, R., Stevens, D., Krapp, M., and Rocha, M.: The PRIMAP-hist national historical emissions time series, Earth Syst. Sci. Data Discuss., 2016, 1-44, 10.5194/essd-2016-12, 2016.

Hoesly, R. M., Smith, S. J., Feng, L., Klimont, Z., Janssens-Maenhout, G., Pitkanen, T., Seibert, J. J., Vu, L., Andres, R. J., Bolt, R. M., Bond, T. C., Dawidowski, L., Kholod, N., Kurokawa, J. I., Li, M., Liu, L., Lu, Z., Moura, M. C. P., O'Rourke, P. R., and Zhang, Q.: Historical (1750–2014) anthropogenic emissions of reactive gases and aerosols from the Community Emissions Data System (CEDS), Geosci. Model Dev., 11, 369-408, 10.5194/gmd-11-369-2018, 2018.

Holmes, C. D., Prather, M. J., Sovde, O. A., and Myhre, G.: Future methane, hydroxyl, and their uncertainties: key climate and emission parameters for future predictions, Atmospheric Chemistry and Physics, 13, 285-302, 2013.

189 Hossaini, R., Chipperfield, M., Montzka, S., Rap, A., Dhomse, S., and Feng, W.: Efficiency of short-lived halogens at
190 influencing climate through depletion of stratospheric ozone, Nature Geoscience, 8, 186-190, 2015.

191 Hurrell, J. W., Holland, M. M., Gent, P. R., Ghan, S., Kay, J. E., Kushner, P. J., Lamarque, J.-F., Large, W. G., Lawrence,
192 D., Lindsay, K., Lipscomb, W. H., Long, M. C., Mahowald, N., Marsh, D. R., Neale, R. B., Rasch, P., Vavrus, S., Vertenstein,
193 M., Bader, D., Collins, W. D., Hack, J. J., Kiehl, J., and Marshall, S.: The Community Earth System Model: A Framework
194 for Collaborative Research, Bulletin of the American Meteorological Society, 94, 1339-1360, 10.1175/bams-d-12-00121.1,
195 2013.

196 Jones, C. D., Arora, V., Friedlingstein, P., Bopp, L., Brovkin, V., Dunne, J., Graven, H., Hoffman, F., Ilyina, T., and John, J.
197 G.: C4MIP–The Coupled Climate–Carbon Cycle Model Intercomparison Project: experimental protocol for CMIP6,
198 Geoscientific Model Development, 9, 2853-2880, 2016.

199 Keeling, C. D., Bacastow, R. B., Bainbridge, A. E., Ekdahl, C. A., Guenther, P. R., Waterman, L. S., and Chin, J. F.:
200 Atmospheric carbon dioxide variations at Mauna Loa observatory, Hawaii, Tellus, 28, 538-551, 1976.

201 Atmospheric CO2 records from sites in the SIO air sampling network: http://cdiac.esd.ornl.gov/trends/co2/sio-keel.htm,
202 access: May, 2004.

203 Lawrence, D. M., Hurtt, G. C., Arneth, A., Brovkin, V., Calvin, K. V., Jones, A. D., Jones, C. D., Lawrence, P. J., de Noblet-
204 Ducoudré, N., and Pongratz, J.: The Land Use Model Intercomparison Project (LUMIP) contribution to CMIP6: rationale
205 and experimental design, Geoscientific Model Development, 9, 2973-2998, 2016.

206 Matthes, K., Funke, B., Anderson, M., Barnard, L., Beer, J., Charbonneau, P., Clilverd, M., Dudok de Wit, T., Haberreiter,
207 M., and Hendry, A.: Solar forcing for CMIP6 (v3. 2), Geoscientific Model Development, 10, 2247-2302, 2017.

208 Meehl, G. A., Covey, C., Delworth, T., Latif, M., McAvaney, B., Mitchell, J. F., Stouffer, R. J., and Taylor, K. E.: The WCRP
209 CMIP3 multimodel dataset: A new era in climate change research, Bulletin of the American Meteorological Society, 88,
210 1383-1394, 2007.

211 Meinshausen, M., Raper, S. C. B., and Wigley, T. M. L.: Emulating coupled atmosphere-ocean and carbon cycle models with
212 a simpler model, MAGICC6: Part I – Model Description and Calibration, Atmospheric Chemistry and Physics 11, 1417-
213 1456, 2011a.

214 Meinshausen, M., Smith, S., Calvin, K., Daniel, J., Kainuma, M., Lamarque, J. F., Matsumoto, K., Montzka, S., Raper, S.,
215 Riahi, K., Thomson, A., Velders, G., and van Vuuren, D. P.: The RCP greenhouse gas concentrations and their extensions
216 from 1765 to 2300, Climatic Change, 109, 213-241, 10.1007/s10584-011-0156-z, 2011b.

217 Meinshausen, M., Wigley, T. M. L., and Raper, S. C. B.: Emulating atmosphere-ocean and carbon cycle models with a
218 simpler model, MAGICC6: Part 2– Applications, Atmospheric Chemistry and Physics 11, 1457-1471, 2011c.

219 Meinshausen, M., Vogel, E., Nauels, A., Lorbacher, K., Meinshausen, N., Etheridge, D. M., Fraser, P. J., Montzka, S. A.,
220 Rayner, P. J., Trudinger, C. M., Krummel, P. B., Beyerle, U., Canadell, J. G., Daniel, J. S., Enting, I. G., Law, R. M., Lunder,
221 C. R., O'Doherty, S., Prinn, R. G., Reimann, S., Rubino, M., Velders, G. J. M., Vollmer, M. K., Wang, R. H. J., and Weiss,

R.: Historical greenhouse gas concentrations for climate modelling (CMIP6), Geosci. Model Dev., 10, 2057-2116, 10.5194/gmd-10-2057-2017, 2017.

Mengel, M., Nauels, A., Rogelj, J., and Schleussner, C.-F.: Committed sea-level rise under the Paris Agreement and the legacy of delayed mitigation action, Nature communications, 9, 601, 2018.

Montzka, S., McFarland, M., Andersen, S., Miller, B., Fahey, D., Hall, B., Hu, L., Siso, C., and Elkins, J.: Recent trends in global emissions of hydrochlorofluorocarbons and hydrofluorocarbons: Reflecting on the 2007 adjustments to the Montreal Protocol, The Journal of Physical Chemistry A, 119, 4439-4449, 2015.

Montzka, S. A., Dutton, G. S., Yu, P., Ray, E., Portmann, R. W., Daniel, J. S., Kuijpers, L., Hall, B. D., Mondeel, D., Siso, C., Nance, J. D., Rigby, M., Manning, A. J., Hu, L., Moore, F., Miller, B. R., and Elkins, J. W.: An unexpected and persistent increase in global emissions of ozone-depleting CFC-11, Nature, 557, 413-417, 10.1038/s41586-018-0106-2, 2018.

Morgenstern, O., Braesicke, P., Hurwitz, M. M., O'Connor, F. M., Bushell, A. C., Johnson, C. E., and Pyle, J. A.: The World Avoided by the Montreal Protocol, Geophysical Research Letters, 35, 10.1029/2008gl034590, 2008.

Myhre, G., Shindell, D., Breon, F. M., Collins, W., Fuglestvedt, J., Huang, J., Koch, D., Lamarque, J. F., Lee, D., Mendoza, B., Nakajima, T., Robock, A., Stephens, G., Takemura, T., and Zhang, H.: Anthropogenic and Natural Radiative Forcing, in: Climate Change 2013: The Physical Science Basis. Contribution of Working Group I to the Fifth Assessment, Report of the Intergovernmental Panel on Climate Change, edited by: Stocker, T. F., Qin, D., Plattner, G.-K., Tignor, M., Allen, S. K., Boschung, J., Nauels, A., Xia, Y., Bex, V., and Midgley, P. M., Cambridge University Press, Cambridge, New York, 2013.

Nisbet, E. G., Dlugokencky, E. J., Manning, M. R., Lowry, D., Fisher, R. E., France, J. L., Michel, S. E., Miller, J. B., White, J. W. C., Vaughn, B., Bousquet, P., Pyle, J. A., Warwick, N. J., Cain, M., Brownlow, R., Zazzeri, G., Lanoisellé, M., Manning, A. C., Gloor, E., Worthy, D. E. J., Brunke, E.-G., Labuschagne, C., Wolff, E. W., and Ganesan, A. L.: Rising atmospheric methane: 2007–2014 growth and isotopic shift, Global Biogeochemical Cycles, 30, 1356-1370, 10.1002/2016gb005406, 2016.

NOAA ESRL GMD: Atmospheric Carbon Dioxide Dry Air Mole Fractions from quasi-continuous measurements at Mauna Loa, Hawaii. K.W. Thoning, D. R. K., and A. Crotwell (Ed.), National Oceanic and Atmospheric Administration (NOAA), Earth System Research Laboratory (ESRL), Global Monitoring Division (GMD): Boulder, Colorado, USA, 2014a.

NOAA ESRL GMD: Atmospheric Carbon Dioxide Dry Air Mole Fractions from quasi-continuous measurements at Barrow, Alaska. K.W. Thoning, D. R. K., and A. Crotwell (Ed.), National Oceanic and Atmospheric Administration (NOAA), Earth System Research Laboratory (ESRL), Global Monitoring Division (GMD): Boulder, Colorado, USA, 2014b.

NOAA ESRL GMD: Atmospheric Carbon Dioxide Dry Air Mole Fractions from quasi-continuous measurements at South Pole. K.W. Thoning, D. R. K., and A. Crotwell (Ed.), National Oceanic and Atmospheric Administration (NOAA), Earth System Research Laboratory (ESRL), Global Monitoring Division (GMD): Boulder, Colorado, USA, 2014c.

NOAA ESRL GMD: Atmospheric Carbon Dioxide Dry Air Mole Fractions from quasi-continuous measurements at American Samoa. K.W. Thoning, D. R. K., and A. Crotwell (Ed.), National Oceanic and Atmospheric Administration (NOAA), Earth System Research Laboratory (ESRL), Global Monitoring Division (GMD): Boulder, Colorado, USA, 2014d.

O'Neill, B. C., Tebaldi, C., Vuuren, D. P. v., Eyring, V., Friedlingstein, P., Hurtt, G., Knutti, R., Kriegler, E., Lamarque, J.-F., and Lowe, J.: The scenario model intercomparison project (ScenarioMIP) for CMIP6, Geoscientific Model Development, 9, 3461-3482, 2016.

Prather, M. J., Holmes, C. D., and Hsu, J.: Reactive greenhouse gas scenarios: Systematic exploration of uncertainties and the role of atmospheric chemistry, Geophysical Research Letters, 39, 2012.

Prinn, R., Cunnold, D., Rasmussen, R., Simmonds, P., Alyea, F., Crawford, A., Fraser, P., and Rosen, R.: Atmospheric emissions and trends of nitrous oxide deduced from 10 years of ALE–GAGE data, Journal of Geophysical Research: Atmospheres, 95, 18369-18385, 1990.

Prinn, R. G., Weiss, R. F., Arduini, J., Arnold, T., DeWitt, H. L., Fraser, P. J., Ganesan, A. L., Gasore, J., Harth, C. M., Hermansen, O., Kim, J., Krummel, P. B., Li, S., Loh, Z. M., Lunder, C. R., Maione, M., Manning, A. J., Miller, B. R., Mitrevski, B., Mühle, J., O'Doherty, S., Park, S., Reimann, S., Rigby, M., Saito, T., Salameh, P. K., Schmidt, R., Simmonds, P. G., Steele, L. P., Vollmer, M. K., Wang, R. H., Yao, B., Yokouchi, Y., Young, D., and Zhou, L.: History of chemically and radiatively important atmospheric gases from the Advanced Global Atmospheric Gases Experiment (AGAGE), Earth Syst. Sci. Data, 10, 985-1018, 10.5194/essd-10-985-2018, 2018.

Ray, E. A., Moore, F. L., Elkins, J. W., Rosenlof, K. H., Laube, J. C., Röckmann, T., Marsh, D. R., and Andrews, A. E.: Quantification of the SF6 lifetime based on mesospheric loss measured in the stratospheric polar vortex, Journal of Geophysical Research: Atmospheres, 122, 4626-4638, 10.1002/2016JD026198, 2017.

Rigby, M., Montzka, S. A., Prinn, R. G., White, J. W. C., Young, D., O'Doherty, S., Lunt, M. F., Ganesan, A. L., Manning, A. J., Simmonds, P. G., Salameh, P. K., Harth, C. M., Mühle, J., Weiss, R. F., Fraser, P. J., Steele, L. P., Krummel, P. B., McCulloch, A., and Park, S.: Role of atmospheric oxidation in recent methane growth, Proceedings of the National Academy of Sciences, 114, 5373-5377, 10.1073/pnas.1616426114, 2017.

Rigby, M., Park, S., Saito, T., Western, L. M., Redington, A. L., Fang, X., Henne, S., Manning, A. J., Prinn, R. G., Dutton, G. S., Fraser, P. J., Ganesan, A. L., Hall, B. D., Harth, C. M., Kim, J., Kim, K. R., Krummel, P. B., Lee, T., Li, S., Liang, Q., Lunt, M. F., Montzka, S. A., Mühle, J., O'Doherty, S., Park, M. K., Reimann, S., Salameh, P. K., Simmonds, P., Tunnicliffe, R. L., Weiss, R. F., Yokouchi, Y., and Young, D.: Increase in CFC-11 emissions from eastern China based on atmospheric observations, Nature, 569, 546-550, 10.1038/s41586-019-1193-4, 2019.

Rogelj, J., Schaeffer, M., Meinshausen, M., Shindell, D. T., Hare, W., Klimont, Z., Velders, G. J., Amann, M., and Schellnhuber, H. J.: Disentangling the effects of CO2 and short-lived climate forcer mitigation, Proceedings of the National Academy of Sciences, 111, 16325-16330, 2014.

Rogelj, J., Meinshausen, M., Schaeffer, M., Knutti, R., and Riahi, K.: Impact of short-lived non-CO2 mitigation on carbon budgets for stabilizing global warming, Environmental Research Letters, 10, 2015.

Royer, D. L.: CO2-forced climate thresholds during the Phanerozoic, Geochim Cosmochim Ac, 70, 5665-5675, 2006.

Saunois, M., Bousquet, P., Poulter, B., Peregon, A., Ciais, P., Canadell, J. G., Dlugokencky, E. J., Etiope, G., Bastviken, D., Houweling, S., Janssens-Maenhout, G., Tubiello, F. N., Castaldi, S., Jackson, R. B., Alexe, M., Arora, V. K., Beerling, D. J.,

Bergamaschi, P., Blake, D. R., Brailsford, G., Brovkin, V., Bruhwiler, L., Crevoisier, C., Crill, P., Covey, K., Curry, C., Frankenberg, C., Gedney, N., Höglund-Isaksson, L., Ishizawa, M., Ito, A., Joos, F., Kim, H. S., Kleinen, T., Krummel, P., Lamarque, J. F., Langenfelds, R., Locatelli, R., Machida, T., Maksyutov, S., McDonald, K. C., Marshall, J., Melton, J. R., Morino, I., Naik, V., O'Doherty, S., Parmentier, F. J. W., Patra, P. K., Peng, C., Peng, S., Peters, G. P., Pison, I., Prigent, C., Prinn, R., Ramonet, M., Riley, W. J., Saito, M., Santini, M., Schroeder, R., Simpson, I. J., Spahni, R., Steele, P., Takizawa, A., Thornton, B. F., Tian, H., Tohjima, Y., Viovy, N., Voulgarakis, A., van Weele, M., van der Werf, G. R., Weiss, R., Wiedinmyer, C., Wilton, D. J., Wiltshire, A., Worthy, D., Wunch, D., Xu, X., Yoshida, Y., Zhang, B., Zhang, Z., and Zhu, Q.: The global methane budget 2000–2012, Earth Syst. Sci. Data, 8, 697-751, 10.5194/essd-8-697-2016, 2016.

Schaefer, H., Fletcher, S. E. M., Veidt, C., Lassey, K. R., Brailsford, G. W., Bromley, T. M., Dlugokencky, E. J., Michel, S. E., Miller, J. B., Levin, I., Lowe, D. C., Martin, R. J., Vaughn, B. H., and White, J. W. C.: A 21st-century shift from fossil-fuel to biogenic methane emissions indicated by ¹³CH<sub>4</sub&gt, Science, 352, 80, 10.1126/science.aad2705, 2016.

Schneider, L., and Kollmuss, A.: Perverse effects of carbon markets on HFC-23 and SF6 abatement projects in Russia, Nature Climate Change, 5, 1061, 10.1038/nclimate2772, 2015.

Schneider, L. R.: Perverse incentives under the CDM: an evaluation of HFC-23 destruction projects, Climate Policy, 11, 851-864, 10.3763/cpol.2010.0096, 2011.

Schneider von Deimling, T., Meinshausen, M., Levermann, A., Huber, V., Frieler, K., Lawrence, D. M., and Brovkin, V.: Estimating the near-surface permafrost-carbon feedback on global warming, Biogeosciences, 9, 649-665, 10.5194/bg-9-649-2012, 2012.

Schneider von Deimling, T., Grosse, G., Strauss, J., Schirrmeister, L., Morgenstern, A., Schaphoff, S., Meinshausen, M., and Boike, J.: Observation-based modelling of permafrost carbon fluxes with accounting for deep carbon deposits and thermokarst activity, Biogeosciences, 12, 3469-3488, 2015.

Smith, C. J., Kramer, R. J., Myhre, G., Forster, P. M., Soden, B. J., Andrews, T., Boucher, O., Faluvegi, G., Fläschner, D., Hodnebrog, Ø., Kasoar, M., Kharin, V., Kirkevåg, A., Lamarque, J.-F., Mülmenstädt, J., Olivié, D., Richardson, T., Samset, B. H., Shindell, D., Stier, P., Takemura, T., Voulgarakis, A., and Watson-Parris, D.: Understanding Rapid Adjustments to Diverse Forcing Agents, Geophysical Research Letters, 45, 12,023-012,031, 10.1029/2018gl079826, 2018.

Smith, P., Davis, S. J., Creutzig, F., Fuss, S., Minx, J., Gabrielle, B., Kato, E., Jackson, R. B., Cowie, A., and Kriegler, E.: Biophysical and economic limits to negative CO 2 emissions, Nature climate change, 6, 42-50, 2016.

Stevens, B., Fiedler, S., Kinne, S., Peters, K., Rast, S., Müsse, J., Smith, S. J., and Mauritsen, T.: MACv2-SP: A parameterization of anthropogenic aerosol optical properties and an associated Twomey effect for use in CMIP6, Geoscientific Model Development, 10, 433-452, 2017.

Taylor, K. E., Stouffer, R. J., and Meehl, G. A.: An overview of CMIP5 and the experiment design, Bulletin of the American Meteorological Society, 93, 485-498, 2012.

Toohey, M., Stevens, B., Schmidt, H., and Timmreck, C.: Easy Volcanic Aerosol (EVA v1.0): an idealized forcing generator for climate simulations, Geosci. Model Dev., 9, 4049-4070, 10.5194/gmd-9-4049-2016, 2016.

Tsutsumi, Y., Mori, K., Hirahara, T., Ikegami, M., and Conway, T. J.: Technical report of global analysis method for major greenhouse gases by the World Data Center for greenhouse gases, WMO/TD, 2009.

Velders, G., and Daniel, J.: Uncertainty analysis of projections of ozone-depleting substances: mixing ratios, EESC, ODPs, and GWPs, Atmospheric Chemistry and Physics, 14, 2757-2776, 2014a.

Velders, G. J. M., Andersen, S. O., Daniel, J. S., Fahey, D. W., and McFarland, M.: The importance of the Montreal Protocol in protecting climate, P Natl Acad Sci USA, 104, 4814-4819, 2007.

Velders, G. J. M., and Daniel, J. S.: Uncertainty analysis of projections of ozone-depleting substances: mixing ratios, EESC, ODPs, and GWPs, Atmos. Chem. Phys., 14, 2757-2776, 10.5194/acp-14-2757-2014, 2014b.

Velders, G. J. M., Fahey, D. W., Daniel, J. S., Andersen, S. O., and McFarland, M.: Future atmospheric abundances and climate forcings from scenarios of global and regional hydrofluorocarbon (HFC) emissions, Atmospheric Environment, 123, 200-209, https://doi.org/10.1016/j.atmosenv.2015.10.071, 2015.

Vollmer, M. K., Young, D., Trudinger, C. M., Mühle, J., Henne, S., Rigby, M., Park, S., Li, S., Guillevic, M., Mitrevski, B., Harth, C. M., Miller, B. R., Reimann, S., Yao, B., Steele, L. P., Wyss, S. A., Lunder, C. R., Arduini, J., McCulloch, A., Wu, S., Rhee, T. S., Wang, R. H. J., Salameh, P. K., Hermansen, O., Hill, M., Langenfelds, R. L., Ivy, D., O'Doherty, S., Krummel, P. B., Maione, M., Etheridge, D. M., Zhou, L., Fraser, P. J., Prinn, R. G., Weiss, R. F., and Simmonds, P. G.: Atmospheric histories and emissions of chlorofluorocarbons CFC-13 (CClF3), ΣCFC-114 (C2Cl2F4), and CFC-115 (C2ClF5), Atmos. Chem. Phys., 18, 979-1002, 10.5194/acp-18-979-2018, 2018.

Welp, L. R., Patra, P. K., Rödenbeck, C., Nemani, R., Bi, J., Piper, S. C., and Keeling, R. F.: Increasing summer net CO2 uptake in high northern ecosystems inferred from atmospheric inversions and remote sensing, Atmos. Chem. Phys.(Discuss), submitted, 2016.

WMO: Scientific Assessment of Ozone Depletion: 2006, World Meteorological Organization, Geneva, Switzerland, 572, 2006.

WMO: Scientific Assessment of Ozone Depletion: 2014, World Meteorological Organization, Geneva, Switzerland, 416, 2014.

Worden, J. R., Bloom, A. A., Pandey, S., Jiang, Z., Worden, H. M., Walker, T. W., Houweling, S., and Röckmann, T.: Reduced biomass burning emissions reconcile conflicting estimates of the post-2006 atmospheric methane budget, Nature Communications, 8, 2227, 10.1038/s41467-017-02246-0, 2017.

13 Figures

SSP1
Sustainability
SSP2
Middle
of the road
SSP3
Regional
rivalry
SSP4
Inequality
SSP5
Fossil-fuel
development
Global-mean temperature
5
4.5
4
3.5
3
2.5
2
1.5
1
0.5
0
SSP5-8.5
SSP3-7.0
SSP4-6.0
SSP2-4.5
SSP4-3.4
SSP5-3.4-OS
SSP1-2.6
SSP1-1.9
Low NTCF
Mitigation
2100
2050
Today 2020
1750

Figure 1

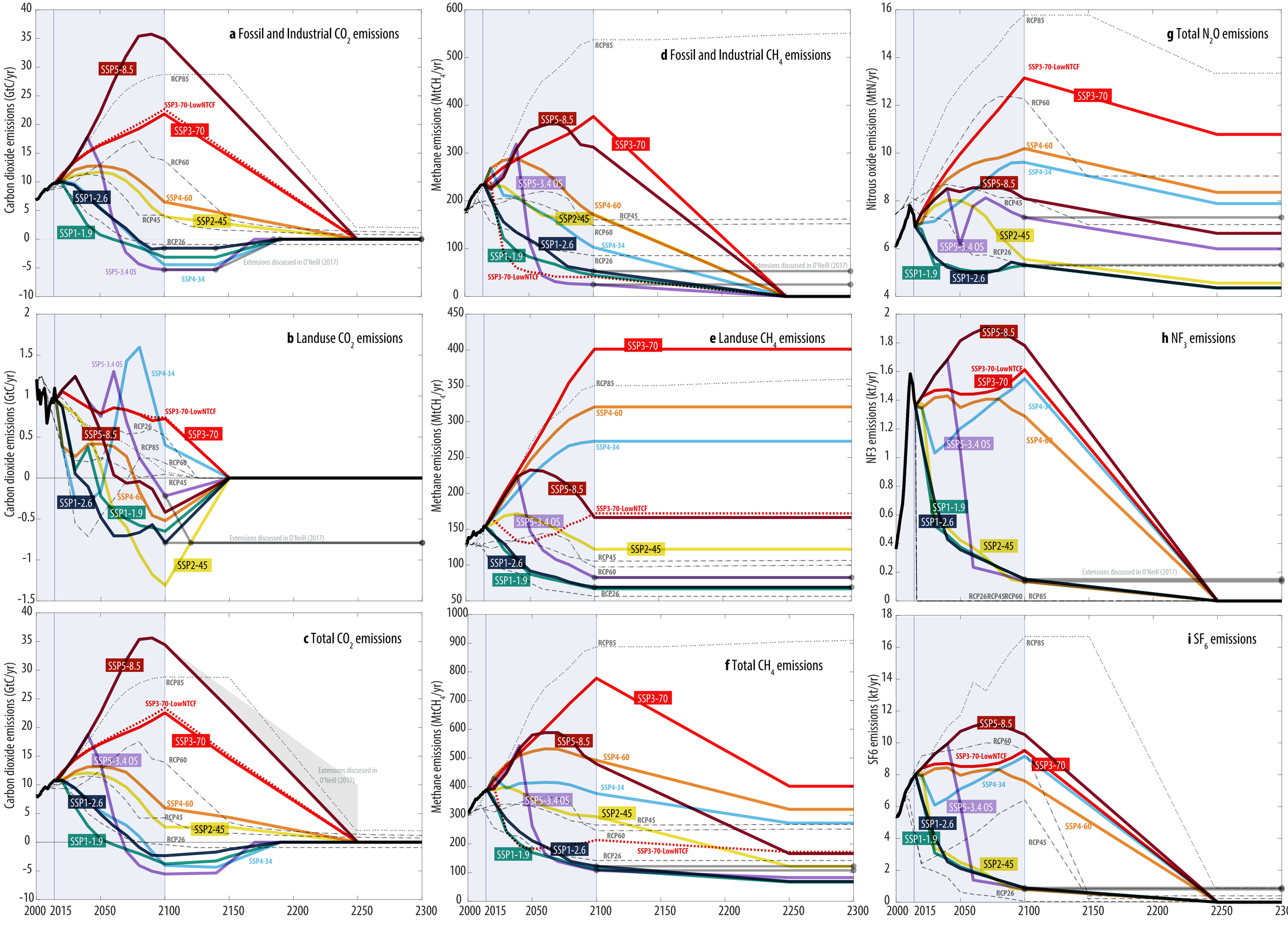
a Fossil and Industrial CO2 emissions
Carbon dioxide emissions (GtC/yr)
SSP5-8.5
RCP85
SSP3-70-LowNTCF
SSP3-70
RCP60
SSP1-2.6
SSP4-60
SSP2-45
RCP45
SSP1-1.9
RCP26
SSP5-3.4 OS
SSP4-34
Extensions discussed in O'Neill (2017)
d Fossil and Industrial CH4 emissions
Methane emissions (MtCH4/yr)
g Total N2O emissions
Nitrous oxide emissions (MtN/yr)
b Landuse CO2 emissions
e Landuse CH4 emissions
h NF3 emissions
NF3 emissions (kt/yr)
RCP26RCP45RCP60
c Total CO2 emissions
f Total CH4 emissions
i SF6 emissions
SF6 emissions (kt/yr)
2000 2015 2050 2100 2150 2200 2250 2300

Figure 2

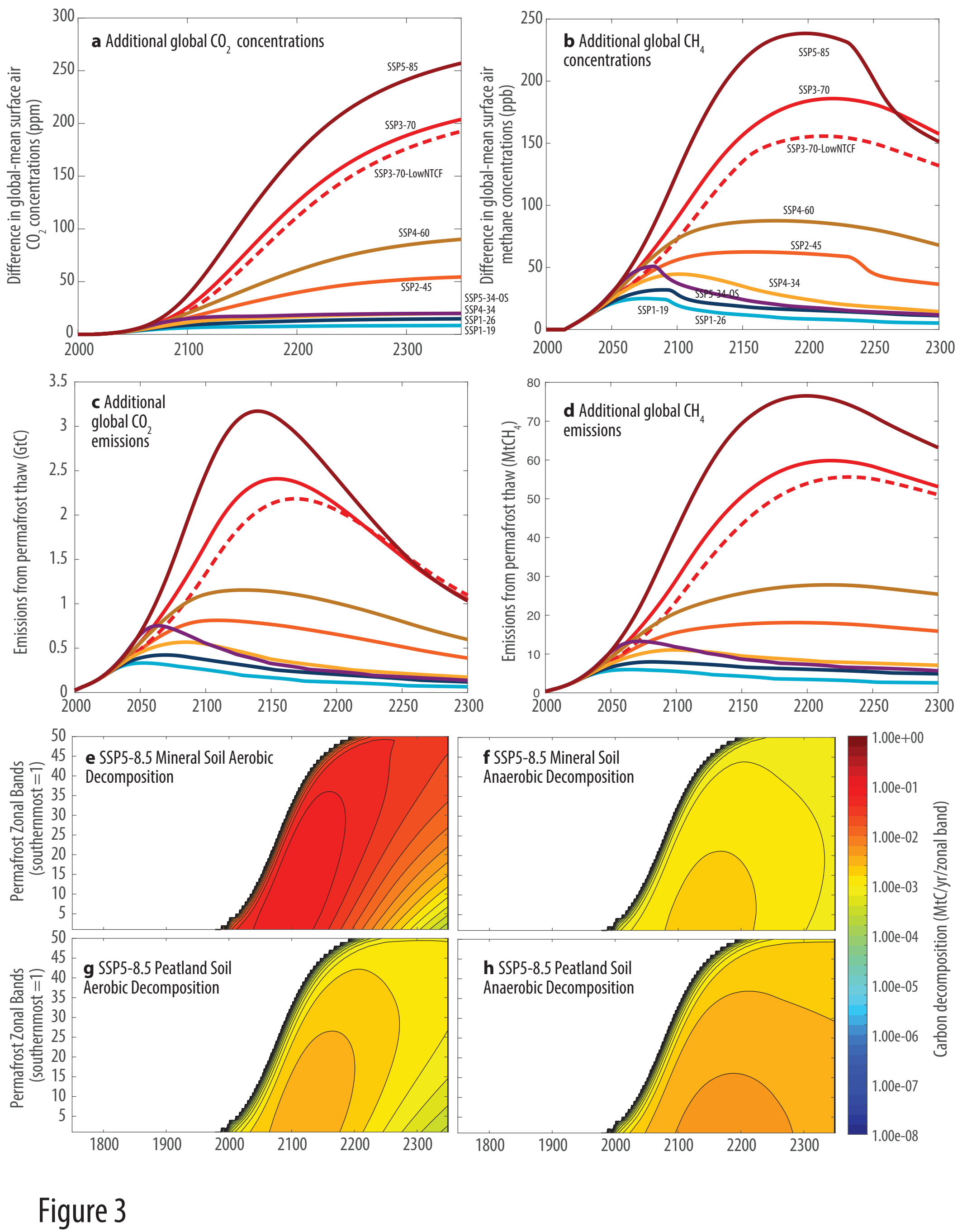
a Additional global CO2 concentrations
Difference in global-mean surface air CO2 concentrations (ppm)
SSP5-85
SSP3-70
SSP3-70-LowNTCF
SSP4-60
SSP2-45
SSP5-34-OS
SSP4-34
SSP1-26
SSP1-19
b Additional global CH4 concentrations
Difference in global-mean surface air methane concentrations (ppb)
c Additional global CO2 emissions
Emissions from permafrost thaw (GtC)
d Additional global CH4 emissions
Emissions from permafrost thaw (MtCH4)
e SSP5-8.5 Mineral Soil Aerobic Decomposition
f SSP5-8.5 Mineral Soil Anaerobic Decomposition
g SSP5-8.5 Peatland Soil Aerobic Decomposition
h SSP5-8.5 Peatland Soil Anaerobic Decomposition
Permafrost Zonal Bands (southernmost =1)
Carbon decomposition (MtC/yr/zonal band)

Figure 3

a Carbon Dioxide

Radiative Forcing relative to OLBL first run (C_0 = 389ppm) (W/m²)

CO_2 mole fraction (ppm)

IPCC TAR ill - CO_2 & All RF

IPCC TAR II - CO_2 & All RF

IPCC TAR I - CO_2 & All RF

Etminan II - CO_2

Etminan II - All RF

This Study - CO_2

This Study - All RF

Etminan I - All RF

OLBL

b Methane

Radiative Forcing relative to OLBL first run (M_0 =1800ppb) (W/m²)

CH_4 mole fraction (ppb)

IPCC TAR - CH_4 & All RF

Etminan I - All RF & CH_4

Etminan II - CH_4

Etminan II - All RF

This Study - CH_4

This Study - All RF

c Nitrous Oxide

Radiative Forcing relative to OLBL first run (N_0 =323ppb) (W/m²)

N_2O mole fraction (ppb)

IPCC TAR - N_2O & All RF

This Study - N_2O

This Study - All RF

Etminan - All RF & N_2O

Etminan - All RF

Etminan - N_2O

Etminan II - N_2O

Etminan I - All RF

Etminan II - All RF

d Errors (differences between 48 Oslo LBL model cases compared to parameterisations)

The ranges for N_2O, CH_4 and CO_2 indicate the concentration settings for the 48 Oslo LBL model cases

N_2O (ppb): 323 200 525

CH_4 (ppb): 1800 750 3500 340 | 1800 750 3500 340 | 1800 750 3500 340 | 1800 750 3500 340

CO_2 = 389 ppm | CO_2 = 180 ppm | CO_2 = 700 ppm | CO_2 = 2000 ppm

This study's approximation of OLBL

Etminan II simplified formula with adj. pre-ind

Etminan I simplified formula

Fit error

Total forcing difference between fit and OLBL model (W/m2)

48 Oslo LBL cases

Figure 4

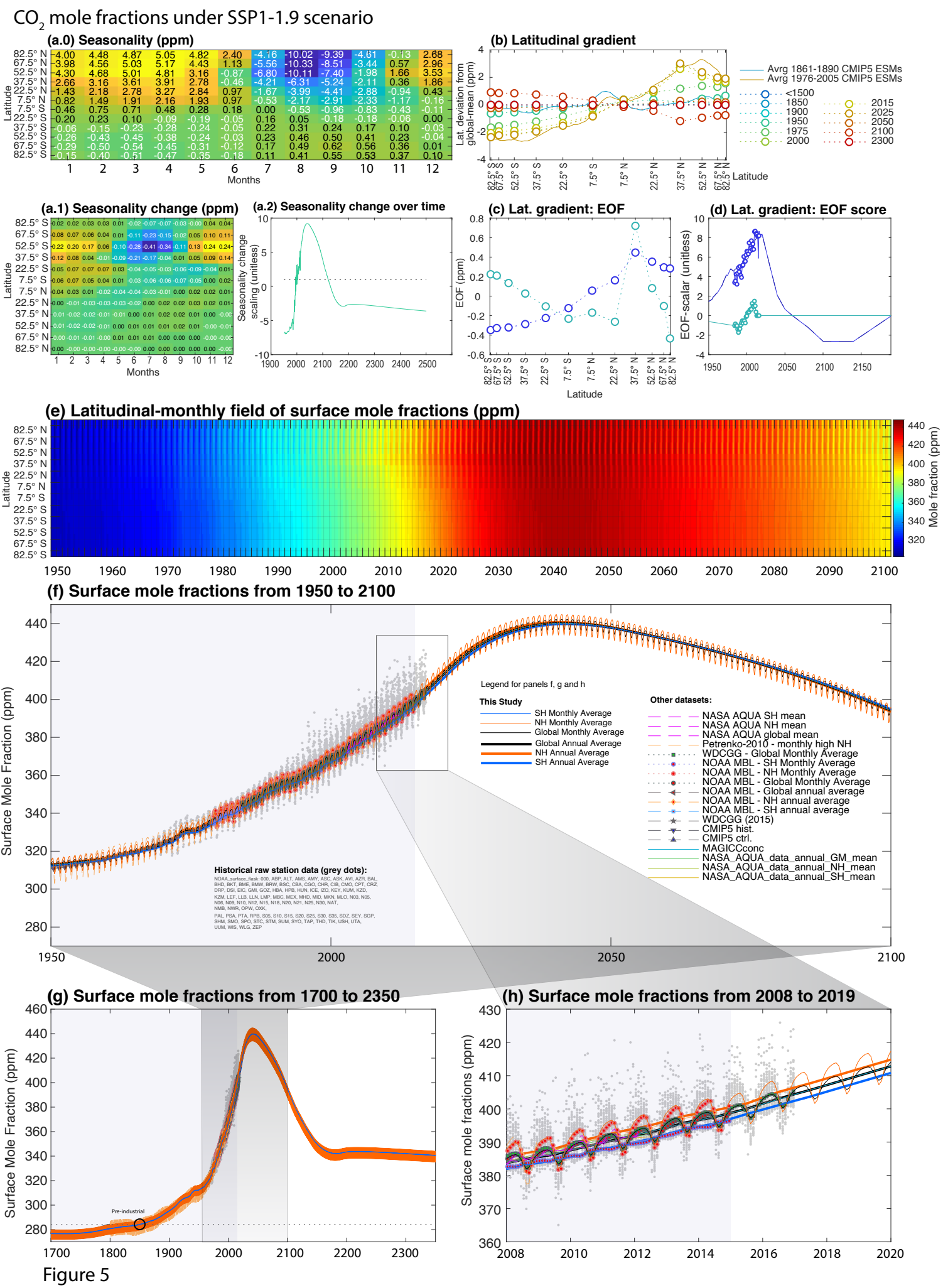
CO2 mole fractions under SSP1-1.9 scenario
(a.0) Seasonality (ppm)
Latitude
Months
(b) Latitudinal gradient
Lat. deviation from global-mean (ppm)
Avrg 1861-1890 CMIP5 ESMs
Avrg 1976-2005 CMIP5 ESMs
<1500
1850
1900
1950
1975
2000
2015
2025
2050
2100
2300
(a.1) Seasonality change (ppm)
(a.2) Seasonality change over time
Seasonality change scaling (unitless)
(c) Lat. gradient: EOF
EOF (ppm)
(d) Lat. gradient: EOF score
EOF-scalar (unitless)
(e) Latitudinal-monthly field of surface mole fractions (ppm)
Mole fraction (ppm)
(f) Surface mole fractions from 1950 to 2100
Surface Mole Fraction (ppm)
Legend for panels f, g and h
This Study
SH Monthly Average
NH Monthly Average
Global Monthly Average
Global Annual Average
NH Annual Average
SH Annual Average
Other datasets:
NASA AQUA SH mean
NASA AQUA NH mean
NASA AQUA global mean
Petrenko-2010 - monthly high NH
WDCGG - Global Monthly Average
NOAA MBL - SH Monthly Average
NOAA MBL - NH Monthly Average
NOAA MBL - Global Monthly Average
NOAA MBL - Global annual average
NOAA MBL - NH annual average
NOAA MBL - SH annual average
WDCGG (2015)
CMIP5 hist.
CMIP5 ctrl.
MAGICCconc
NASA_AQUA_data_annual_GM_mean
NASA_AQUA_data_annual_NH_mean
NASA_AQUA_data_annual_SH_mean
Historical raw station data (grey dots):
(g) Surface mole fractions from 1700 to 2350
Pre-industrial
(h) Surface mole fractions from 2008 to 2019
Surface mole fractions (ppm)

Figure 5

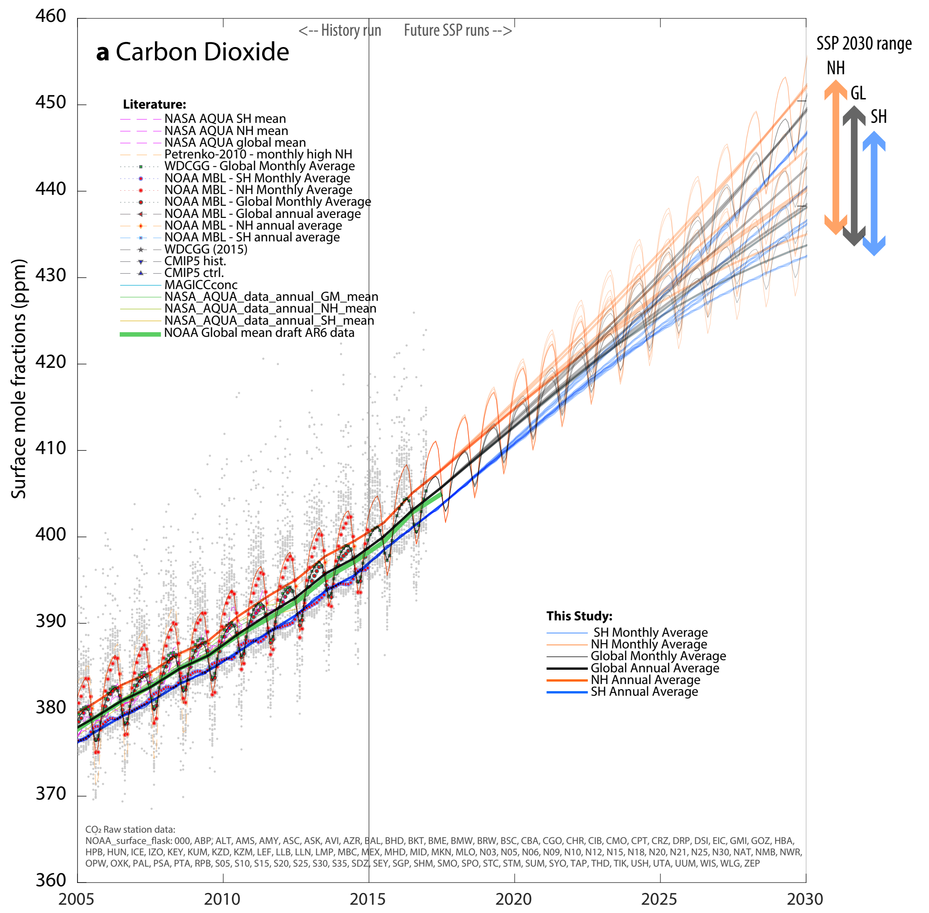
a Carbon Dioxide
<-- History run
Future SSP runs -->
Surface mole fractions (ppm)
460
450
440
430
420
410
400
390
380
370
360
2005
2010
2015
2020
2025
2030
Literature:
NASA AQUA SH mean
NASA AQUA NH mean
NASA AQUA global mean
Petrenko-2010 - monthly high NH
WDCGG - Global Monthly Average
NOAA MBL - SH Monthly Average
NOAA MBL - NH Monthly Average
NOAA MBL - Global Monthly Average
NOAA MBL - Global annual average
NOAA MBL - NH annual average
NOAA MBL - SH annual average
WDCGG (2015)
CMIP5 hist.
CMIP5 ctrl.
MAGICCconc
NASA_AQUA_data_annual_GM_mean
NASA_AQUA_data_annual_NH_mean
NASA_AQUA_data_annual_SH_mean
NOAA Global mean draft AR6 data
This Study:
SH Monthly Average
NH Monthly Average
Global Monthly Average
Global Annual Average
NH Annual Average
SH Annual Average
SSP 2030 range
NH
GL
SH
CO2 Raw station data:
NOAA_surface_flask: 000, ABP, ALT, AMS, AMY, ASC, ASK, AVI, AZR, BAL, BHD, BKT, BME, BMW, BRW, BSC, CBA, CGO, CHR, CIB, CMO, CPT, CRZ, DRP, DSI, EIC, GMI, GOZ, HBA, HPB, HUN, ICE, IZO, KEY, KUM, KZD, KZM, LEF, LLB, LLN, LMP, MBC, MEX, MHD, MID, MKN, MLO, N03, N05, N06, N09, N10, N12, N15, N18, N20, N21, N25, N30, NAT, NMB, NWR, OPW, OXK, PAL, PSA, PTA, RPB, S05, S10, S15, S20, S25, S30, S35, SDZ, SEY, SGP, SHM, SMO, SPO, STC, STM, SUM, SYO, TAP, THD, TIK, USH, UTA, UUM, WIS, WLG, ZEP

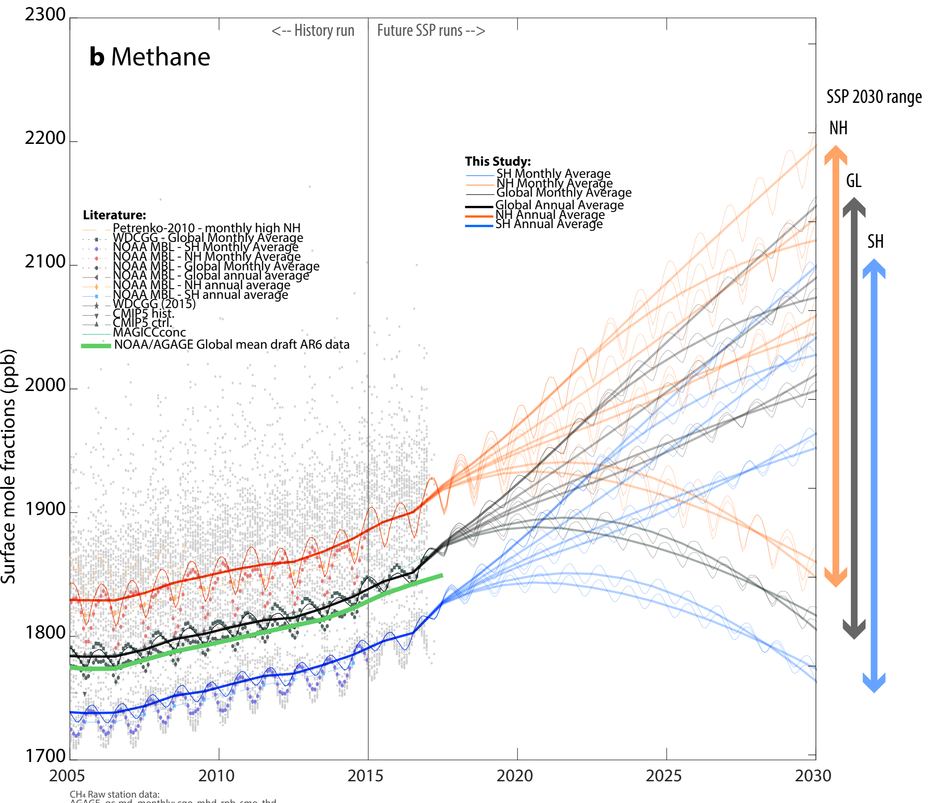
b Methane
<-- History run
Future SSP runs -->
Surface mole fractions (ppb)
2300
2200
2100
2000
1900
1800
1700
2005
2010
2015
2020
2025
2030
Literature:
Petrenko-2010 - monthly high NH
WDCGG - Global Monthly Average
NOAA MBL - SH Monthly Average
NOAA MBL - NH Monthly Average
NOAA MBL - Global Monthly Average
NOAA MBL - Global annual average
NOAA MBL - NH annual average
NOAA MBL - SH annual average
WDCGG (2015)
CMIP5 hist.
CMIP5 ctrl.
MAGICCconc
NOAA/AGAGE Global mean draft AR6 data
This Study:
SH Monthly Average
NH Monthly Average
Global Monthly Average
Global Annual Average
NH Annual Average
SH Annual Average
SSP 2030 range
NH
GL
SH
CH4 Raw station data:
AGAGE_gc-md_monthly: cgo, mhd, rpb, smo, thd
NOAA_surface_flask: 000, ABP, ALT, AMS, AMY, ASC, ASK, AVI, AZR, BAL, BHD, BKT, BME, BMW, BRW, BSC, CBA, CGO, CHR, CIB, CMO, CPT, CRZ, DRP, DSI, EIC, GMI, GOZ, HBA, HPB, HUN, ICE, ITN, IZO, KEY, KUM, KZD, KZM, LEF, LLB, LLN, LMP, MBC, MEX, MHD, MID, MKN, MLO, N03, N05, N06, N09, N10, N12, N15, N18, N20, N21, N25, N30, NAT, NMB, NWR, OPW, OXK, PAL, PSA, PTA, RPB, S05, S10, S15, S20, S25, S30, S35, SDZ, SEY, SGP, SHM, SMO, SPO, STM, SUM, SYO, TAP, THD, TIK, USH, UTA, UUM, WIS, WKT, WLG, ZEP

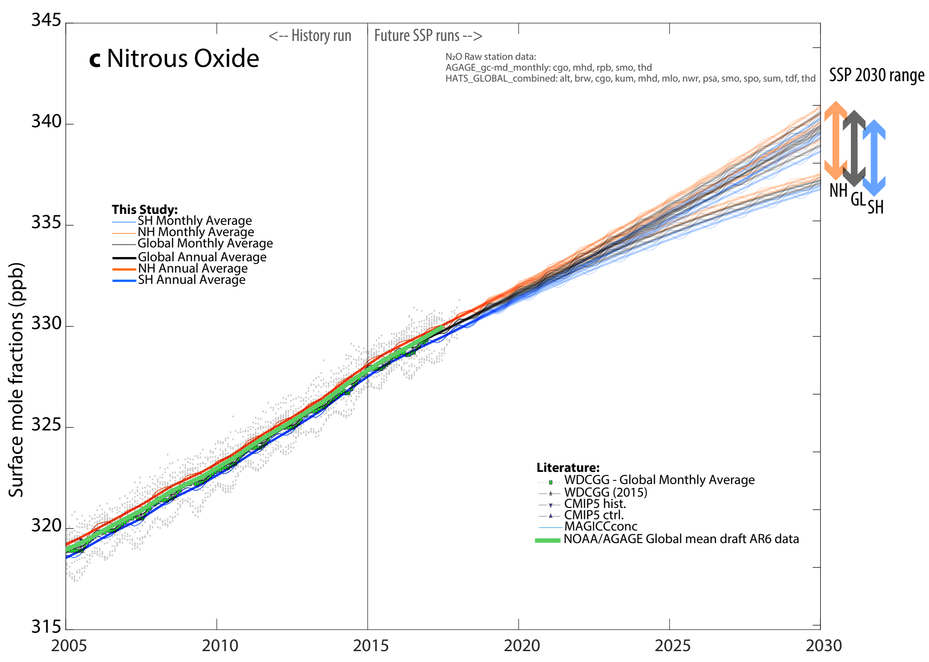
c Nitrous Oxide
<-- History run
Future SSP runs -->
N2O Raw station data:
AGAGE_gc-md_monthly: cgo, mhd, rpb, smo, thd
HATS_GLOBAL_combined: alt, brw, cgo, kum, mhd, mlo, nwr, psa, smo, spo, sum, tdf, thd
Surface mole fractions (ppb)
345
340
335
330
325
320
315
2005
2010
2015
2020
2025
2030
This Study:
SH Monthly Average
NH Monthly Average
Global Monthly Average
Global Annual Average
NH Annual Average
SH Annual Average
Literature:
WDCGG - Global Monthly Average
WDCGG (2015)
CMIP5 hist.
CMIP5 ctrl.
MAGICCconc
NOAA/AGAGE Global mean draft AR6 data
SSP 2030 range
NH
GL
SH

Figure 6

SSP scenarios greenhouse gas radiative forcings

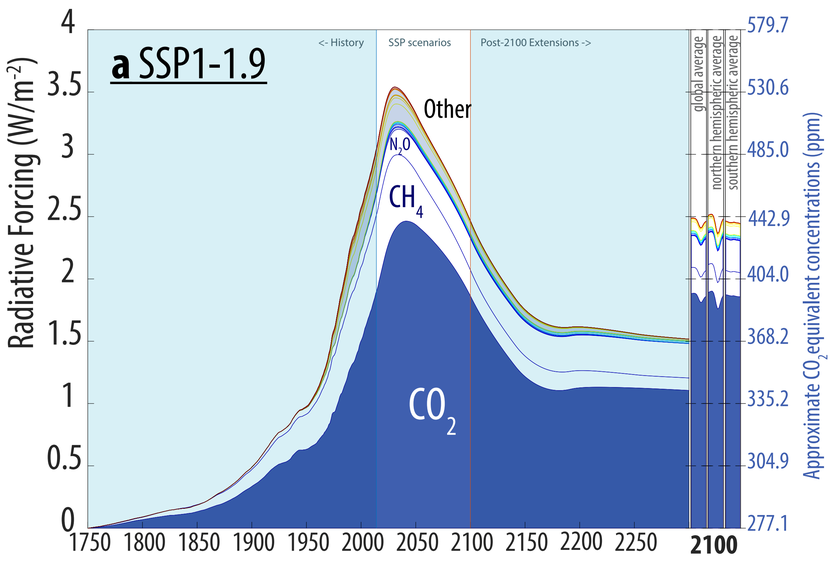

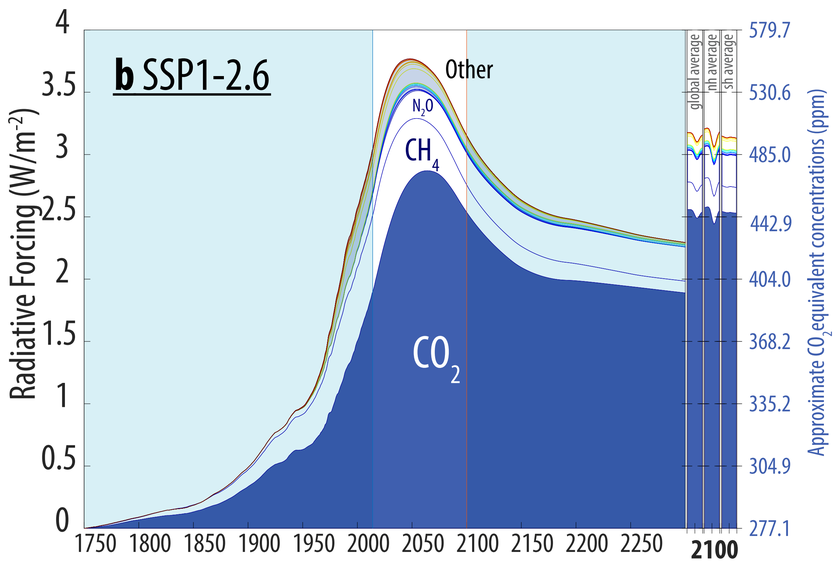

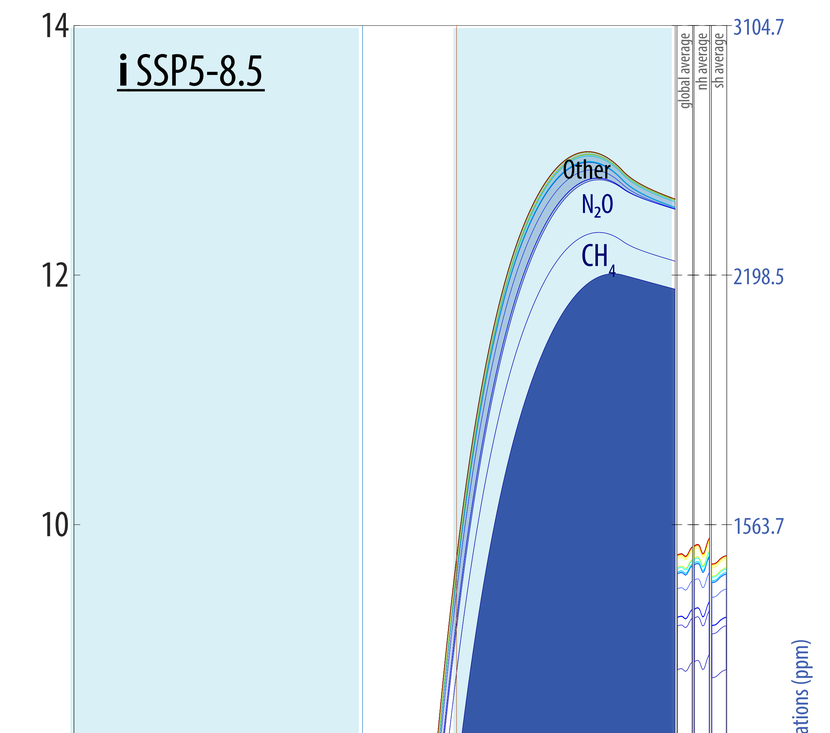

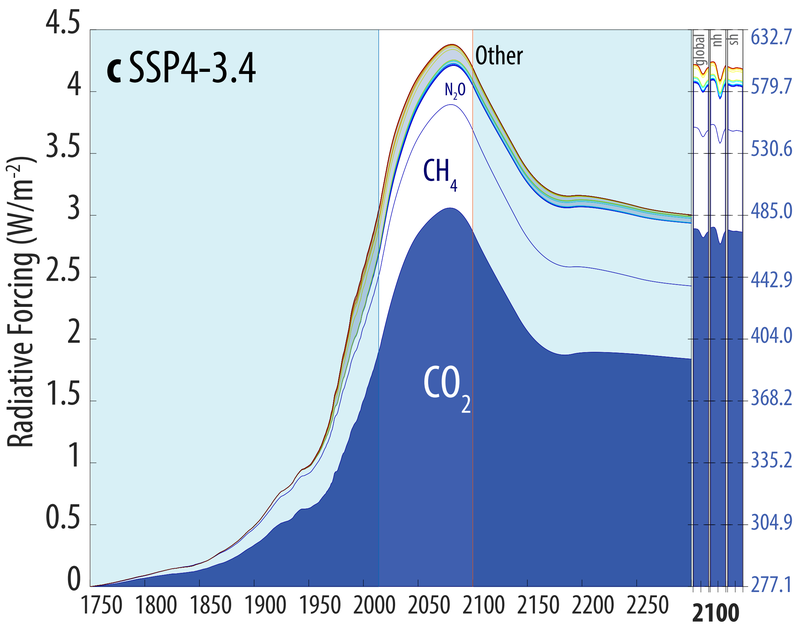

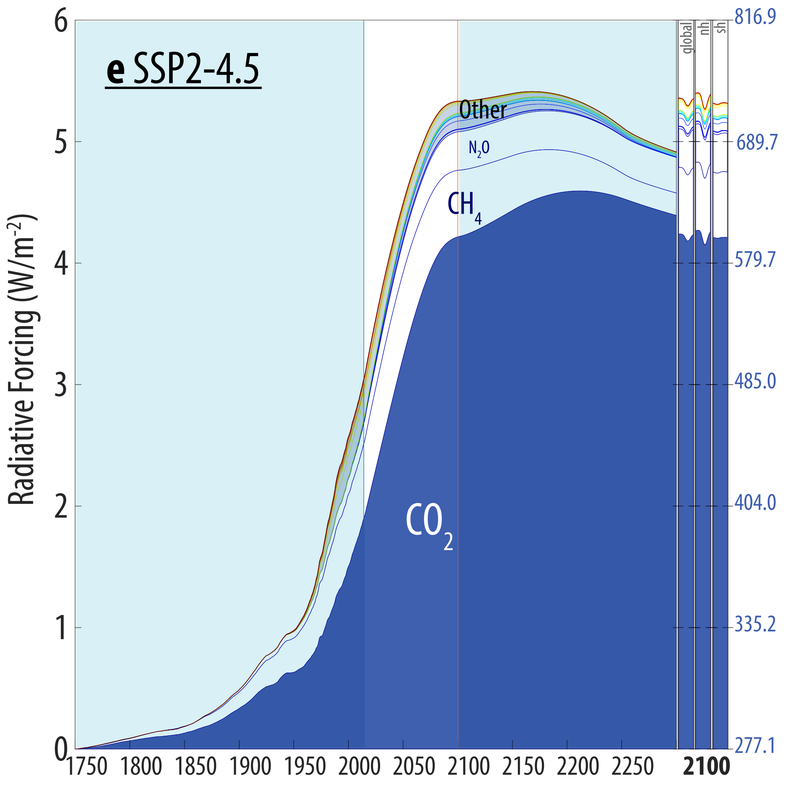

Legend of gases:

N_2O
CH_4
CO_2

Other greenhouse gases

HFC-43-10mee	$c\text{-}C_4F_8$	HCFC-22	CH_2Cl_2
HFC-365mfc	C_5F_{18}	HCFC-141b	CH_3Cl
HFC-245fa	C_7F_{16}	HCFC-142b	CH_3CCl_3
HFC-134a	C_6F_{14}	CFC-115	CCl_4
HFC-236fa	C_5F_{12}	CFC-114	$CHCl_3$
HFC-227ea	C_4F_{10}	CFC-113	CH_3Br
HFC-152a	C_3F_8	CFC-11	Halon-2402
HFC-143a	C_2F_6	CFC-12	Halon-1301
HFC-125	CF_4		Halon-1211
HFC-32	SO_2F_2		
HFC-23	SF_6		
	NF_3		

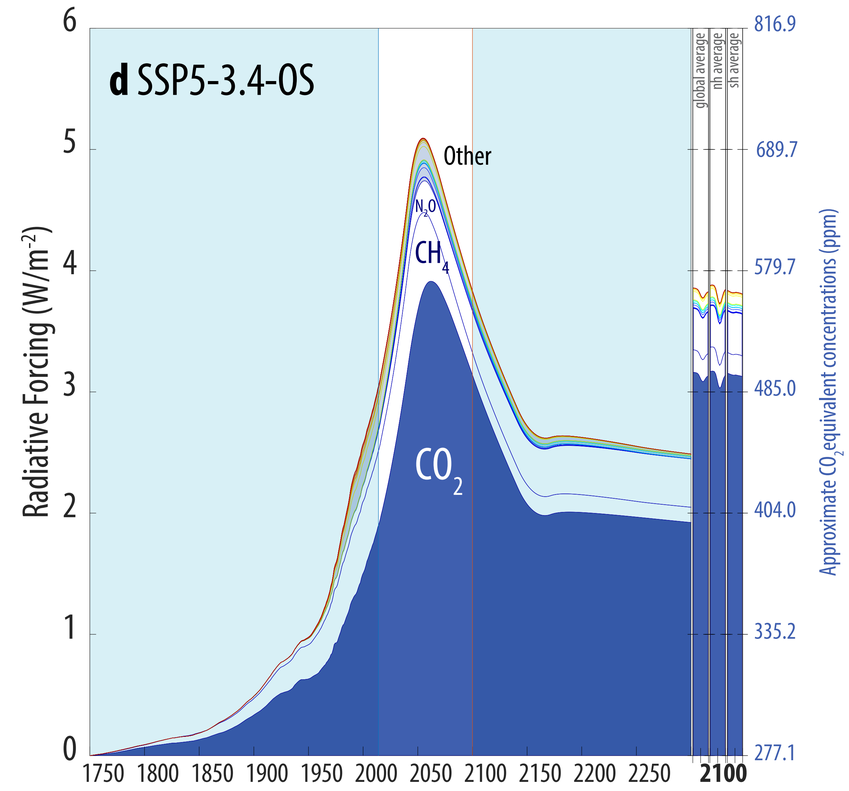

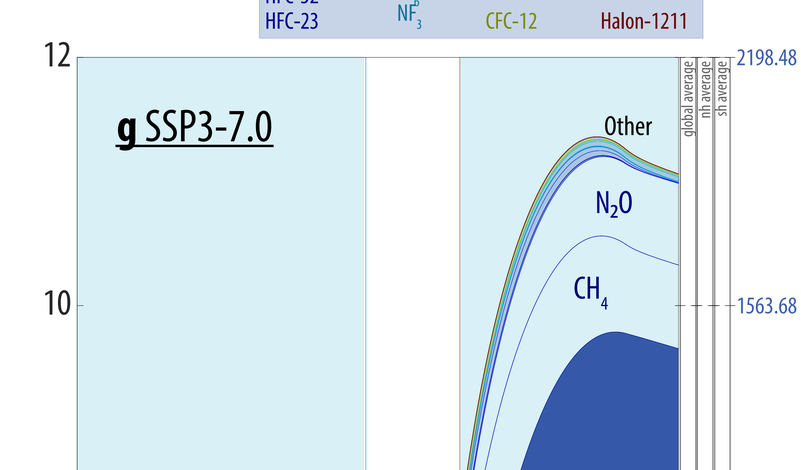

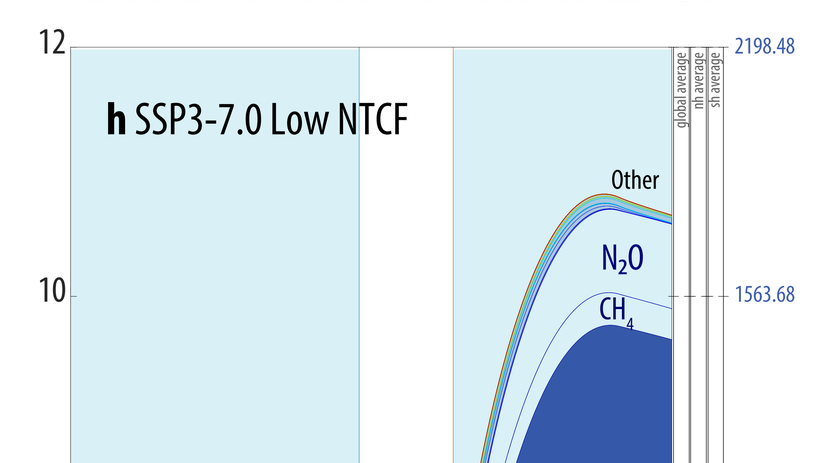

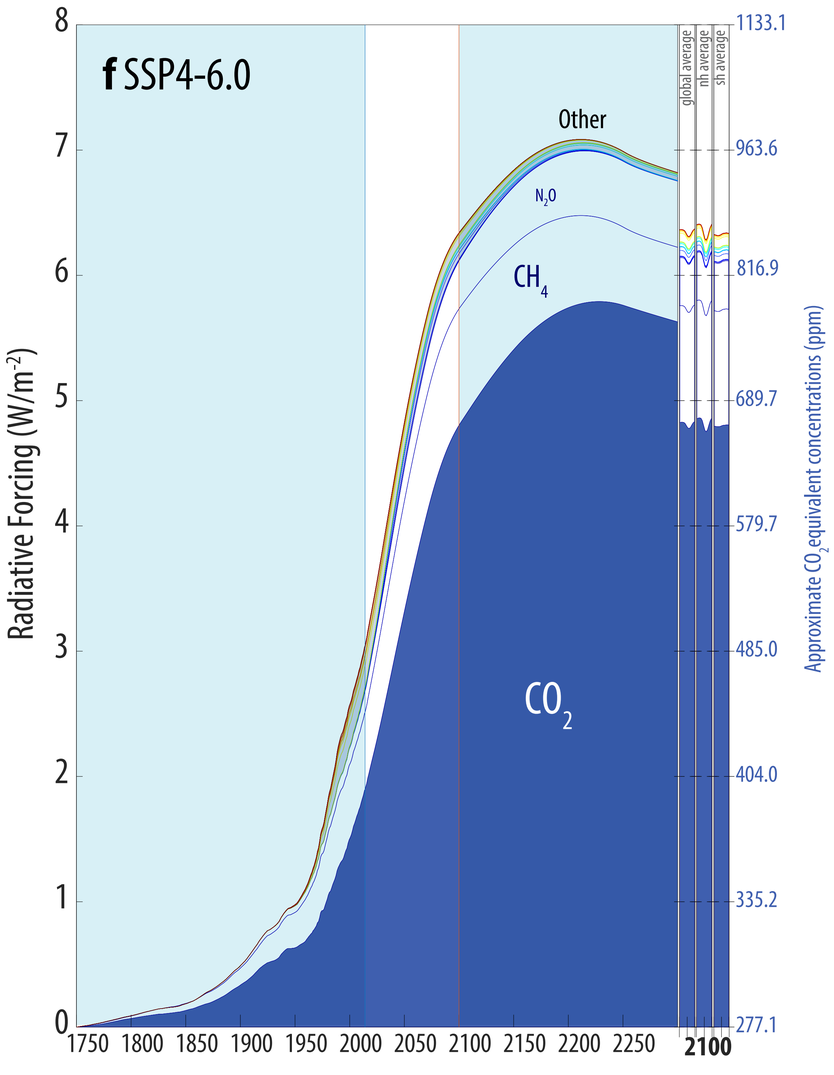

Figure 7

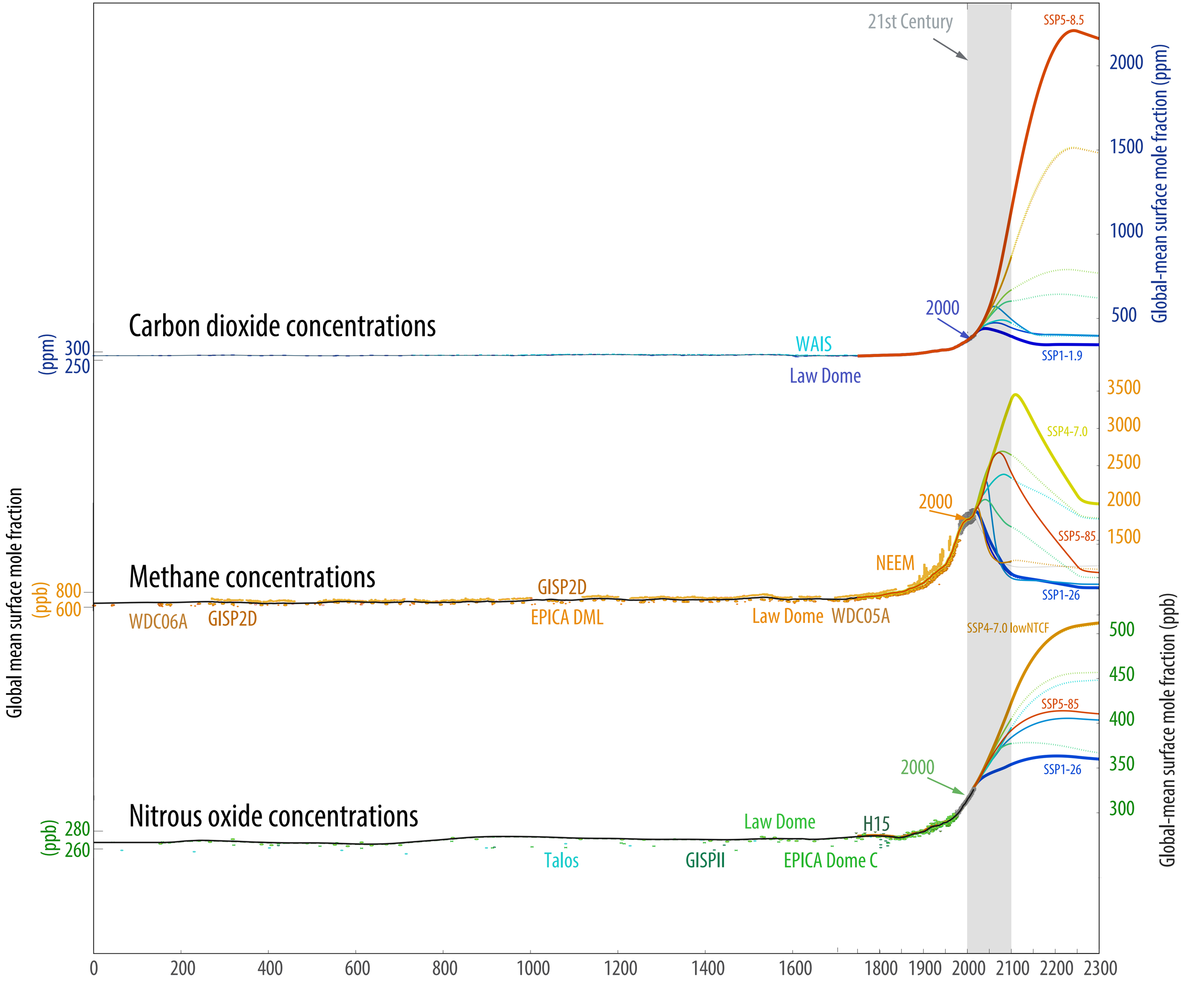
Carbon dioxide concentrations
(ppm)
300
250
21st Century
SSP5-8.5
2000
WAIS
Law Dome
SSP1-1.9
2000
1500
1000
500
Global-mean surface mole fraction (ppm)
Methane concentrations
(ppb)
800
600
WDC06A
GISP2D
GISP2D
EPICA DML
Law Dome
WDC05A
NEEM
2000
SSP4-7.0
SSP5-85
SSP1-26
3500
3000
2500
2000
1500
Nitrous oxide concentrations
(ppb)
280
260
Talos
GISPII
Law Dome
H15
EPICA Dome C
2000
SSP4-7.0 lowNTCF
SSP5-85
SSP1-26
500
450
400
350
300
Global mean surface mole fraction
Global-mean surface mole fraction (ppb)
0
200
400
600
800
1000
1200
1400
1600
1800
1900
2000
2100
2200
2300

Figure 8

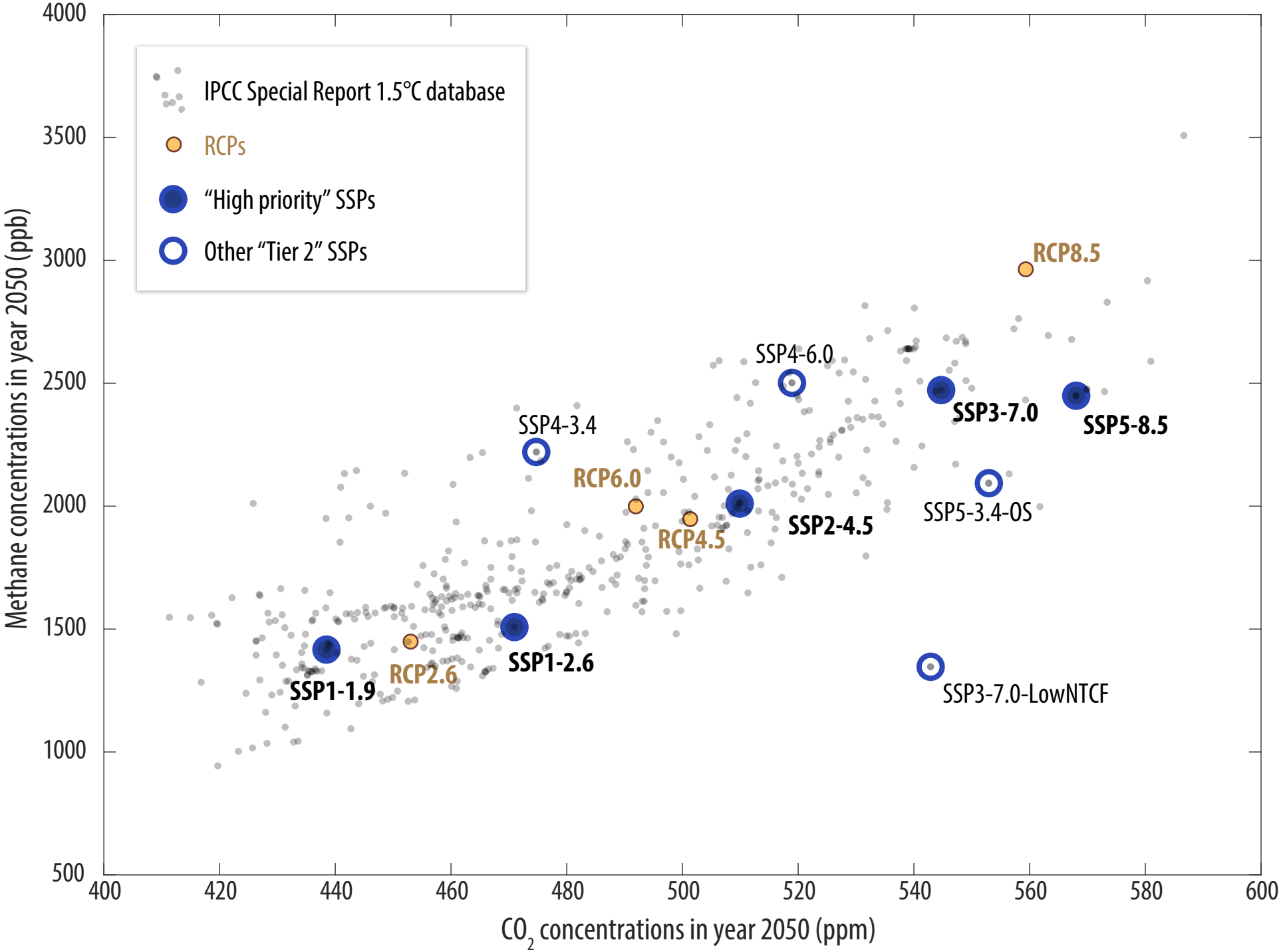
IPCC Special Report 1.5°C database
RCPs
"High priority" SSPs
Other "Tier 2" SSPs
RCP8.5
SSP4-6.0
SSP3-7.0
SSP5-8.5
SSP4-3.4
RCP6.0
RCP4.5
SSP2-4.5
SSP5-3.4-OS
SSP1-2.6
RCP2.6
SSP1-1.9
SSP3-7.0-LowNTCF
Methane concentrations in year 2050 (ppb)
CO_2 concentrations in year 2050 (ppm)
4000
3500
3000
2500
2000
1500
1000
500
400
420
440
460
480
500
520
540
560
580
600

Figure 9

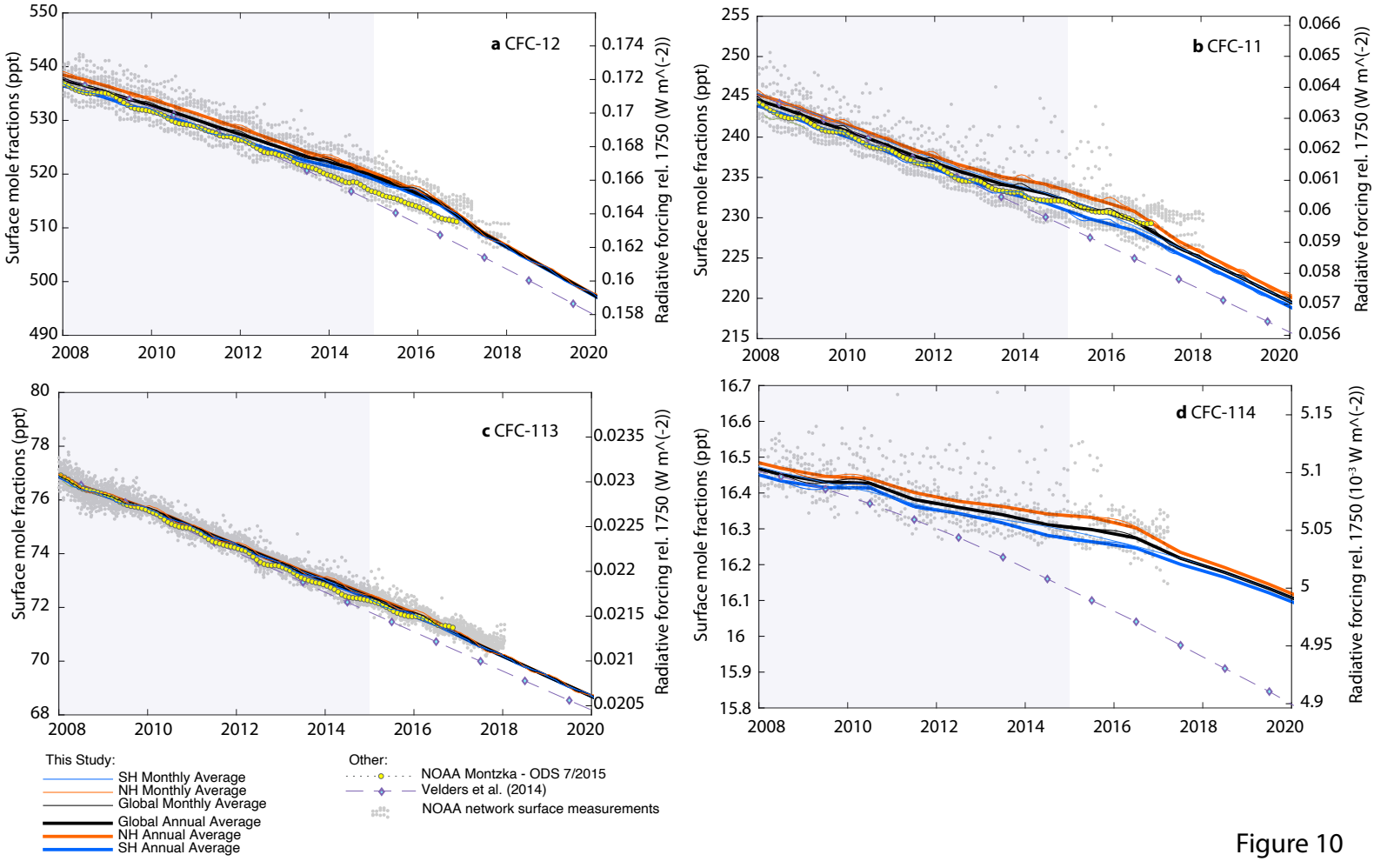
a CFC-12
b CFC-11
c CFC-113
d CFC-114
Surface mole fractions (ppt)
Radiative forcing rel. 1750 (W m^(-2))
Radiative forcing rel. 1750 (10^-3 W m^(-2))
This Study:
SH Monthly Average
NH Monthly Average
Global Monthly Average
Global Annual Average
NH Annual Average
SH Annual Average
Other:
NOAA Montzka - ODS 7/2015
Velders et al. (2014)
NOAA network surface measurements

Figure 10

a CO_2 concentrations 2000-2100

CMIP5 recommendation:
RCP3-PD / RCP26
RCP45
RCP6
RCP85

CMIP5 emissions run with CMIP6 settings:
RCP3-PD / RCP26
RCP45
RCP6
RCP85

CMIP6 recommendation:

2015-2100	Long-term extension after 2100
	SSP1-19
	SSP1-26
	SSP5-34-OS
	SSP4-34
	SSP2-45
	SSP4-60
	SSP3-70
	SSP3-70-LowNTCF
	SSP5-85

Global-mean surface mole fraction (ppm)

b CO_2 concentrations 1750-2300

Global-mean surface mole fraction (ppm)

c CH_4 concentrations 2000-2100

Global-mean surface mole fraction (ppb)

d CH_4 concentrations 1750-2300

Global-mean surface mole fraction (ppb)

e N_2O concentrations 2000-2100

Global-mean surface mole fraction (ppb)

f N_2O concentrations 1750-2300

Global-mean surface mole fraction (ppb)

Figure 11

a

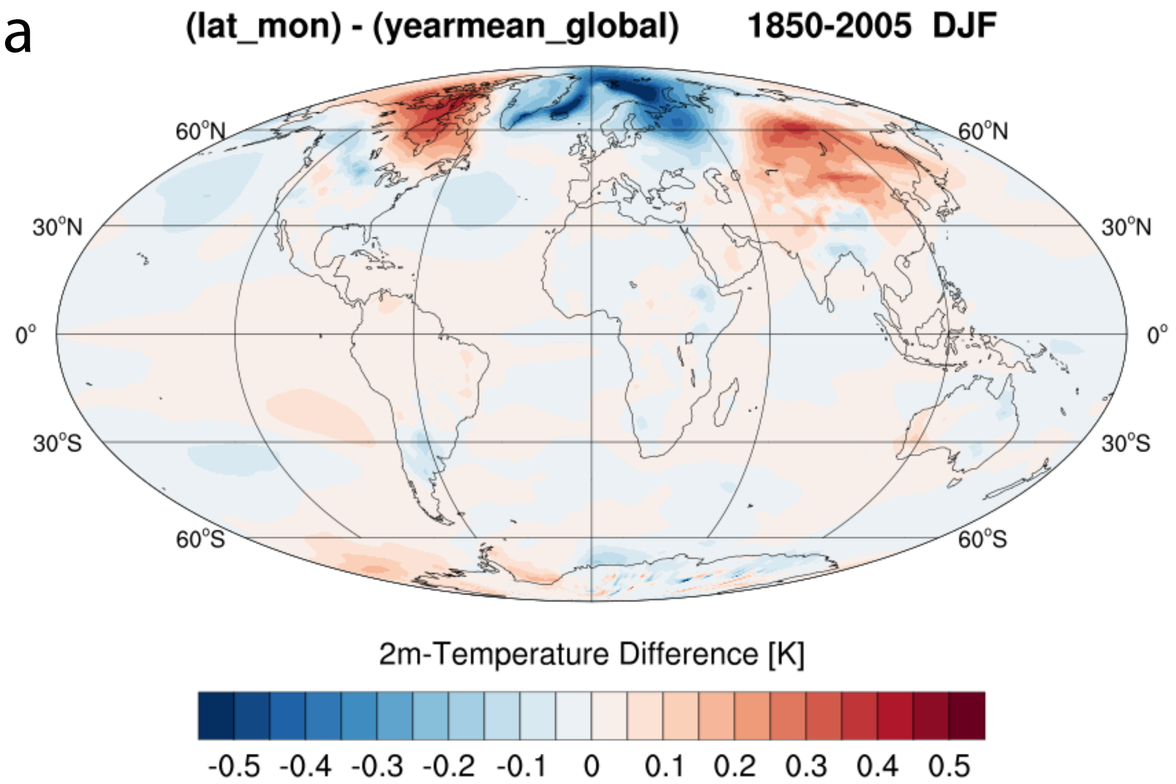

b

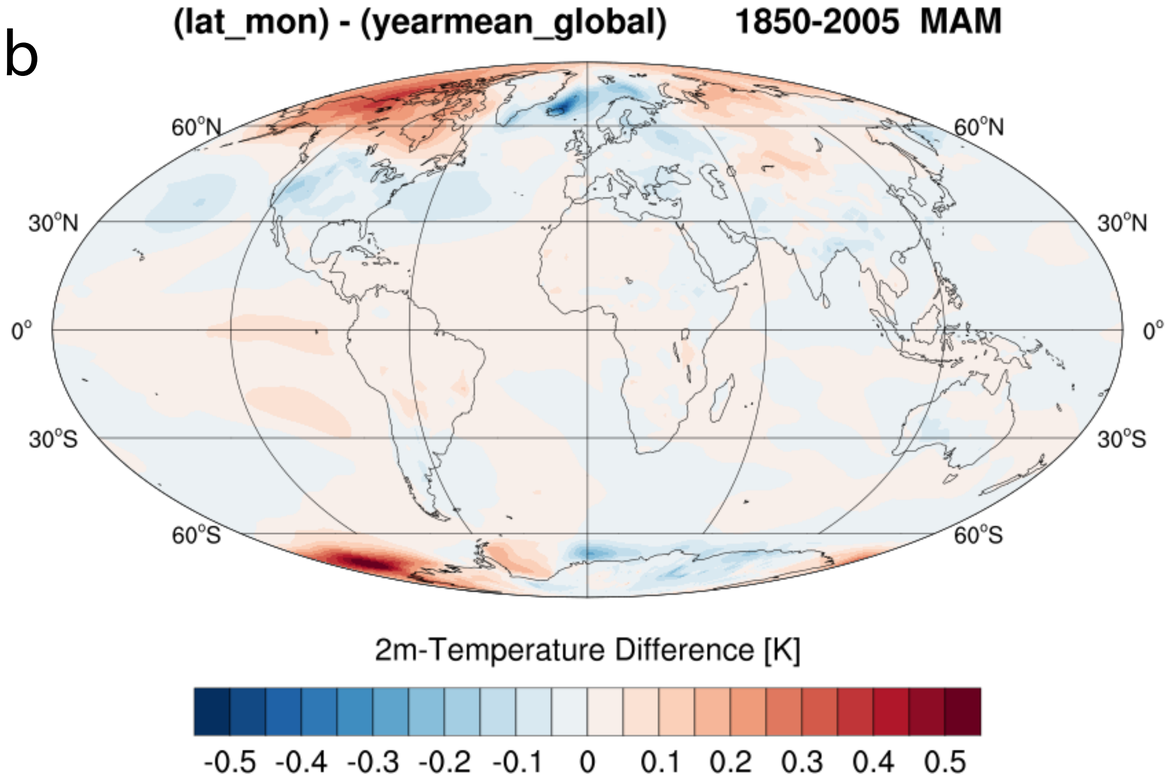

(lat_mon) - (yearmean_global) 1850-2005 DJF

(lat_mon) - (yearmean_global) 1850-2005 MAM

c

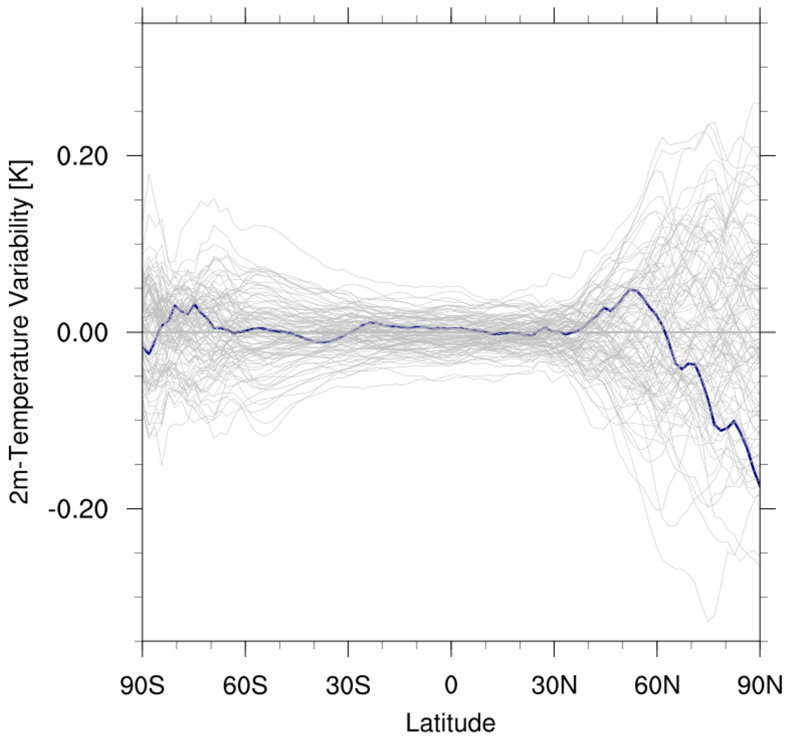

d

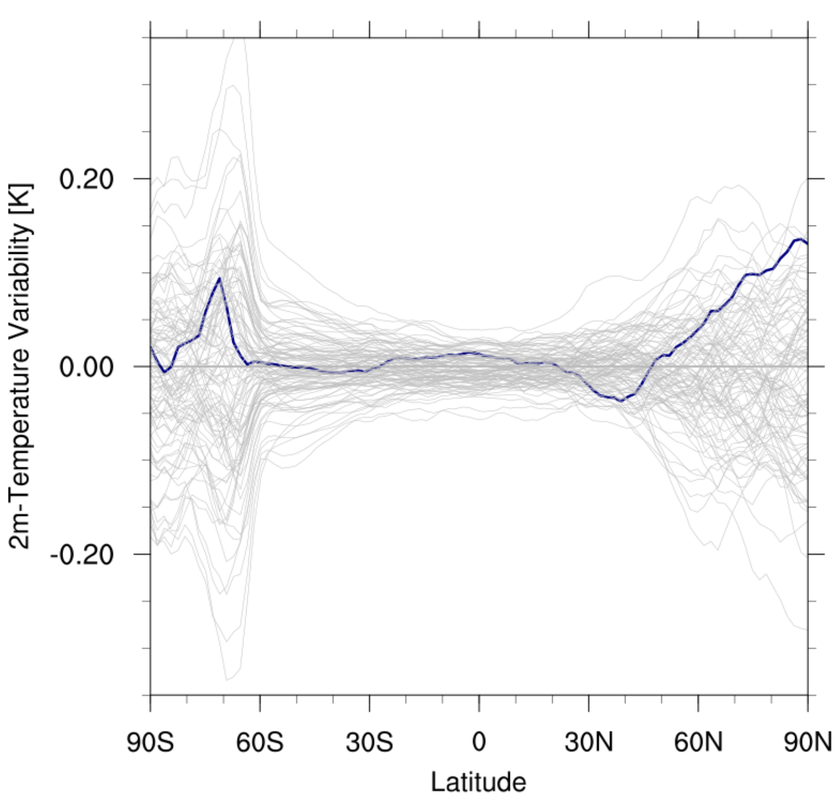

Figure 12